General Disclaimer

One or more of the Following Statements may affect this Document

- This document has been reproduced from the best copy furnished by the organizational source. It is being released in the interest of making available as much information as possible.

- This document may contain data, which exceeds the sheet parameters. It was furnished in this condition by the organizational source and is the best copy available.

- This document may contain tone-on-tone or color graphs, charts and/or pictures, which have been reproduced in black and white.

- This document is paginated as submitted by the original source.

- Portions of this document are not fully legible due to the historical nature of some of the material. However, it is the best reproduction available from the original submission.

(NASA-CR-167967) EXPERIMENTAL VERIFICATION OF THE NEUBER RELATION AT ROOM AND ELEVATED TEMPERATURES M.S. Thesis (Michigan State Univ.) 100 p HC A05/MF A01 CSCL 20K

N83-19121

Unclas
G3/39 02755

EXPERIMENTAL VERIFICATION OF THE NEUBER RELATION AT ROOM AND ELEVATED TEMPERATURES

By

Lonnie J. Lucas

A THESIS

Submitted to
Michigan State University
in partial fulfillment of the requirements
for the degree of

MASTER OF SCIENCE

Department of Metallurgy, Mechanics and Materials Science

1982

ABSTRACT

EXPERIMENTAL VERIFICATION OF THE NEUBER RELATION AT ROOM AND ELEVATED TEMPERATURES

By

Lonnie J. Lucas

The accuracy of the Neuber equation at room temperature and 1,200°F was experimentally determined under cyclic load conditions with hold times. All strains were measured with an interferometric technique at both the local and remote regions of notched specimens. At room temperature, strains were obtained for the initial response at one load level and for cyclically stable conditions at four load levels. Stresses in notched members were simulated by subjecting smooth specimens to the same strains as were recorded on the notched specimen. Local stress-strain response was then predicted with excellent accuracy by subjecting a smooth specimen to limits established by the Neuber Equation. Data at 1,200°F were obtained with the same experimental techniques but only in the cyclically stable conditions. The Neuber prediction at this temperature gave relatively accurate results in terms of predicting stress and strain points. However, predicted interaction of the creep and stress relaxation behavior differed from experimentally measured values.

ACKNOWLEDGMENTS

This thesis project was funded by the National Aeronautics and Space Administration.

I would like to thank my wife, Beth, for her help during the period of this work. I would also like to thank Shari Sawdey and Michelle Ward for their help in preparing the figures and typing. A special thank you goes to Dr. John Martin who is an excellent teacher, advisor and friend.

TABLE OF CONTENTS

LIST OF TABLES

LIST OF FIGURES

CHAPTER 1

INTRODUCTION

There has been a demand in recent years for the aircraft industry to provide a more energy efficient turbine propulsion system. Part of this task involves trying to understand the limitations of the current materials and structures being used, especially in the 'hot section' of the engine (1)*. The hot section components include the turbine blades, vanes, and combustors which operate under severe stresses and temperatures. To make improvements in these parts it is first necessary to compile test data which describe the events leading up to failure. Theoretical models can then be developed and compared with experimental data until the failure modes and component lives may be predicted.

The combustor, fabricated from the alloy Hastelloy X, is one component which has gone through the initial testing phase and is now being examined from a theoretical standpoint. Failures in the combustor liner have been attributed to thermal-mechanical fatigue which causes cracking and

---

*Numbers in parenthesis refer to references listed in the reference table. Numbers in brackets refer to equations.

buckling (2). A number of constitutive theories have been proposed for predicting the nonlinear stress-strain behavior near holes which serve as cracking sites in the liner (3). When these theories are incorporated into finite element codes, the final package becomes very complex and requires a large computer facility.

The purpose of this study is to examine a more basic theory, namely the Neuber relation, to see how well it can predict local stress-strain behavior in notched specimens of Hastelloy X. For cyclic loading the Neuber equation is written,

$$(\Delta\sigma)(\Delta\varepsilon) = (K_t')^2 (\Delta S)(\Delta e) \qquad [1]$$

where: $\Delta\sigma$ and $\Delta\varepsilon$ are the notch root stress and strain ranges, respectively;

ΔS and Δe are the remote stress and strain ranges, respectively;

K_t' is the elastic stress concentration factor.

Much of the work involving Neuber's relation has focused on stress redistribution near a notch (4) and the accompanying variation in the stress and strain concentration factors throughout fatigue life (5,6,7). One of these researchers, Guillot (6), evaluated Neuber's equation at moderately elevated temperatures (500°F) and found that conservative results were obtained for life predictions in 1018 steel and 7475 aluminum. Both Bofferding (5) and

Guillot (6) used an Interferometric Strain Gage (I.S.G.) (8-11) to measure notch root strains.

Equation [1] by itself is indeterminate. Knowing the remote stress or strain range leaves three unknowns. The relationship between stress and strain at both the remote and local locations is needed. Crews and Hardrath (12) assumed that the notch stress could be found by reproducing measured notch strains in smooth samples. This assumption was upheld by Stadnick (13) and other researchers (14,15) who showed that the smooth specimen simulation gave good results in predicting fatigue lives of notched specimens. For this study it was assumed that smooth specimens could be used to supply the needed stress-strain relationship.

Stadnick and Morrow (16) worked on automating the techniques for performing tests on smooth specimens that were controlled according to the Neuber Equation. They evaluated various approaches for subjecting a smooth specimen to the same stresses and strains which would exist at a notch. These methods consisted of manual control, and analog or digital computer control of the Neuber parameters.

Separate research efforts have been devoted to using smooth specimens to simulate notch root response, developing laser based measurement devices and establishing high temperature testing techniques. This study utilized all of these tools to determine the accuracy of Neuber's equation for cyclic loading of notched specimens at temperatures up to 1,200°F.

CHAPTER 2

INTERFEROMETRIC STRAIN GAGE

2.1 Fundamentals of the I.S.G.

The Interferometric Strain Gage is a noncontacting laser device capable of measuring strains over a very short gage length (50-100 microns). Figure 1 illustrates the fundamental principles upon which the I.S.G. is designed. This cut-away view shows two surface indentations which form the gage length on a specimen. Parallel rays reflecting off the indentations have a path difference of $d \sin\alpha$, where α is the angle between the normal incident laser beam and the light rays of interest. When the following relation is satisfied,

$$d \sin\alpha = m\lambda \quad (m = 0, \pm 1, \pm 2, \ldots) \qquad [1]$$

where: λ = wavelength of laser light

the laser rays will interfere constructively to form bright interference fringes such as those in Figure 2. Each bright fringe is defined by an integer, m. from Equation [1]. The orientation of the fringe patterns with respect to the laser is shown in Figure 3.

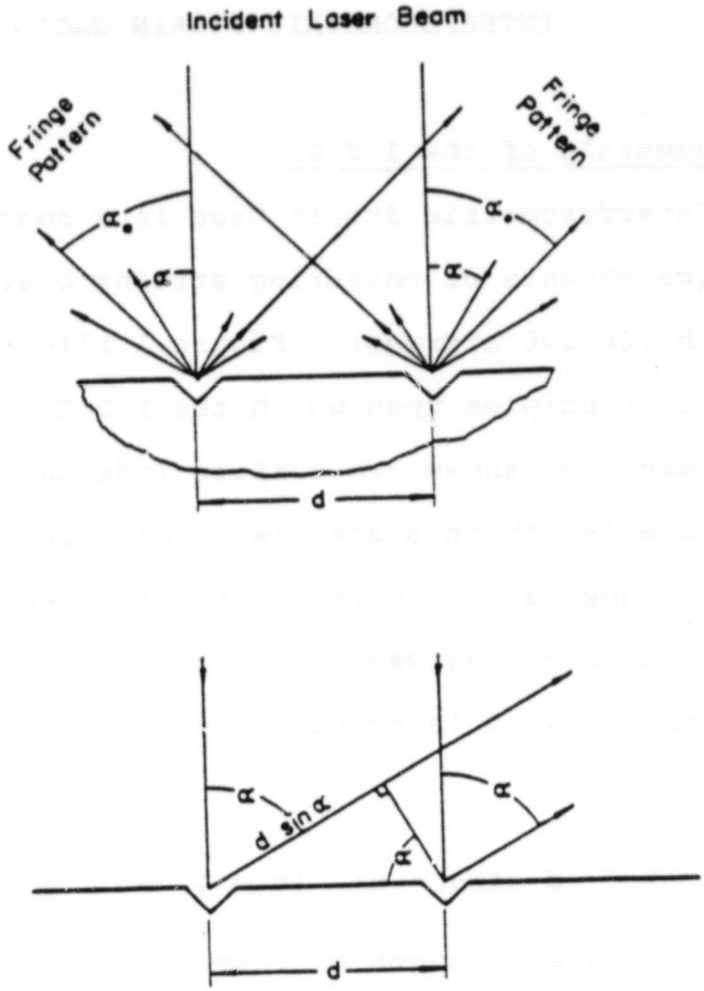

FIGURE 1 FRINGE PATTERN GENERATION PRINCIPLES

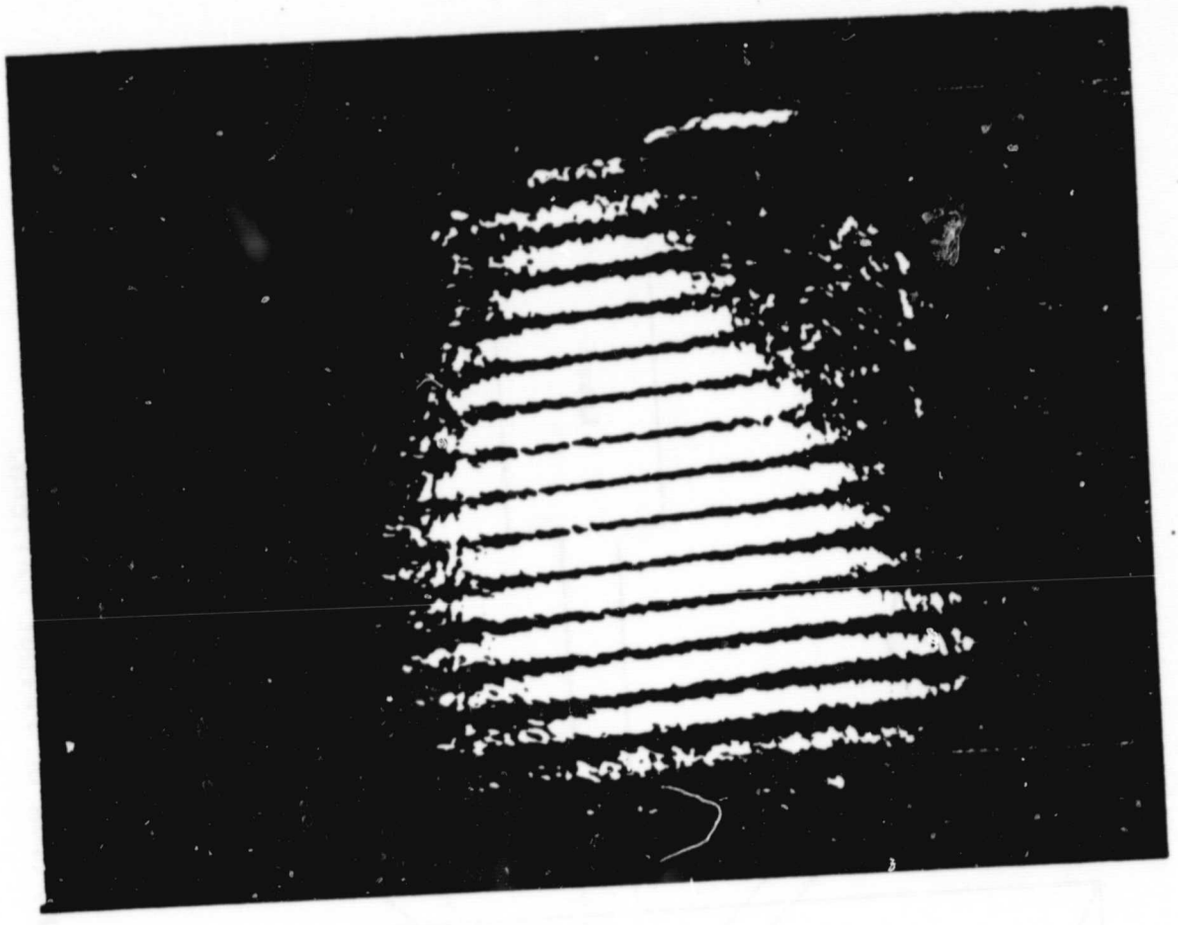

FIGURE 2 INTERFERENCE PATTERNS

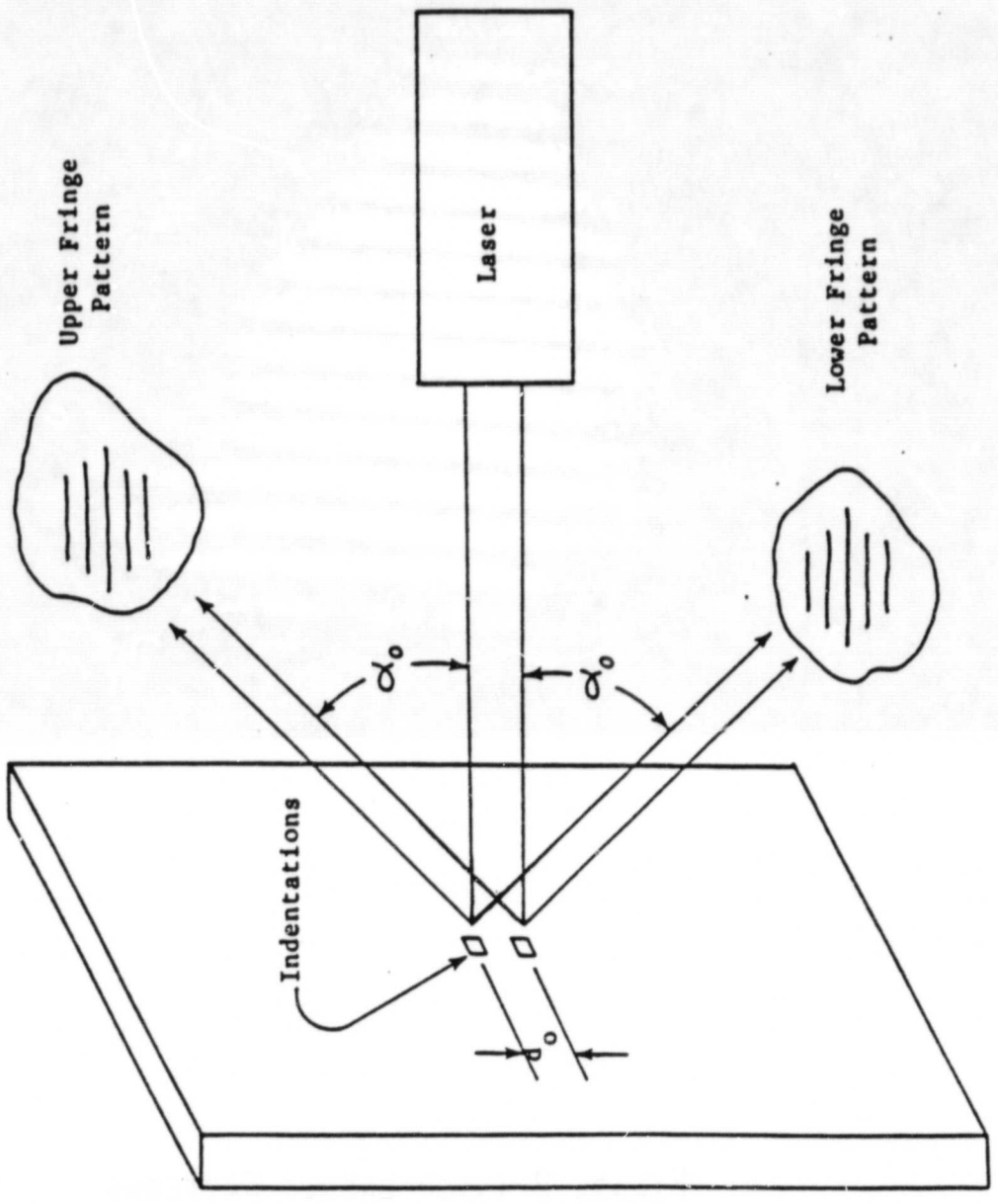

FIGURE 3 ORIENTATION OF FRINGE PATTERNS

When a tensile load is applied to the specimen, the indentations will move apart a distance δd. Since $m\lambda$ is a constant for a given fringe, α must decrease for tensile loads which means that the fringes will move toward the laser beam. For compressive loads, the spacing d decreases, causing an increase in α and a movement of the fringes away from the incident beam. To monitor this motion, a fixed observation point at angle α_o is chosen. The relationship between fringe motion and displacement is defined as,

$$\delta d = \left(\frac{\lambda}{\sin \alpha_o}\right) \quad \delta m \qquad [2]$$

Where: δm is the fraction of fringes passing the observation point.

Letting $\delta m = 1$ and substituting typical values into Equation [2],

$$\delta d = \left(\frac{6328 \times 10^{-10} m}{\sin 42^\circ}\right) \cong 1 \times 10^{-6} m = 1 \text{ micron}$$

By knowing the initial spacing between indentations, d_o, the strain can be calculated,

$$\varepsilon = \frac{\delta d}{d_o} = \frac{1 \text{ micron}}{100 \text{ microns}} = 1\% \qquad [3]$$

Fringe motion can also be caused by rigid body motion which occurs in most loading schemes. However, these effects are cancelled out since one pattern of fringes moves toward the incident laser while the other pattern moves away. By using the following equation,

$$\varepsilon = \frac{\delta d}{d_o} = \frac{\lambda}{(d_o)\ \sin\ \alpha_o}\ \left(\frac{\delta m_1 + \delta m_2}{2}\right) \qquad [4]$$

Where: δm_1 and δm_2 are the upper and lower fringe patterns.

the relative displacement of the specimen can be averaged out.

A Vicker's hardness tester with a pyramidal diamond (Figure 4) was used to form the indentations. Figure 5 shows scanning electron micrographs of a negative replica from a notched specimen. The upper photo shows two indentations which are 50 microns from the edge of a 0.2 inch diameter hole. The lower photo shows an enlarged view of the replica. The indentations are generally 25 microns on a side and 5 microns deep.

2.2 Hardware and Software for the ISG

A schematic diagram of the ISG is shown in Figure 6. Figure 7 shows the actual components of the ISG. Fringe patterns impinge upon the two servo controlled mirrors positioned at angle α_o and are then reflected onto a pair of photomultiplier tubes (PMT's). A cover with a narrow slit is fitted over the face of each PMT so that only part of one bright fringe may shine through. A bright band of constructive interference is accompanied by a high voltage output from the PMT.

During operation of the system a D/A converter outputs a ramp function to the servo mirrors. This causes the

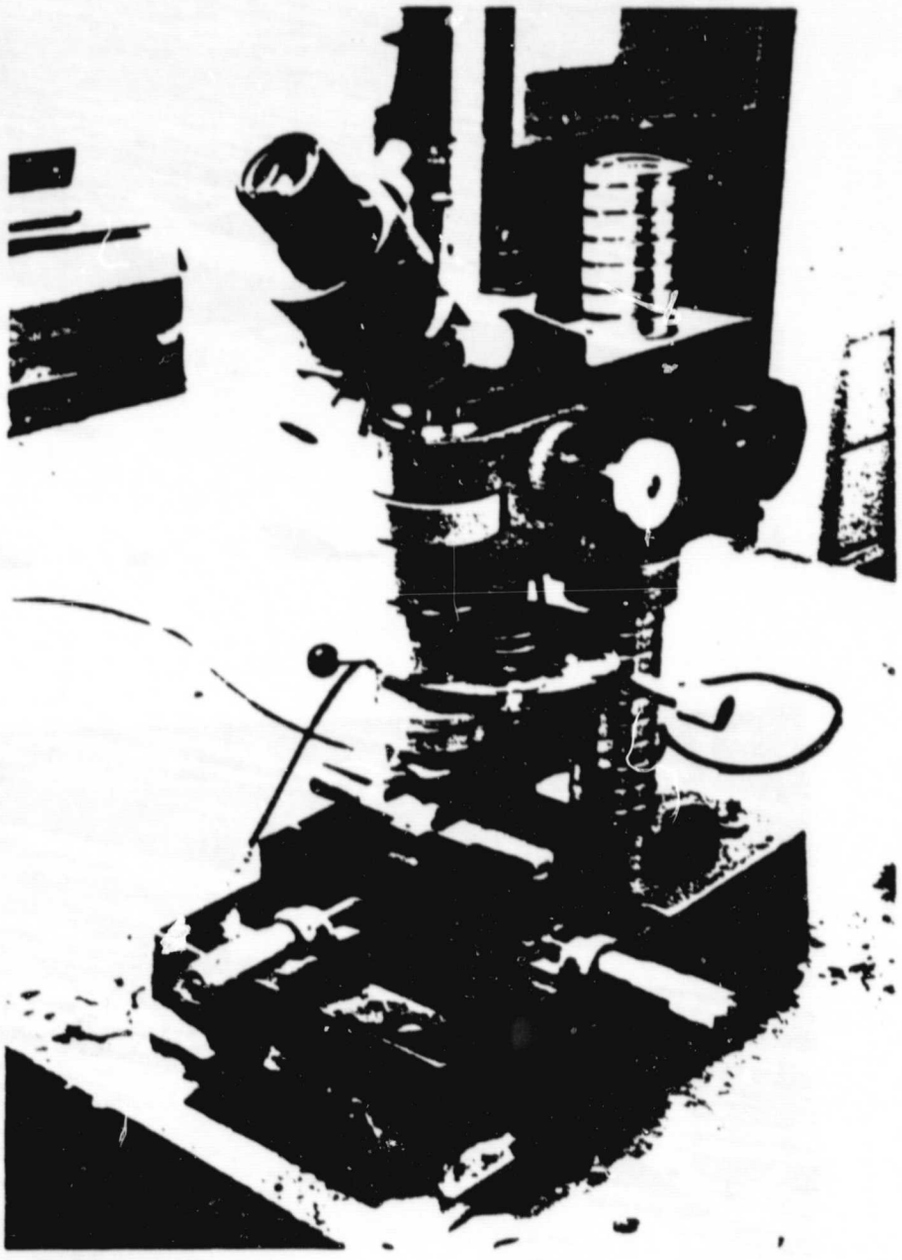

FIGURE 4 VICKERS HARDNESS TESTER

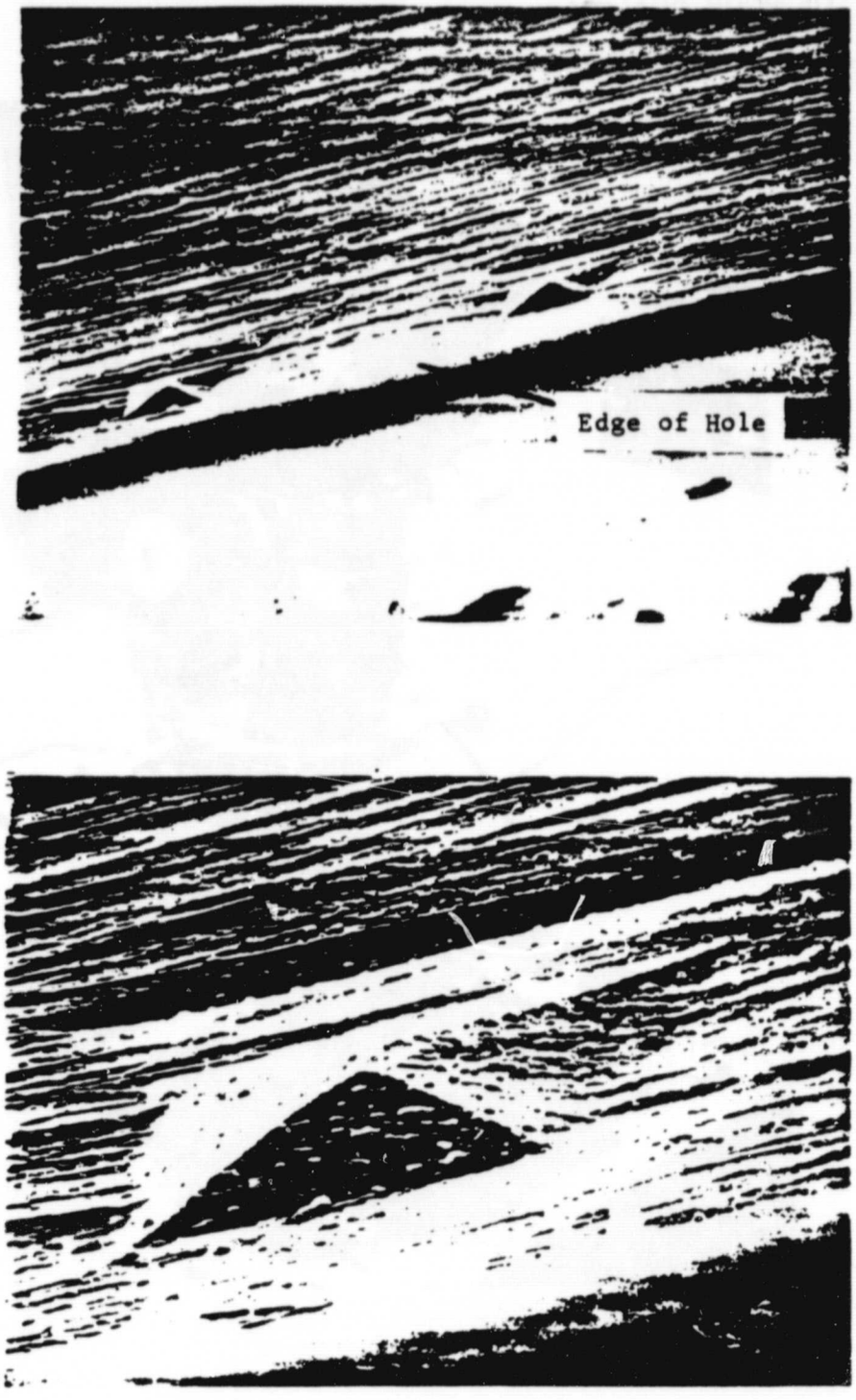

FIGURE 5 NEGATIVE REPLICA OF INDENTATIONS

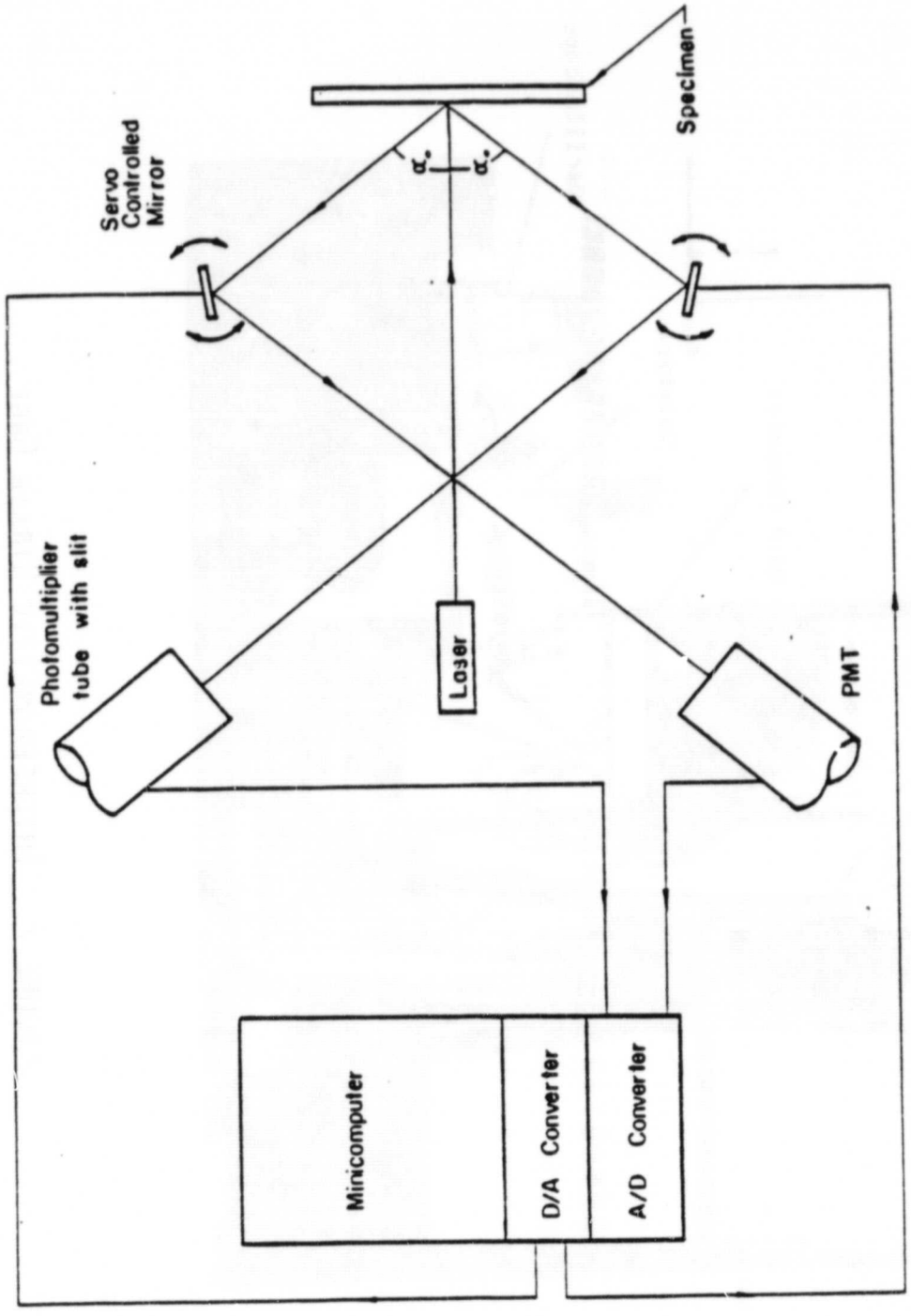

FIGURE 6 SCHEMATIC OF I.S.G.

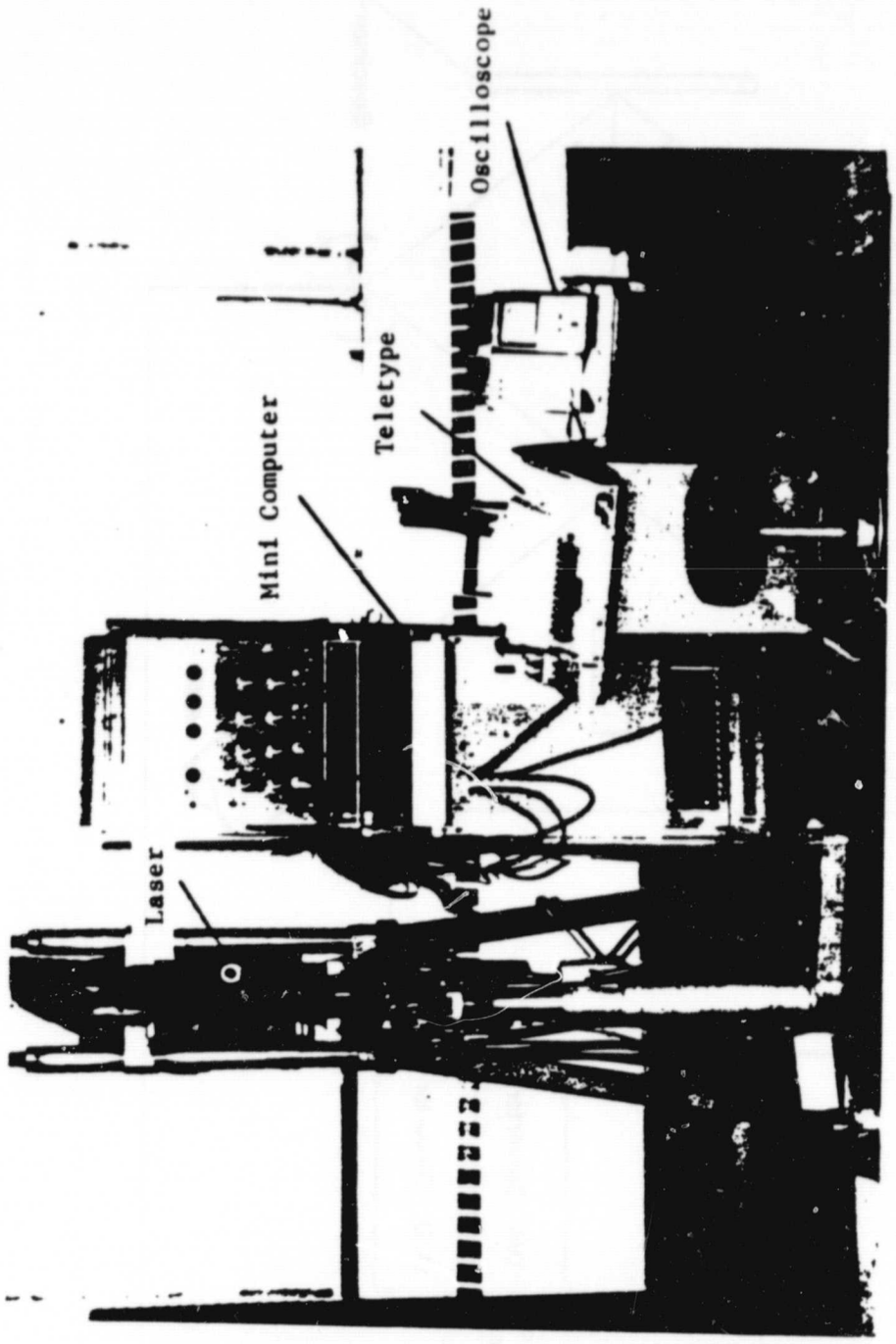

FIGURE 7 INTERFEROMETRIC STRAIN GAGE

mirrors to rotate through a small angle, sweeping several fringes across the slits of the PMT's. A minicomputer divides each sweep into 256 mirror positions and stores an accompanying PMT voltage for each position. In this manner, the computer can locate and store the mirror positions which accompany each maximum (bright) and minimum (dark) fringe band. Applied loads to the specimen cause the fringes to move with respect to α_o and therefore the mirror positions recorded for maximum and minimum fringe bands will also change.

Every 100 milliseconds the mirrors complete a sweep and the change in fringe position is calculated. This allows the analog strain voltage to be determined using Equation [4]. The strain output is continuously available as in standard extensometers but because of the calculation time involved, there are limitations on the strain rates for which data may be obtained. For strain ranges near 0.5% the limit on cyclic frequency is about 0.1 Hz. This speed is quite sufficient for most applications. A more detailed discussion of the I.S.G. may be found in Reference (5).

2.3 The I.S.G. at Elevated Temperatures

The interferometric strain gage offers several advantages over conventional techniques. It operates over a small gage length to obtain strain information at critical locations. It is also noncontacting, which allows it to be used in hostile environments such as those found in high

temperature fatigue applications. Three requirements must be met in order to utilize this gage. One is that the path of the incoming laser beam and rays reflected back by the specimen must not be obstructed. Another is that the reflective ability of the specimen must be maintained. The final requirement is that blackbody radiation emitted from the specimen not overshadow the interference fringes.

The problem of obstruction of light rays depends upon the method of heating the specimen. If an enclosed furnace is used, optical ports for the incident beam and exiting fringes must be provided. Quartz windows with melting temperatures near 4,000°F have been used successfully (17). For this experiment, nigh frequency induction heating was employed. The coils were designed to allow fringes to exit the specimen surface. Figure 8 shows the I.S.G. during a test conducted at 1,200°F. The plexiglass enclosure has a 2 inch wide slit for passing of light rays to and from the specimen. Figure 9 is a closer view of the heating coil and notched specimen.

Since the indentations essentially form the "gage" for the system, their sides must be smooth and reflective. For most metals at high temperature, oxidation begins to break down the integrity of the surface finish. There are three ways of solving the oxidation problem:

1. Protect the specimen in an inert atmosphere.
2. Attach non-oxidizing tabs to the specimen and place the indentations on them.

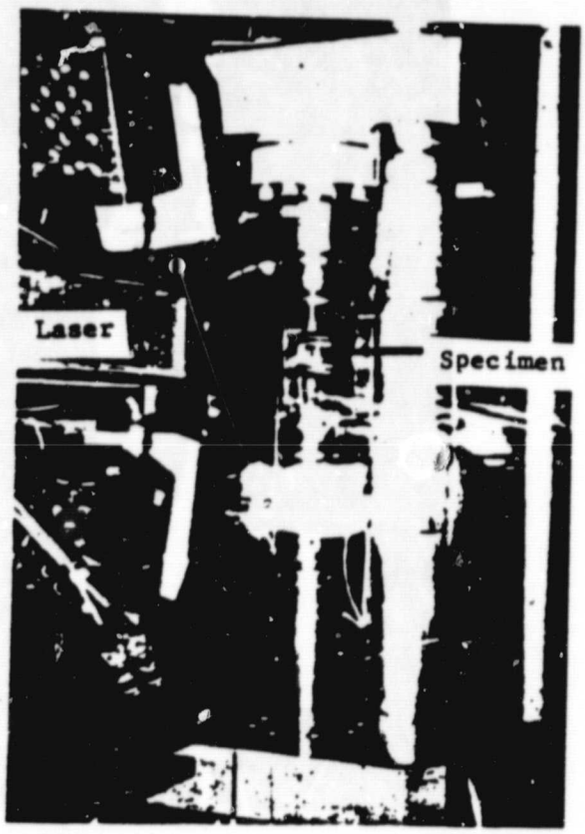

FIGURE 8 INTERFEROMETRIC TECHNIQUE AT 1,200°F

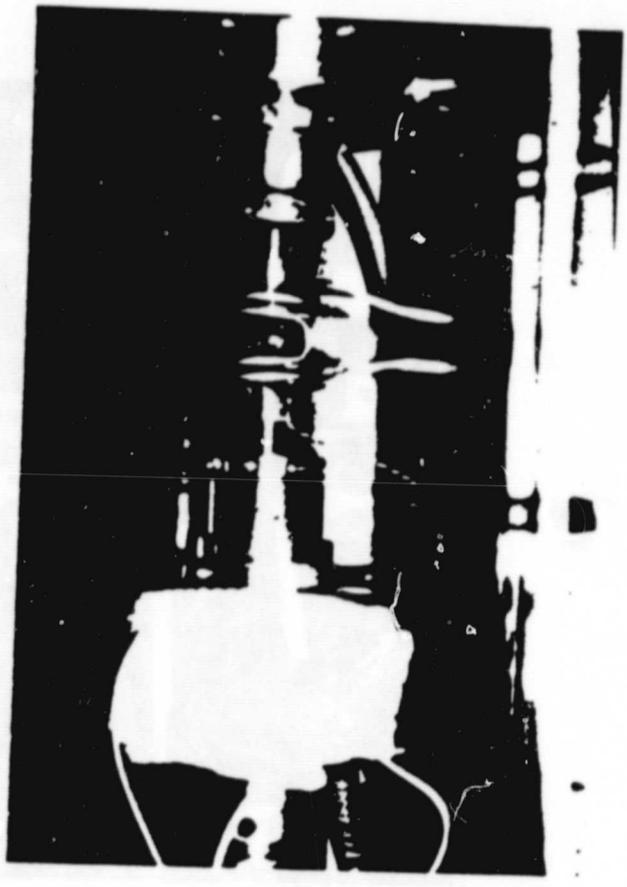

FIGURE 9 INDUCTION HEATING COILS

3. Coat the specimen with a non-oxidizing material.

The latter method was used to retard oxidation in Hastelloy X specimens. A vacuum evaporator was used to deposit 0.14 microns of 40% gold - 60% paladium at 2×10^{-5} torr. For purposes of this study it was concluded that the thin coating would have no significant effect on stress-strain behavior. It should be noted that the coating was applied after indenting the specimen.

Figure 10 is a plot of black-body radiation at various temperatures (17). As temperatures increase, the radiation intensity increases while the wavelength decreases into the region of visible light (.4 to .7 microns). Wavelengths of two common lasers are also plotted in Figure 10. The He-Ne laser (used in this experiment) has a wavelength of 0.633 microns while the argon lasers have more powerful lines at 0.514 microns and 0.488 microns. The best choice for high temperature applications of the I.S.G. would clearly be the argon type laser.

Figures 11 through 13 show the relative intensity of fringe patterns being reflected by a Hastelloy X specimen at various temperatures. The PMT output for a bright fringe is represented as an upper peak of the sine wave type pattern. In Figure 11, the intensity peaks dropped very little as the temperature of the specimen was raised to 1,000°F. Figure 12 shows the effects of oxidation over a ten minute period at 1,100°F. The upper photo in Figure 13 was taken at 1,200°F. The bright fringe bands have been reduced to

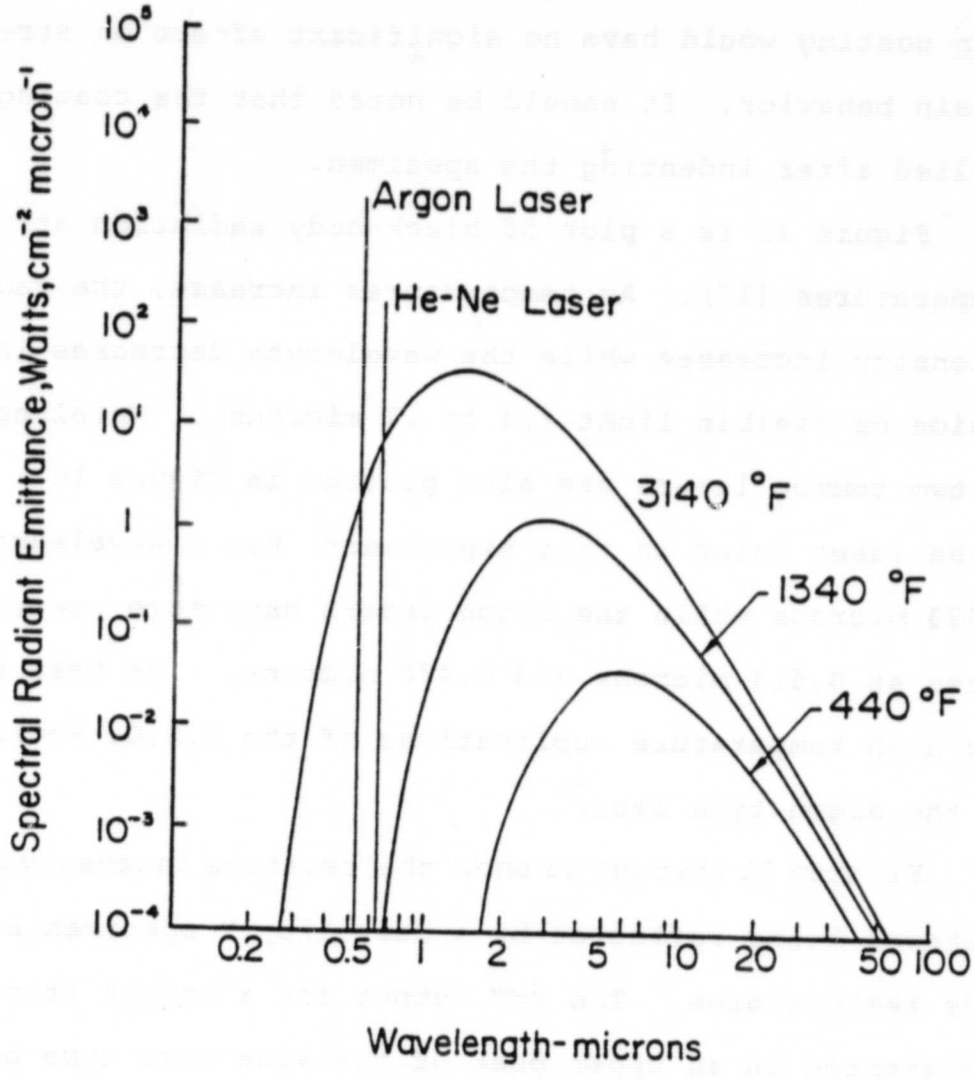

FIGURE 10 BLACK-BODY RADIATION VERSUS WAVELENGTH

ROOM TEMPERATURE

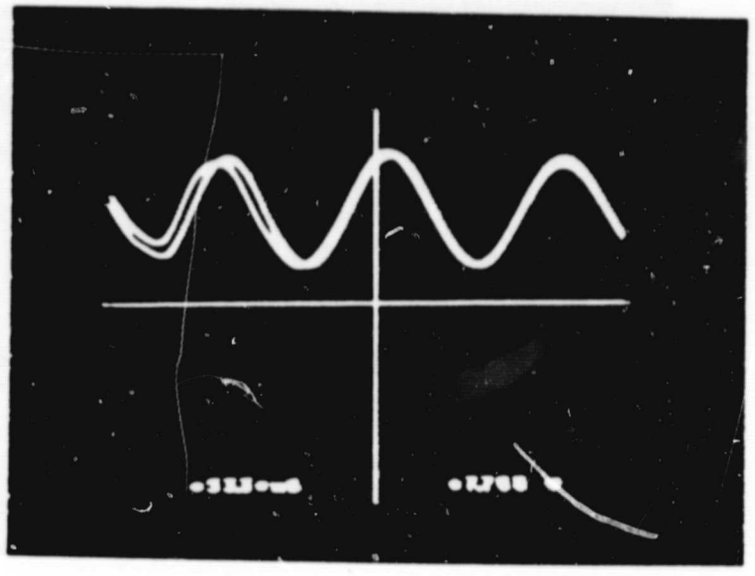

1,000 F

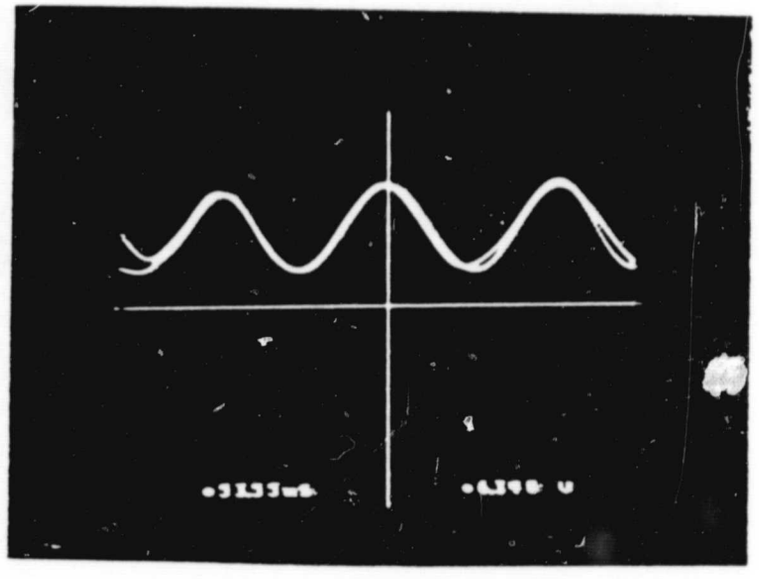

FIGURE 11 FRINGE PATTERN INTENSITY SIGNALS AT 70°F AND 1,200°F

1,100 F

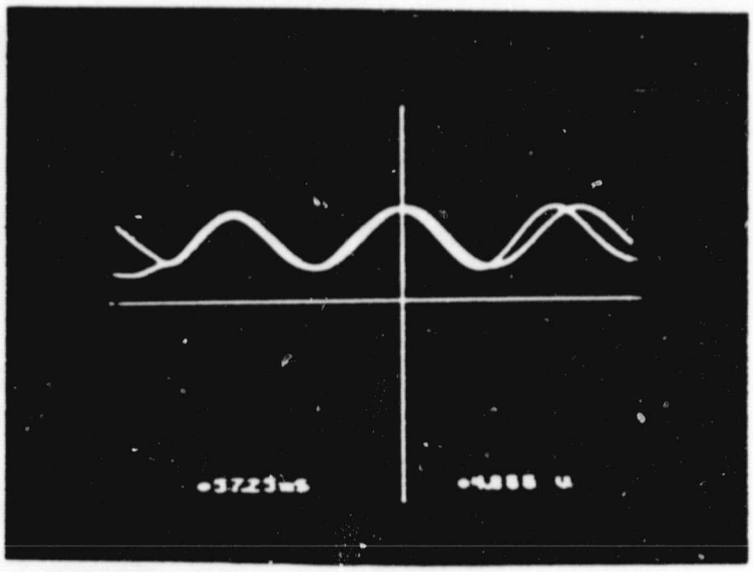

AFTER 10 MINUTES AT 1,100 F

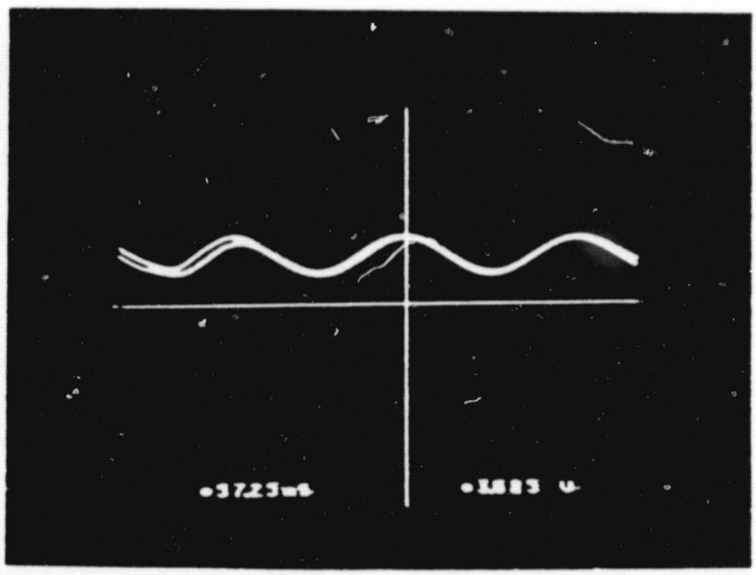

FIGURE 12 FRINGE PATTERN INTENSITY SIGNALS AT 1,100°F

1,200 F

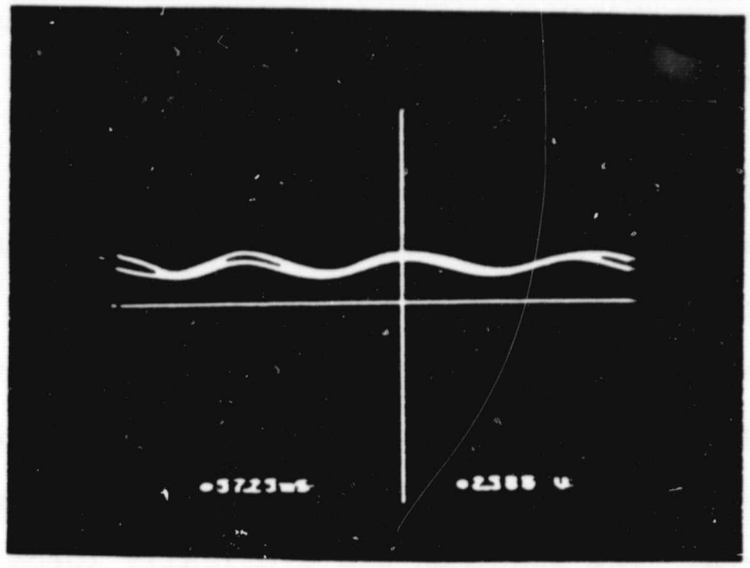

AFTER INCREASING GAIN AT 1,200 F

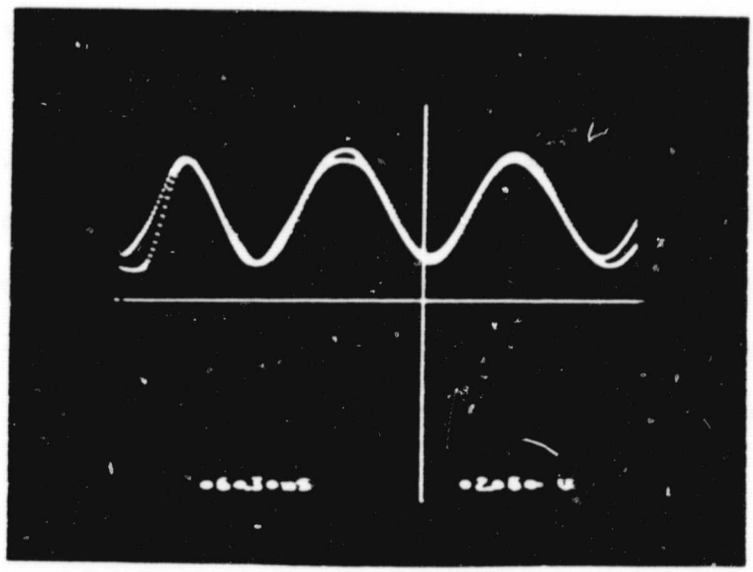

FIGURE 13 FRINGE INTENSITY BEFORE AND AFTER INCREASING PMT GAIN

lower levels due to oxidation and black-body radiation which begins to occur. The bright bands were again made distinguishable in the lower photo of Figure 13 by increasing the gain of the PMT circuit.

2.4 Comparison Test

A test was conducted at room temperature to determine the accuracy of the I.S.G. for the material and strain ranges to be used in the experiment. An MTS extensometer (0.3 inch gage length) and the I.S.G. device were both used to simultaneously monitor the strain in an axial specimen of Hastelloy X. The specimen was cyclically loaded under strain control by using the extensometer to generate a feedback signal. Hysteresis loops were then recorded for various strain ranges. Figure 14 shows the results at four different strain levels. The results for the two measurement devices were superimposed for comparison.

This test showed that the I.S.G. strain values were within 5-10% of the extensometer output. The total strain ranges were predicted exceptionally well. The comparison test allowed confident strain measurements to be made during the remainder of the test program.

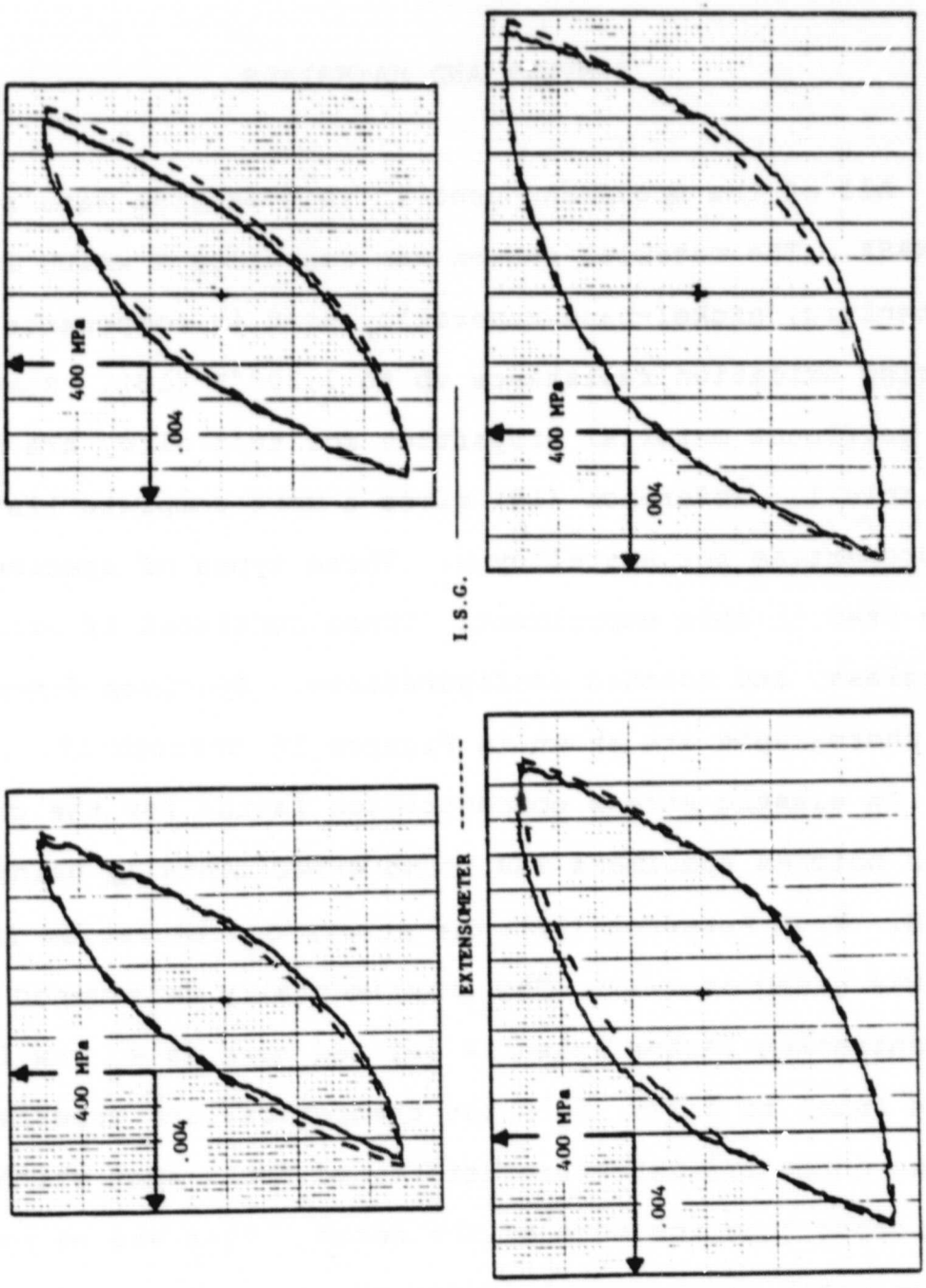

FIGURE 14 COMPARISON OF I.S.G. AND CLIP-ON GAGE STRAIN OUTPUT

CHAPTER 3

SAMPLES AND MATERIALS

All of the specimens used in this program were supplied by NASA. The material chosen was Hastelloy X which is an austenitic, nickel-base superalloy used in components requiring oxidation resistance up to 2,200°F (18). Some of the pertinent material properties for this alloy are given in Table 1. Reference (19) gives a more complete listing of properties for Hastelloy X. Three types of specimens were used in this experiment. These consisted of axial, hourglass, and notched configurations. Specimen dimensions and photographs are shown in Figures 15 through 18.

An elastic stress concentration factor for the circular notches specimens was found experimentally using the I.S.G. From Peterson (20), the stress concentration factor, K_t, was given as 2.37. The experimentally determined stress concentration factor which is defined here as K_t' was found to be equal to 2.27. Both the theoretical and experimental stress concentrations were determined for a spot which was 50 microns from the edge of the notch. This was as near to the notch as the small indentations could be made. Figure 19 shows where five sets of indentations for the I.S.G. were

Table 1. MATERIAL PROPERTIES

Test Temperature		Dynamic Modulus of Elasticity	Ultimate Tensile	0.2% Offset Yield
°C	(°F)	MPa (Ksi x 10^3)	MPa (ksi)	MPA (ksi)
21	(70)	206,850 (30.0)	785.3 (119.9)	360 (52.2)
650	(1,200)	154,448 (22.4)	572.3 (83.0)	272 (39.5)

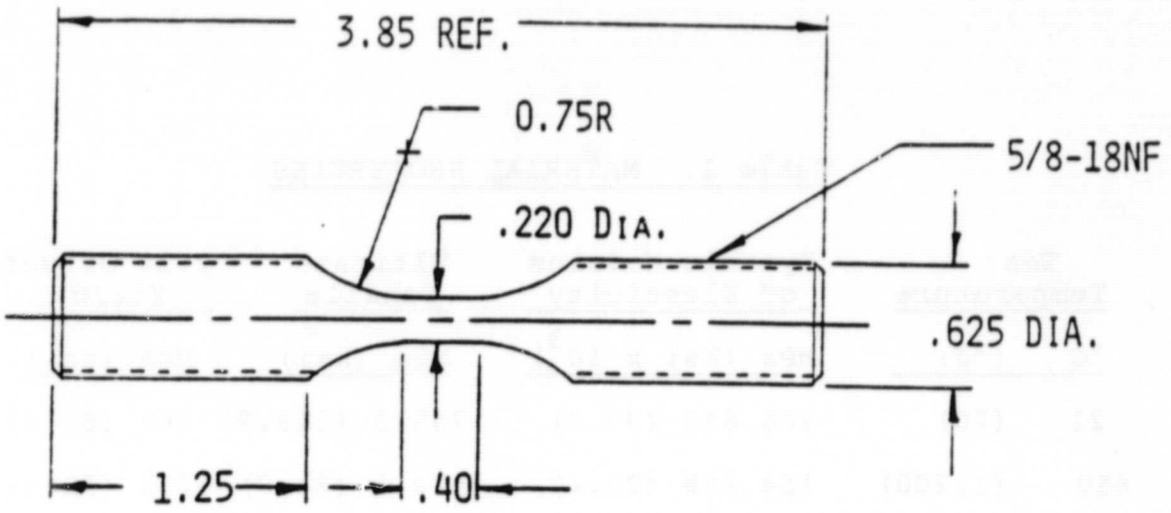

(ALL DIMENSIONS IN INCHES)

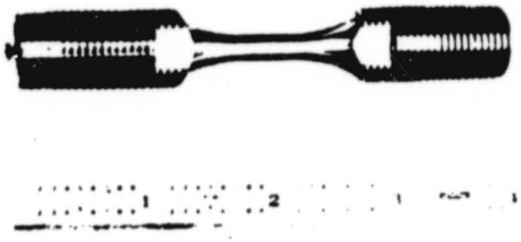

FIGURE 15 SMOOTH AXIAL SPECIMEN

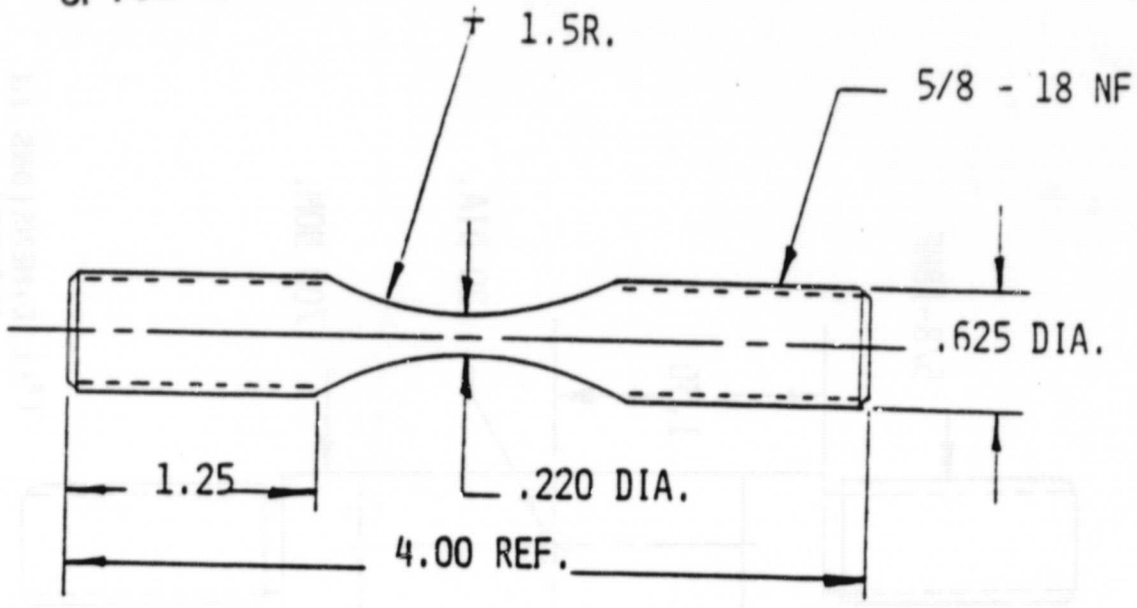

(ALL DIMENSIONS IN INCHES)

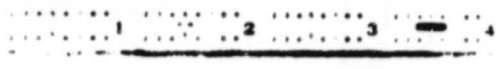

FIGURE 16 HOURGLASS SPECIMEN

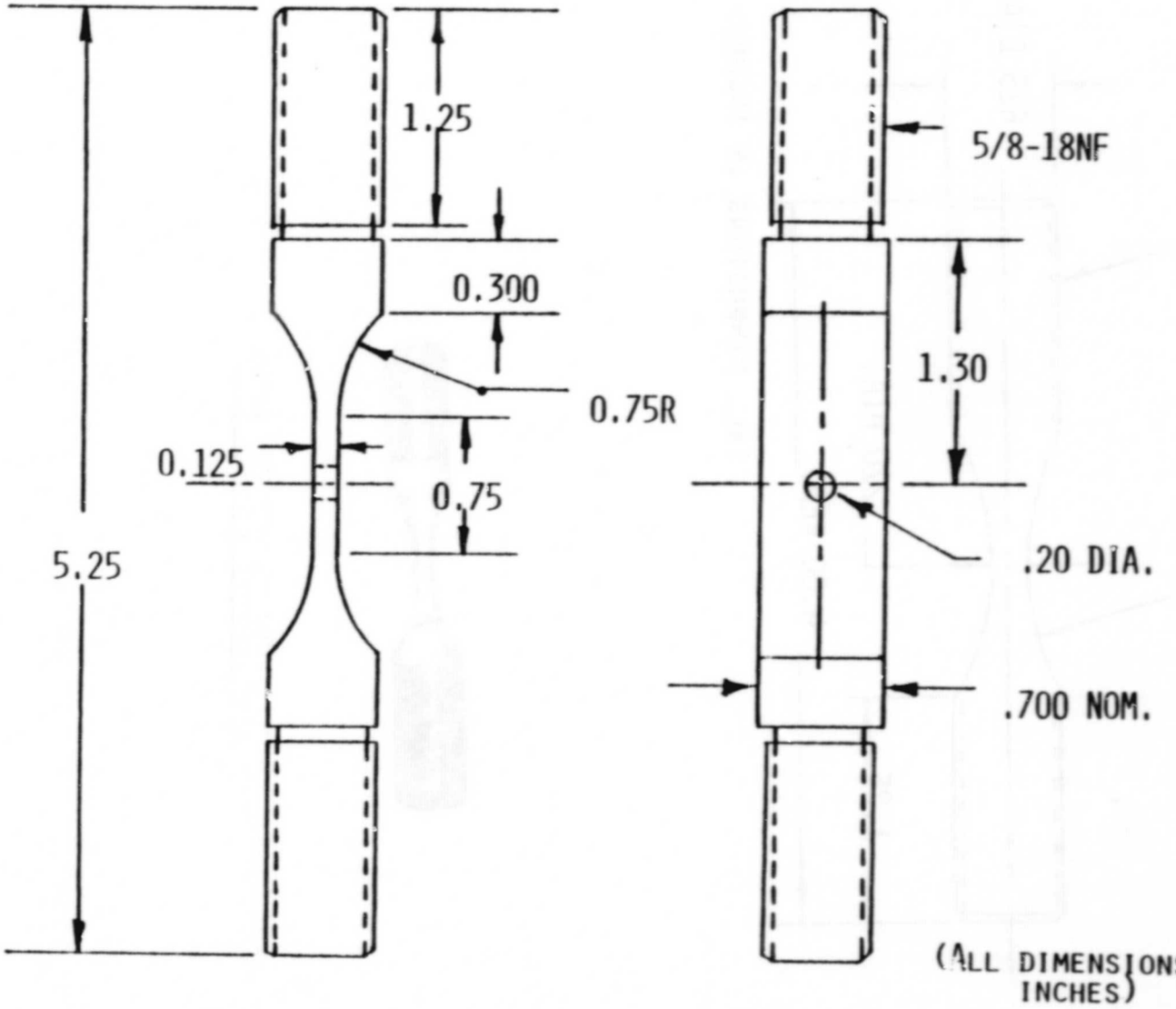

FIGURE 17 NOTCHED SPECIMEN GEOMETRY

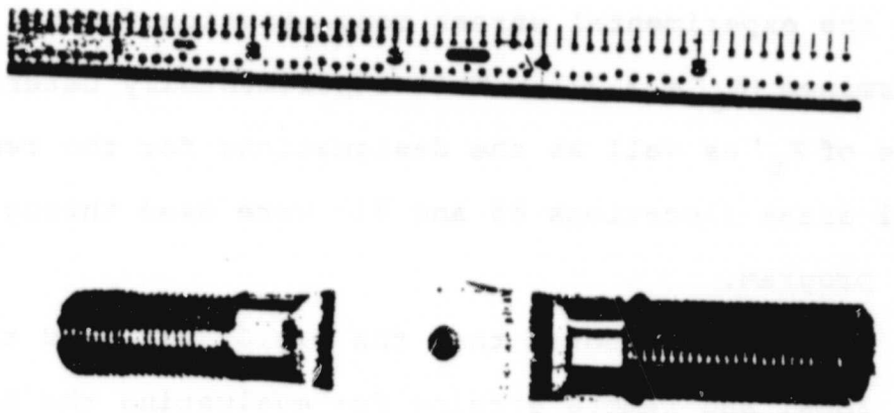

FIGURE 18 NOTCHED SPECIMEN

placed across the width of a notched specimen. Room temperature strain measurements were made at each of these locations while cycling well below the proportional limit. The actual strain data and the calculated strain profile are both shown. By taking the ratio of strains at location #5 and location #1, the strain concentration factor was determined. For elastic strains, the stress and strain concentration factors are equal (21). Using this information the experimental stress concentration factor, K_t', was determined ($K_t' = 2.27$). This experimentally determined value of K_t' as well as the designations for the remote and local areas (locations #5 and #1) were used throughout the test program.

It should be noted that the I.S.G. was used to measure both local and remote strains for evaluating the Neuber equation. Other investigators (5,6) have restricted load levels to insure that the remote region remained linearly elastic. This allowed the remote strain to be calculated by knowing the stress in the net section and the modulus of elasticity. In this experiment, the complications of defining a net section stress were avoided since the remote strain was measured directly. There were also no limitations on plasticity in the remote region. This allowed the Neuber relation to be evaluated over a greater range of loading conditions.

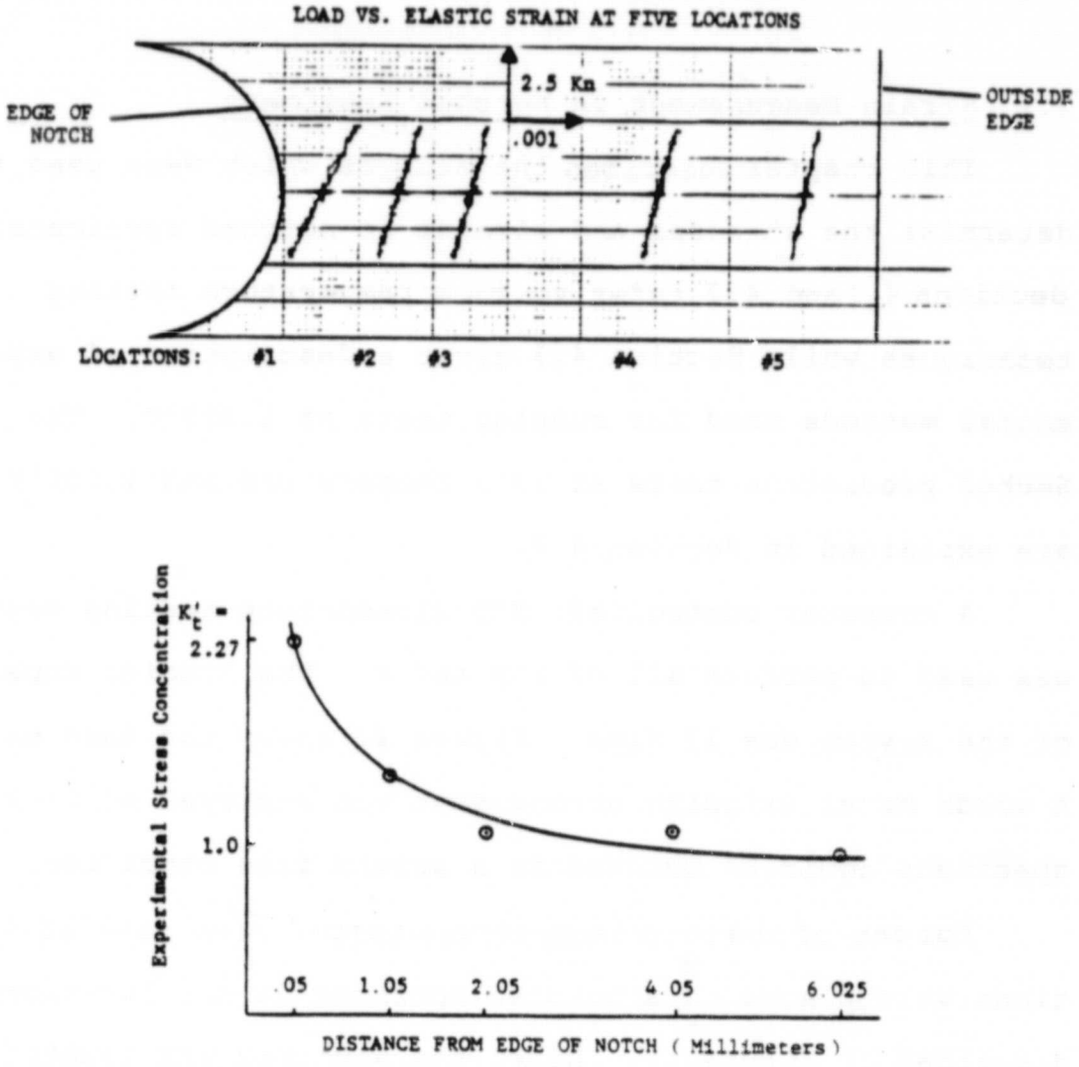

FIGURE 19 DETERMINATION OF STRAIN PROFILE

CHAPTER 4

EXPERIMENTAL METHODS

4.1 Strain Measurement in Notched Specimens

This chapter describes the methods which were used to determine the stresses and strains in notched specimens. Sections 4.1 and 4.2 refer to room temperature testing techniques while Section 4.3 gives a description of experimental methods used for running tests at 1,200°F. The Neuber prediction tests at room temperature and 1,200°F are explained in Section 4.4.

A computer controlled, MTS closed-loop testing machine was used to perform all of the tests. The loading capacity of the system was 12 Kips. Figure 20 shows the test set up. A woods metal gripping arrangement was employed so that specimens could be mounted in a stress free condition.

For one of the room temperature tests, five sets of indentations were placed on a notched specimen at the locations described in Figure 19. After the specimen was mounted, the laser of the I.S.G. was focused on the set of indentations nearest the edge of the notch. Several parameters were then adjusted so that the I.S.G. would function properly. The gain and offset controls for the servo mirrors

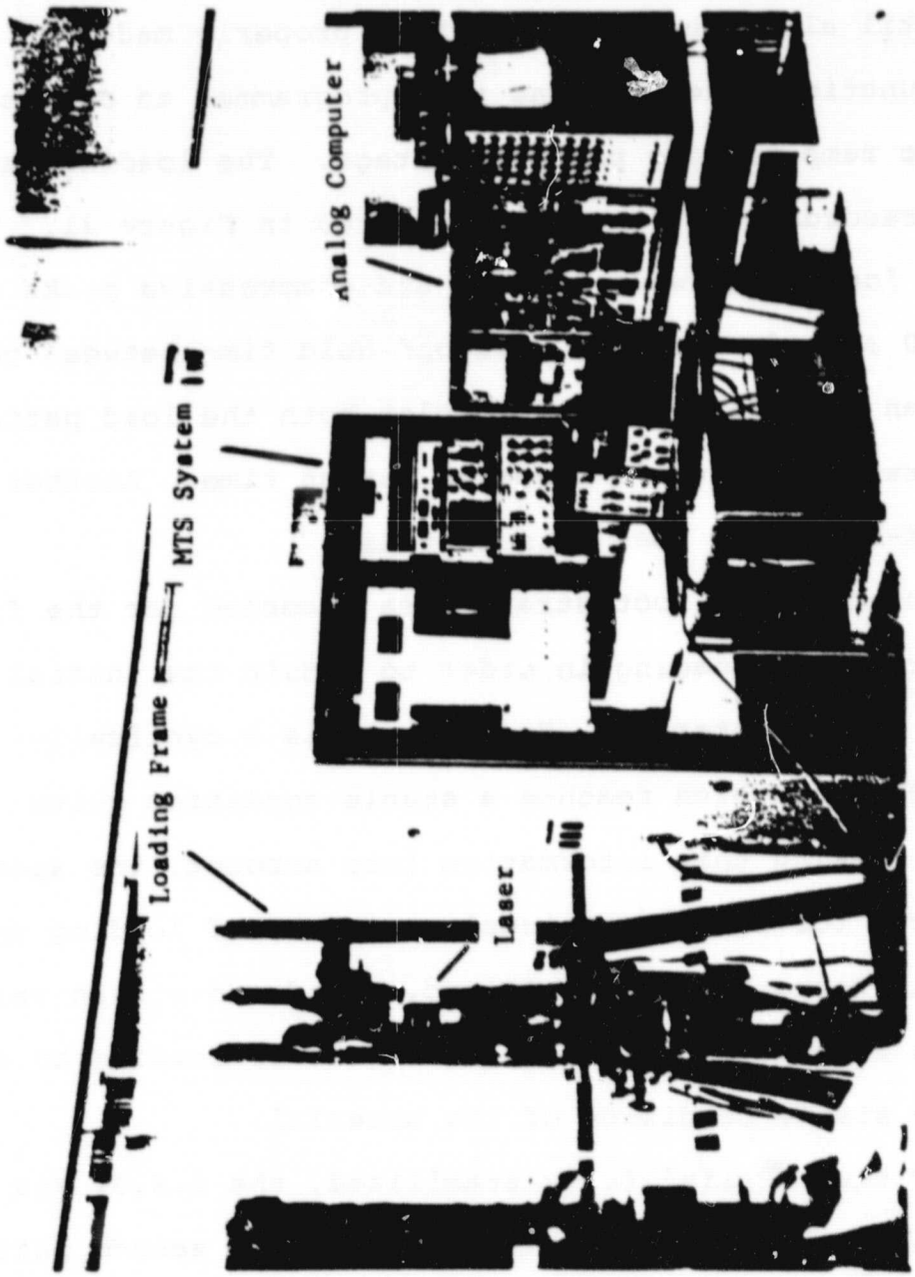

FIGURE 20 TEST SET UP

were set so that the fringe patterns were sweeping symmetrically across the photomultiplier tubes. The electronic analog of the fringe patterns was viewed on an oscilloscope until all adjustments had been properly made.

A function generator was then programmed to output a symmetric ramp loading pattern voltage. The loading pattern and the recording set up is illustrated in Figure 21. The time for loading between tensile and compressive peaks was set at 20 seconds with a 100 second hold time between peaks. A dual pen recorder was used to plot both the load pattern and the resulting strain response versus time. Another plotted X-Y data of load versus strain.

Load and notch root strain were recorded for the first six reversals of loading in order to obtain the initial response of the material. Hastelloy X is a cyclically hardening alloy which reaches a stable condition quite rapidly. Taking this information into account, the specimen was run for fifty additional reversals of loading until the strain response had stabilized. Load and strain values were then recorded for several reversals of loading to describe the stable condition of the material.

With the material fully stabilized, the I.S.G. was focused on the set of indentations which was second farthest from the notch. (See Figure 19 for location #2). Load and strain data were again obtained for several reversals of loading. Similar measurements were performed at locations #3, #4, and #5. At that point, the level of

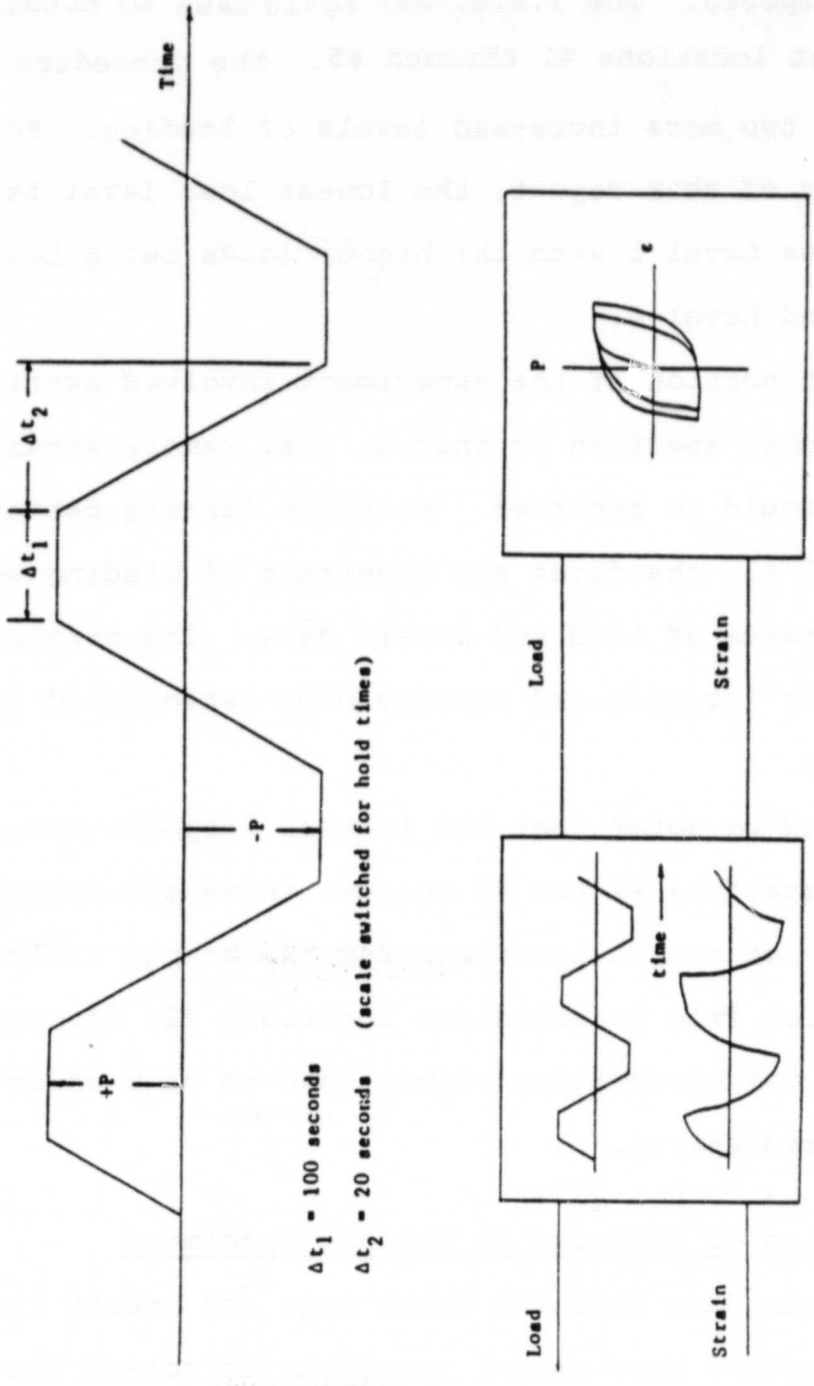

FIGURE 21 LOADING PATTERN AND RECORDING TECHNIQUE

the peaks in the loading pattern was increased. The period of loading remained constant and the 100 second hold times were still imposed. The I.S.G. was again used to obtain strain data at locations #1 through #5. The procedure was repeated for two more increased levels of loading. For the remainder of this report, the lowest load level is referred to as Level 1 with the higher loads being Level 2, Level 3 and Level 4.

The next portion of the experiment involved setting up a new notched specimen so that initial remote strain at location #5 could be recorded. With the loading pattern set for Level #1, the first six reversals of loading were recorded in terms of load and strain data. The stable behavior at this location had already been established in the previous test.

It should be noted that the initial response was recorded for locations #1 and #5 because these are defined as the local and remote locations for the Neuber analysis. The information from intermediate locations #2, #3, and #4 was recorded for observation rather than to be used in the Neuber predictions.

4.2 Simulation of Stresses in Notched Specimens

The strain data from the notch root and remote locations were imposed upon smooth specimens to obtain the stresses. This was the only practical method known for extracting stress information at a notch.

A smooth specimen was set up under strain control with a 0.3 in. gage length extensometer attached. A graph showing the previously obtained strain versus time data at the notch (location #1) was placed on the dual-pen recorder. The strain voltage from the extensometer was fed into the recorder.

As the pen swept across the graph, the operator was required to manually control the test system so that the strain level would exactly duplicate the original I.S.G. data. During this time the stress data were plotted on the other channel of the dual-pen recorder. Stress versus strain plots were also recorded. This method of simulating stresses proved to be very satisfactory from an experimental viewpoint. All parameters such as strain rate, creep, and total strain were reproduced in the smooth specimen as they occurred in the notched plate. The X-Y plots of notch root stress versus strain were considered direct experimental data to which the Neuber predictions could later be compared.

To characterize the overall behavior (and for the eventual Neuber prediction) the remote stresses in the notched member were also determined. To accomplish this, the above procedure was repeated on another smooth specimen using the remote strain plots. Therefore, the stress-strain behavior of a notched specimen had been established for the initial response at Load Level #1 and the stable condition at Load Levels 1 through 4.

4.3 Elevated Temperature Tests

A set of tests similar to those described in Sections 4.1 and 4.2 were conducted at 1,200°F so that Neuber's rule could be evaluated under more adverse circumstances. There were several reasons for choosing this temperature. Although the I.S.G. had produced strain measurements at temperatures up to 1,500°F, the data usually became distorted after a short time. This was due to a breakdown of the Gold-Palladium coating which caused a loss of reflective ability. At 1,200°F the I.S.G. would respond more consistantly for a long period of time. This was important since the loading scheme was lengthy and involved 100 second hold times. Hastelloy X also began to experience time dependent effects at 1,200°F.

The philosophy behind the room temperature and the high temperature experiments was essentially the same. However, the preparation and testing techniques used at high temperature were more complex. After a notched specimen was indented and coated with Gold-Palladium, it had to be carefully mounted so that the induction heating coils would not disrupt the reflected fringe patterns. The specimen was then brought up to temperature using a 5KW induction heater. A chromel-alumel type thermocouple spot welded to the reverse side of the specimen provided temperature feedback (see Figure 22). Cooling coils both above and below the specimen were used to isolate the heat from the load cell and the woods metal pot. The loading

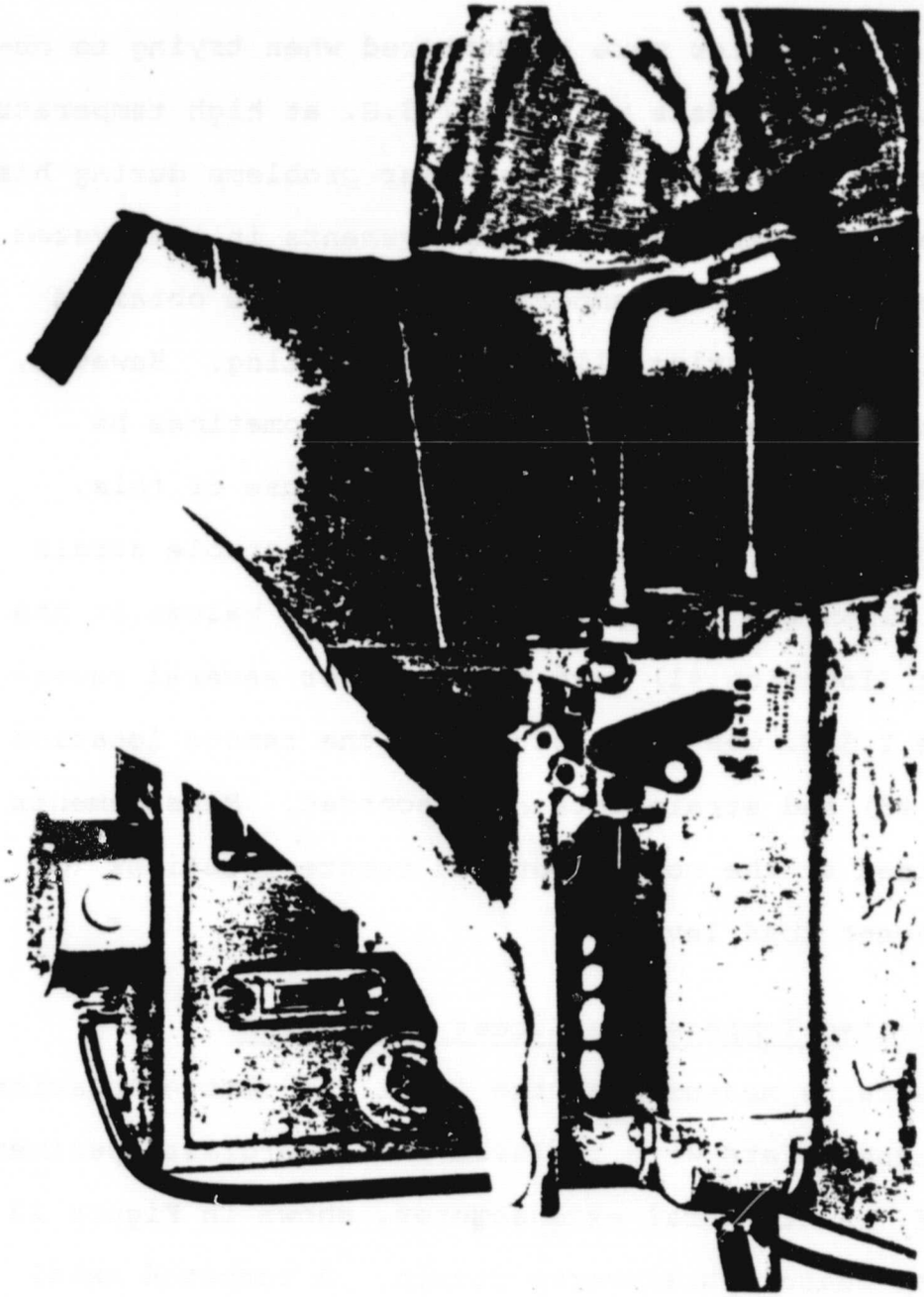

FIGURE 22 SPOTWELDING THERMOCOUPLE TO SPECIMEN

pattern was similar to the one shown in Figure 21. The tensile and compressive peaks were lower than those used at room temperature to allow for the larger amounts of strain at 1,200°F.

Some difficulties were encountered when trying to obtain initial cyclic data with the I.S.G. at high temperature. Bofferding (5) had experienced similar problems during his room temperature experiments. Improvements in the system have since allowed room temperature data to be obtained very consistantly during all phases of testing. However, at elevated temperatures the I.S.G. must sometimes be readjusted after the test has begun. Because of this, the specimen was cycled until it exhibited stable strain response. Then the load pattern and strain values at the notch root (location #1) were recorded for several reversals. The I.S.G. was next focused on the remote location (location #5) and strain data were recorded. Measurements were obtained at the notch root and remote locations for four different load levels.

4.3.1 Elevated Temperature Stress Simulation

The strains measured at the local and remote locations in the notched plate were replayed onto hourglass specimens at 1,200°F. A diametral extensometer, shown in Figure 23 was used to measure transverse strain. A computed axial strain was obtained by combining the load and transverse

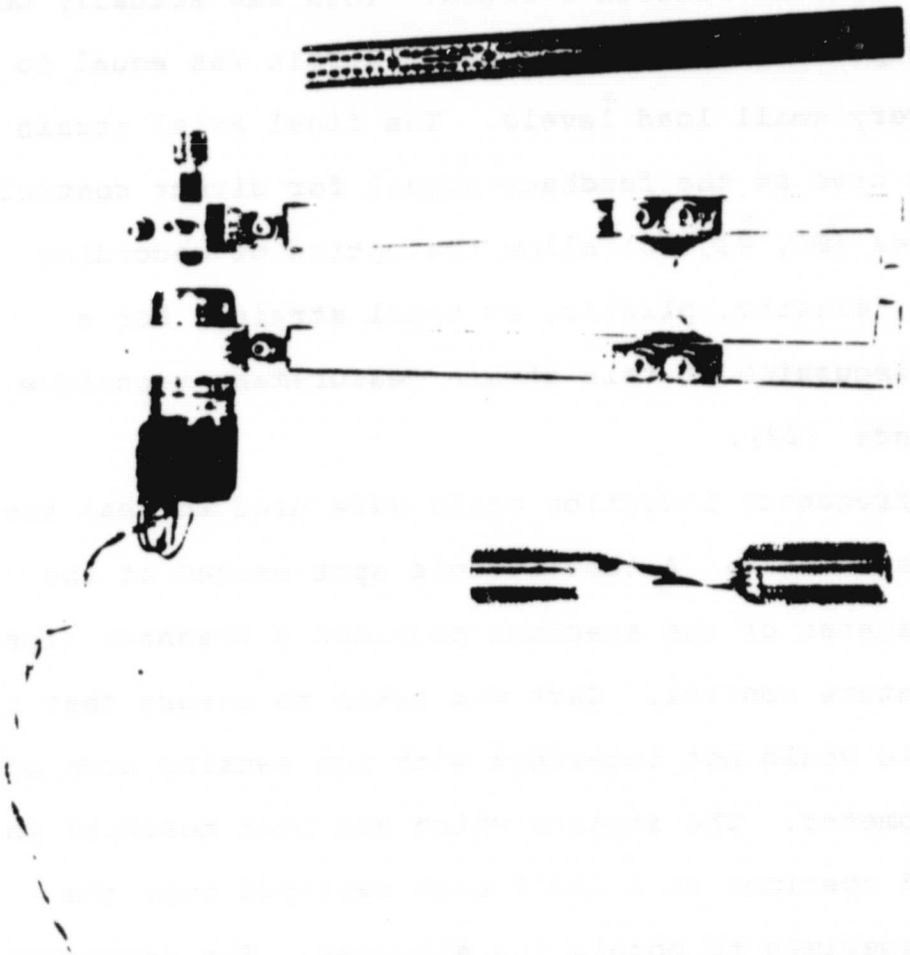

FIGURE 23 DIAMETRAL EXTENSOMETER AND HOURGLASS SPECIMEN

strain voltages in an analog computer circuit. A schematic diagram of the circuit is shown in Figure 24.

The proper output voltage representing total strain was obtained by adjusting three potentiometers. Pot #00 was set so that the transverse strain was increased by a factor of two. Pot #01 was used to dial in the elastic strain voltage, knowing the applied stress and the modulus of elasticity. The last step involved setting pot #02 to obtain the elastic Poisson's ratio. This was actually done by turning pot #02 until the plastic strain was equal to zero for very small load levels. The final axial strain output was used as the feedback signal for direct control. The switches (S1, S2, S3) allow the option of recording transverse, elastic, plastic, or total strain. For a detailed discussion of this strain measurement technique, see Reference (22).

High frequency induction coils were used to heat the hourglass specimens. A thermocouple spot welded at the minimum diameter of the specimen provided a feedback signal for temperature control. Care was taken to insure that the thermocouple would not interfere with the sensing arms of the extensometer. The strains which had been measured in the notched specimen at 1,200°F were replayed onto the hourglass specimen to obtain the stresses. The techniques were the same as those for the room temperature simulation explained in Section 4.2.

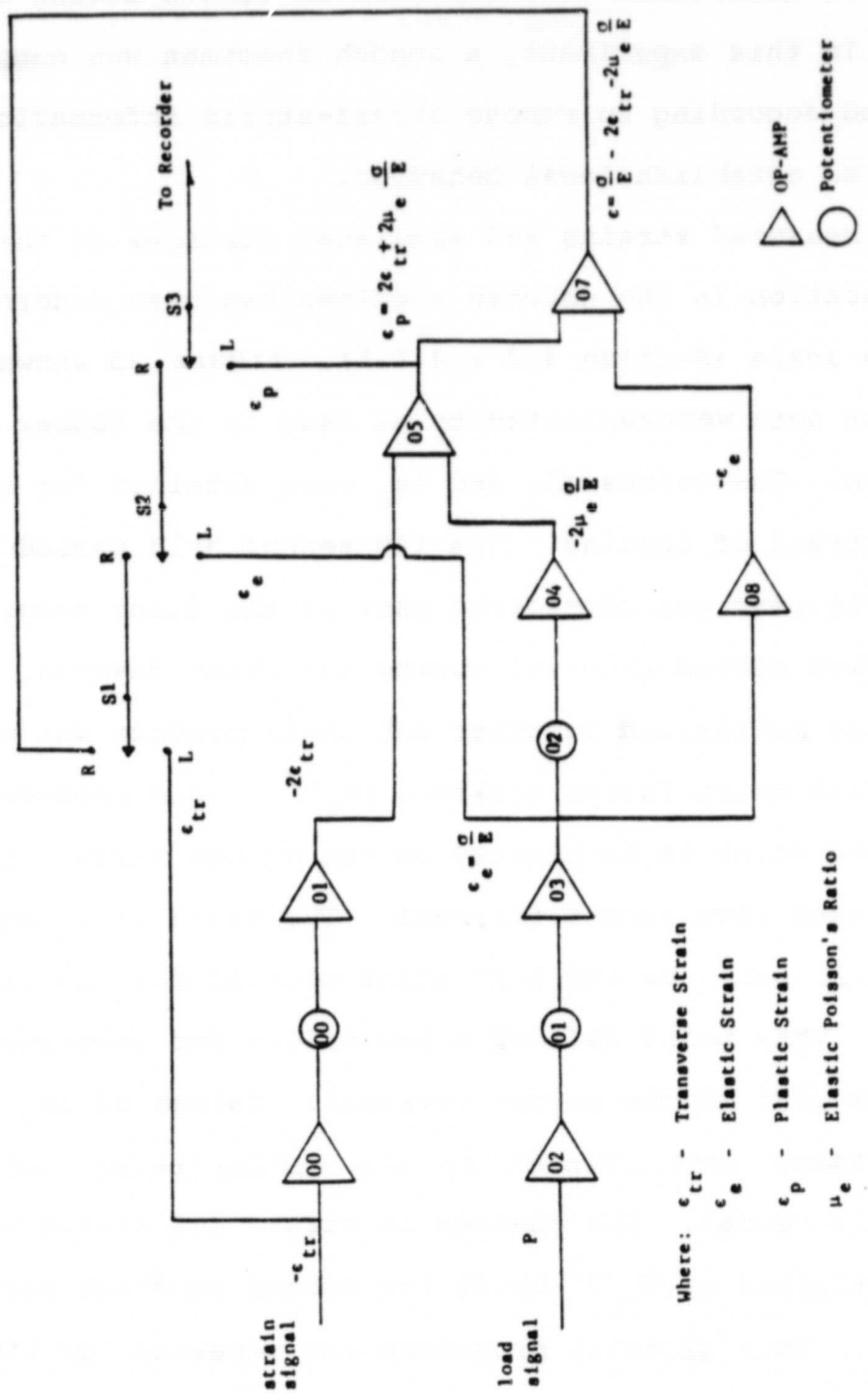

FIGURE 24 ANALOG CIRCUIT FOR TRANSVERSE TO AXIAL STRAIN CONVERSION

4.4 Neuber Prediction of Notch Root Behavior

The Neuber equation allows local behavior in a notched plate to be determined as a function of remote stress and strain. In this experiment, a smooth specimen was manually controlled according to remote stress-strain information in order to establish local behavior.

The measured strains and simulated stresses at the remote location in the notched specimen had been recorded on a time scale (Section 4.2 & 4.3.1). Figure 25 shows how the remote data were replotted to be used in the Neuber prediction. The values ΔS_1 and Δe_1 were obtained for the first reversal of loading. (The 100 second hold period at the tensile peak was considered part of the first reversal.) At each five second interval during the first reversal, ΔS and Δe were multiplied together and their product was multiplied by the notch factor squared, $(K_t')^2$. This procedure allowed one point to be plotted on the Neuber versus time graph at each five second interval. The value of C_1 shown in Figure 25 would be the last point plotted for the first reversal. This point defined a new origin for constructing the Neuber plot of the second reversal. Values of ΔS_2 and Δe_2 were taken with respect to the ending point of the first reversal The changes in stress and strain were again multiplied by $(K_t')^2$ until the second reversal was completed. This plotting procedure was repeated for every subsequent reversal. The Neuber versus time plot was then

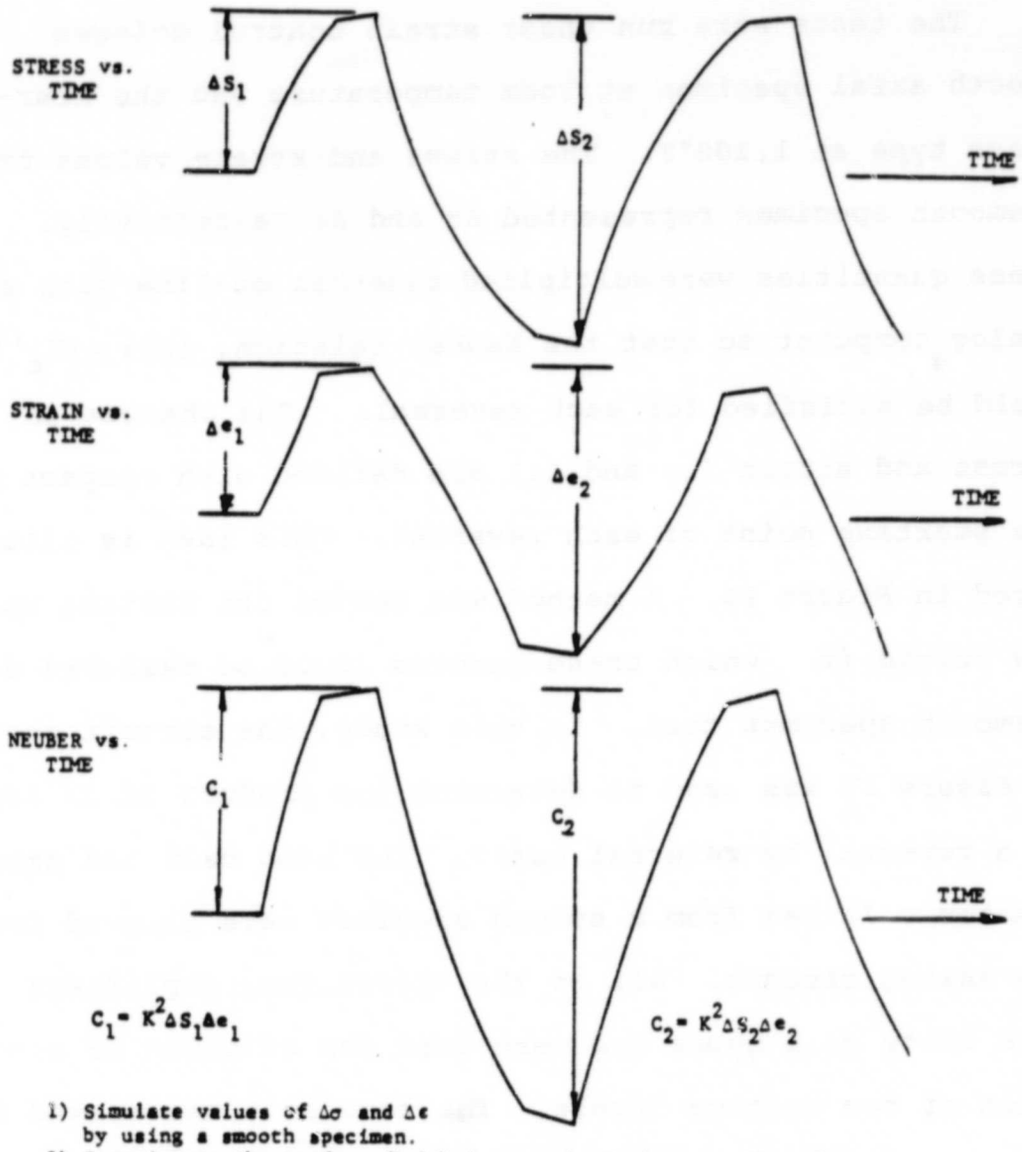

1) Simulate values of $\Delta\sigma$ and $\Delta\epsilon$ by using a smooth specimen.
2) Superimpose the product $(\Delta\sigma)(\Delta\epsilon)$ onto the Neuber vs. Time plot.

FIGURE 25 CONSTRUCTION OF NEUBER VERSUS TIME GRAPH

placed on a recorder so that the product of stress and strain from a smooth specimen could be replayed upon it. This process will now be explained in more detail.

The tests were run under strain control using a smooth axial specimen at room temperature and the hour-glass type at 1,200°F. The stress and strain values from a smooth specimen represented $\Delta\sigma$ and $\Delta\varepsilon$ respectively. These quantities were multiplied together on-line with an analog computer so that the Neuber relation, $\Delta\sigma\Delta\varepsilon = (K_t')^2 \Delta S\Delta e$ could be satisfied for each reversal. The changes in stress and strain ($\Delta\sigma$ and $\Delta\varepsilon$) are defined with respect to the starting point of each reversal. This idea is illustrated in Figure 26. A method was needed for setting up a new origin from which these changes could be measured during a smooth specimen test. In this study, the circuit shown in Figure 27 was used to determine the product of $\Delta\sigma$ and $\Delta\varepsilon$ on a reversal by reversal basis. The load cell and extensometer voltages from a smooth specimen were plugged into the analog circuit. All of the operational amplifiers were unity gain types and were used for addition or subtraction of two voltage levels. The four switches marked S2 could be thrown simultaneously to either the right (R) or left (L) as could the two switches marked S1. With switches S1 thrown to the left, the circuit was in the calibration mode. Reference voltages were set by turning pots #01 and #02 to calibrate the multiplier. After the calibration was

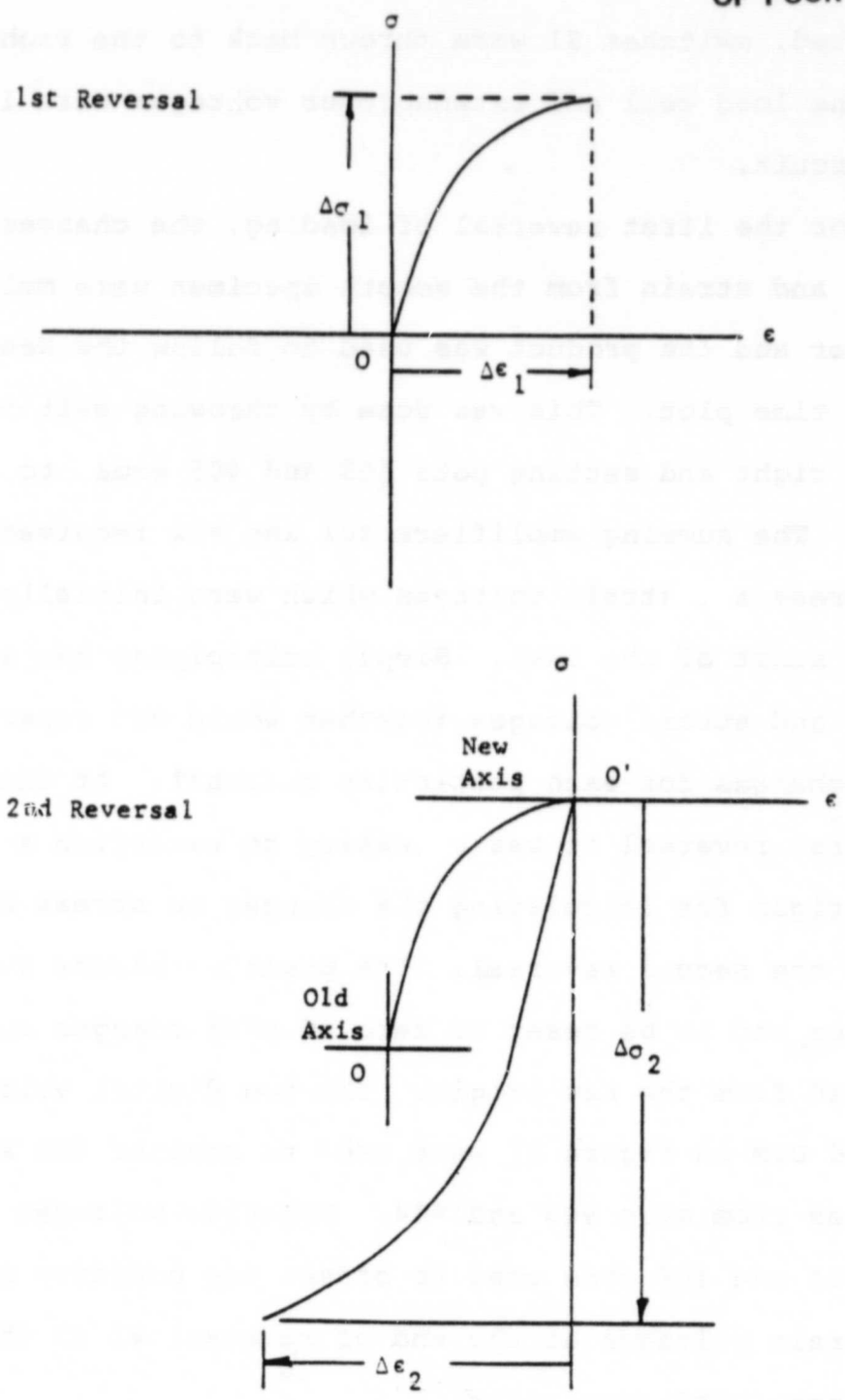

FIGURE 26 THE NEUBER RELATION IS DEFINED FOE EACH SEPERATE REVERSAL

completed, switches S1 were thrown back to the right so that the load cell and extensometer voltages were input to the circuit.

For the first reversal of loading, the changes in stress and strain from the smooth specimen were multiplied together and the product was used to follow the Neuber versus time plot. This was done by throwing switches S2 to the right and setting pots #03 and #05 equal to zero volts. The summing amplifiers #01 and #02 received only the stress and strain voltages which were initially zero at the start of the test. Simply multiplying the actual stress and strain voltages together would not separate their changes for each particular reversal. At the end of the first reversal it was necessary to establish a new voltage origin for calculating the changes in stress and strain during the second reversal. The positive stress and strain voltages had to be reset to zero so that changes could be measured from the new origin. The two digital voltmeters labeled DVM in Figure 27 were used to monitor the sum of voltages from amps #03 and #04. Negative voltages from pots #04 and #06 were used to offset the positive stress and strain voltages at the end of reversal #1 so that the DVM's both read zero volts.

To execute the second reversal, switches S2 were thrown to the left. The negative voltages which had been set by pots #04 and #06 were now being subtracted from the

stress and strain voltages in amps #01 and #02. Therefore, both inputs to the multiplier were zero volts. The changes in stress and strain for the second reversal would be defined in terms of this starting point. Upon completion of the second reversal another new origin was required. Positive voltages from pots #03 and #05 were set to exactly cancel the negative load and strain values as monitored on the DVM's. Switches S2 were then thrown back to the right and the voltage outputs from amps #01 and #02 were again zero. The third reversal was then executed. This procedure was repeated until all of the reversals on the Neuber versus time plot had been retraced.

This technique proved to be a very basic solution to the problem of electronically simulating the Neuber plots. The method of superimposing current test data onto previously obtained plots was the key element throughout this experiment. The interesting point was that the researcher became 'part' of the closed loop by having to manually control the system. The fact that this method allowed information to be replayed with respect to time was very important. It meant that time dependent parameters such as creep and relaxation could be exactly reproduced in smooth specimens.

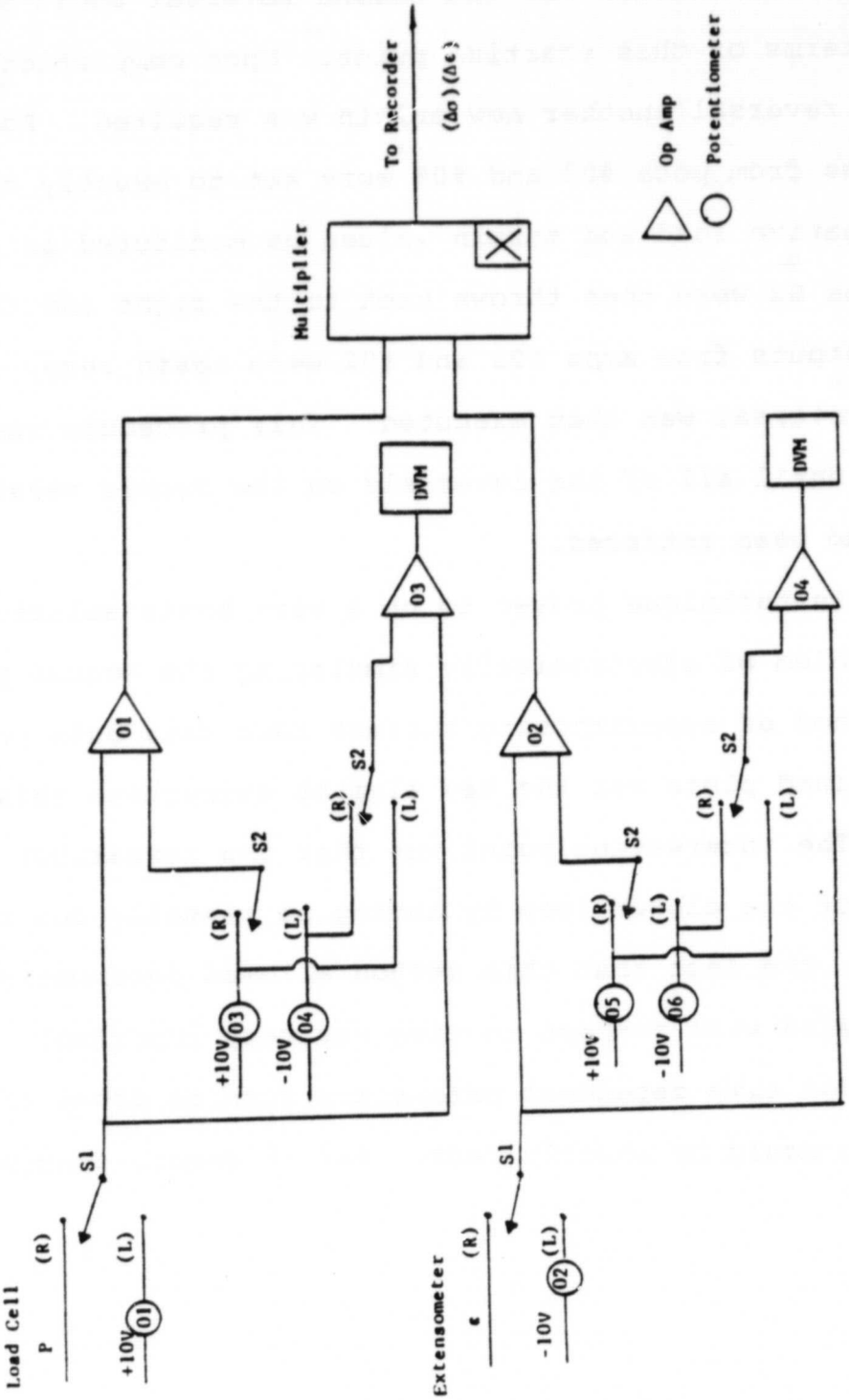

FIGURE 27 ANALOG CIRCUIT FOR NEUBER PREDICTION

CHAPTER 5

EXPERIMENTAL RESULTS AND DISCUSSION

5.1 Room Temperature I.S.G. Measurements

The results are presented in a chronological sequence leading up to a comparison of notch root behavior obtained by two methods: 1) direct strain measurement and stress simulation and 2) Neuber prediction. This chapter contains a large amount of actual data since the experiments were qualitative in many respects.

Figure 28 shows I.S.G. measurements of strain vs. applied load for a notched specimen during the first three cycles of loading. The strain and load data were also plotted on a time scale in Figure 29. The initial loading pattern consisted of constant amplitude completely reversed loading between $\pm$ 14 KN.

The most noticeable effects in notch root behavior were caused by cyclic hardening. The tensile peaks showed a large decrease in strain for each successive cycle due to strain hardening. The compressive strains experienced much less variation during the three cycle period. As a result, an initially tensile mean strain was shifted in the compressive direction. Creep effects were also present in

these room temperature data. This is shown more clearly in the time plot of local strain (Figure 29). The largest amount of creep took place during the first 100 second hold time and then diminished with each successive reversal. It should be noted that the time scale was manually switched from 5 sec/cm to 50 sec/cm for the hold periods.

For remote behavior, cyclic hardening again caused the total strain to decrease for each plotted loop. The effects of creep were minimal for the remote location. The amount of creep at both locations in the specimen decreased as the material stabilized.

When a sufficient number of cycles had been applied to stabilize the material, the I.S.G. was used to record data at four different cyclic load levels which are listed:

Level #	Load (Kn)
1	$\pm$ 14.0
2	$\pm$ 14.5
3	$\pm$ 15.5
4	$\pm$ 16.0

Strain measurements were obtained at each of five locations across the notched specimen (locations were defined in Chapter 3). Figures 30 through 33 each show results for a different load level. (These plots should be viewed without reference to a strain origin since the I.S.G. had to be repositioned for each location.) These figures illustrate the effects of cyclic loading at various distances from the notch. The amount of plastic strain diminished significantly

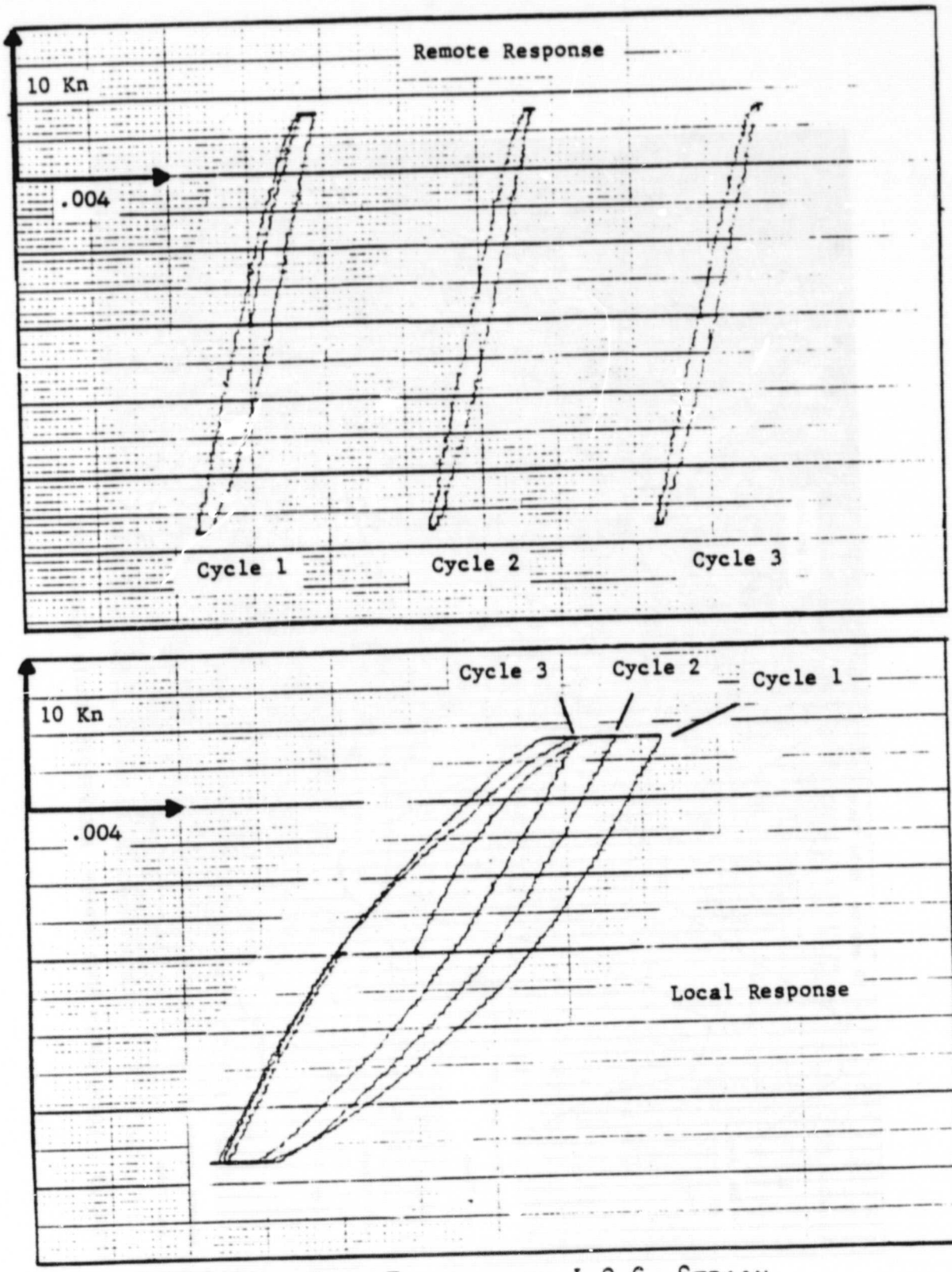

FIGURE 28 ROOM TEMPERATURE I.S.G. STRAIN VERSUS LOAD

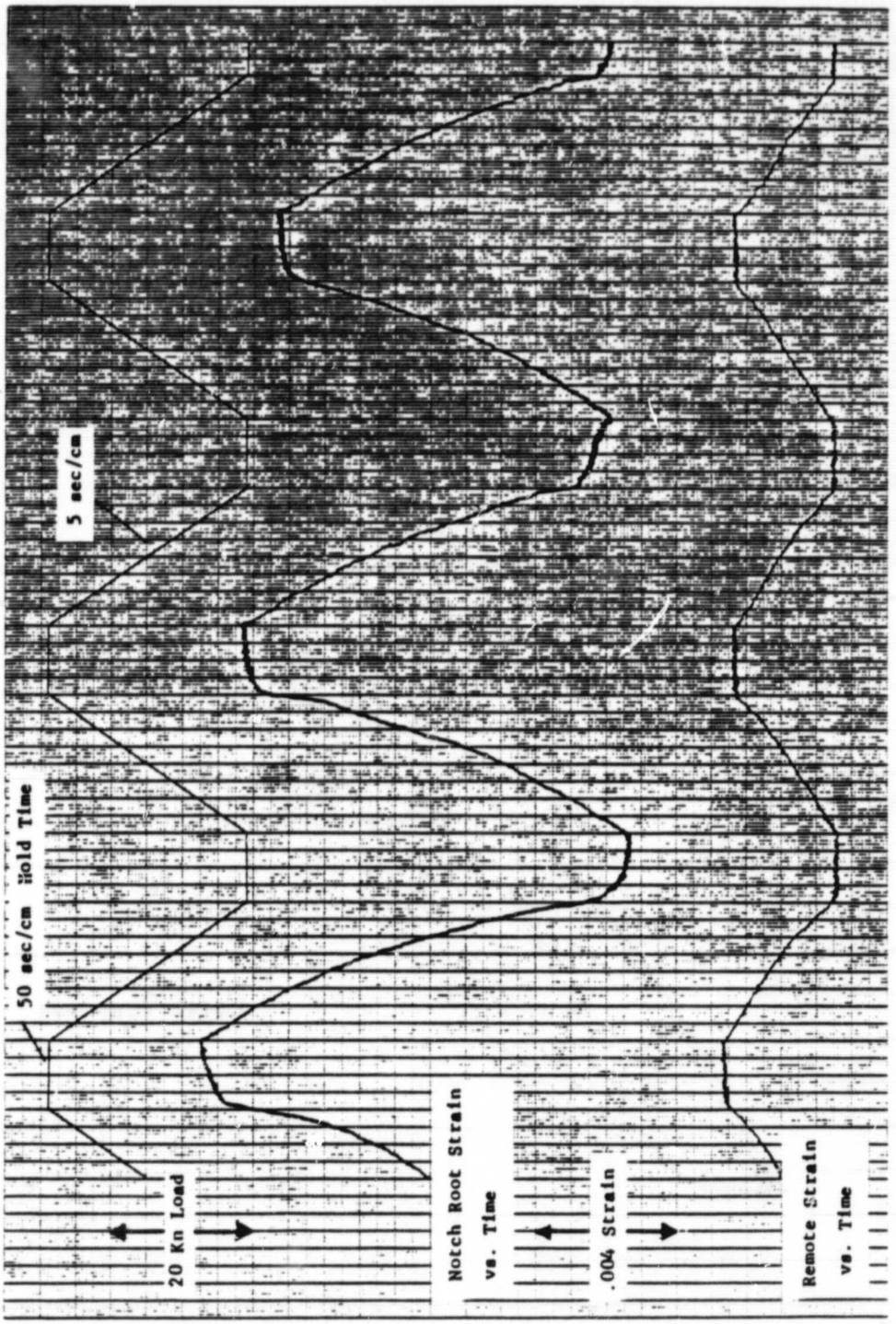

FIGURE 29 LOAD, NOTCH ROOT STRAIN, AND REMOTE STRAIN VERSUS TIME

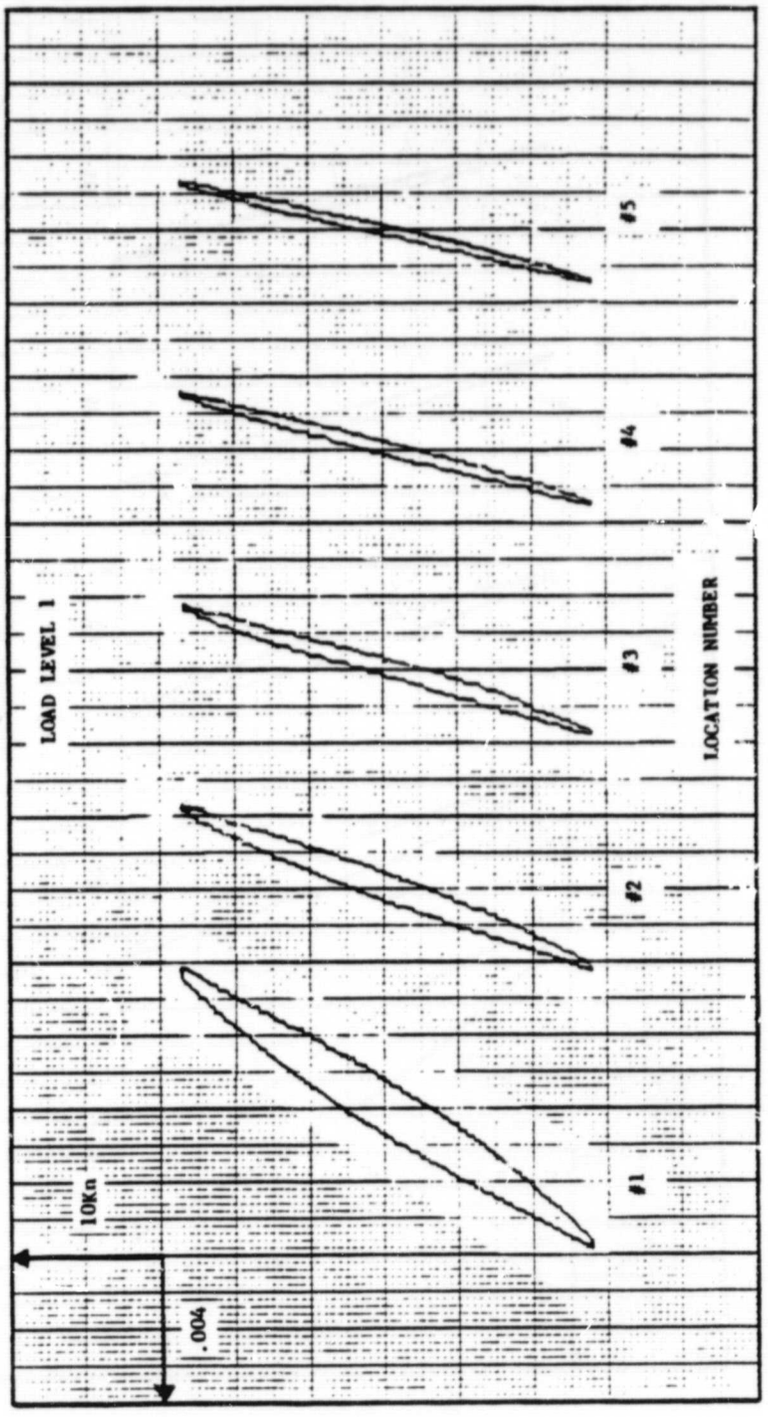

FIGURE 30 LOAD LEVEL 1 VERSUS STRAIN ACROSS NOTCHED SPECIMEN

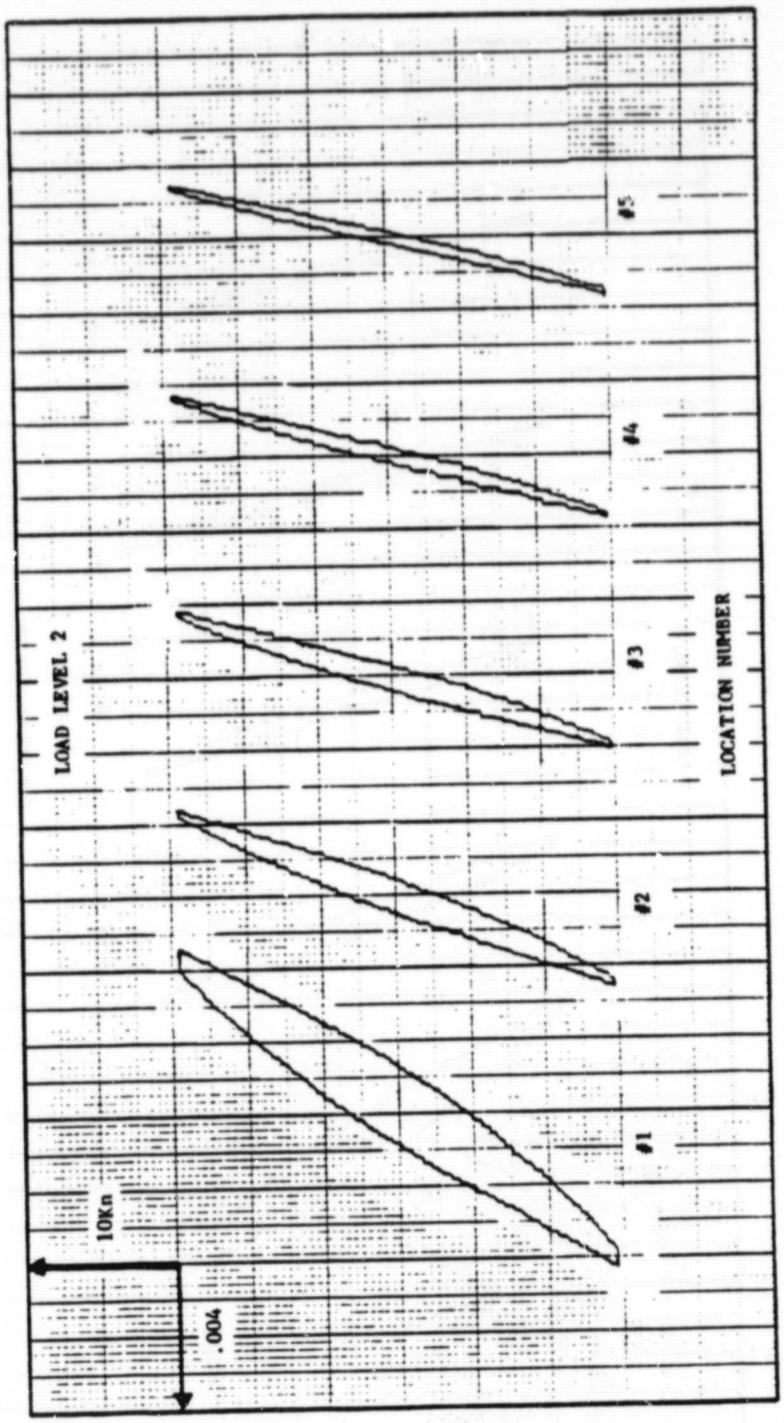

FIGURE 31 LOAD LEVEL 2 VERSUS STRAIN ACROSS NOTCHED SPECIMEN

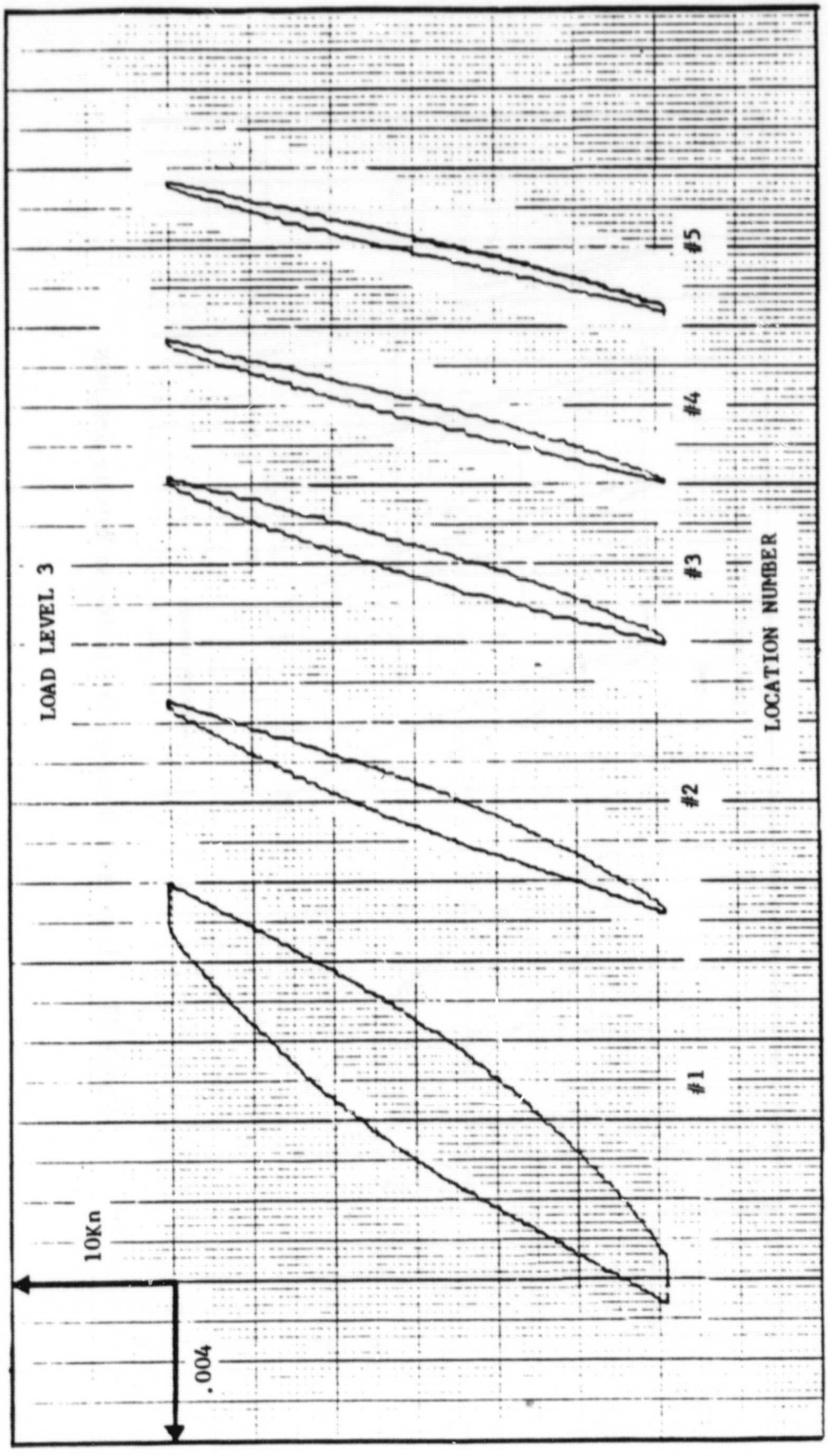

FIGURE 32 LOAD LEVEL 3 VERSUS STRAIN ACROSS NOTCHED SPECIMEN

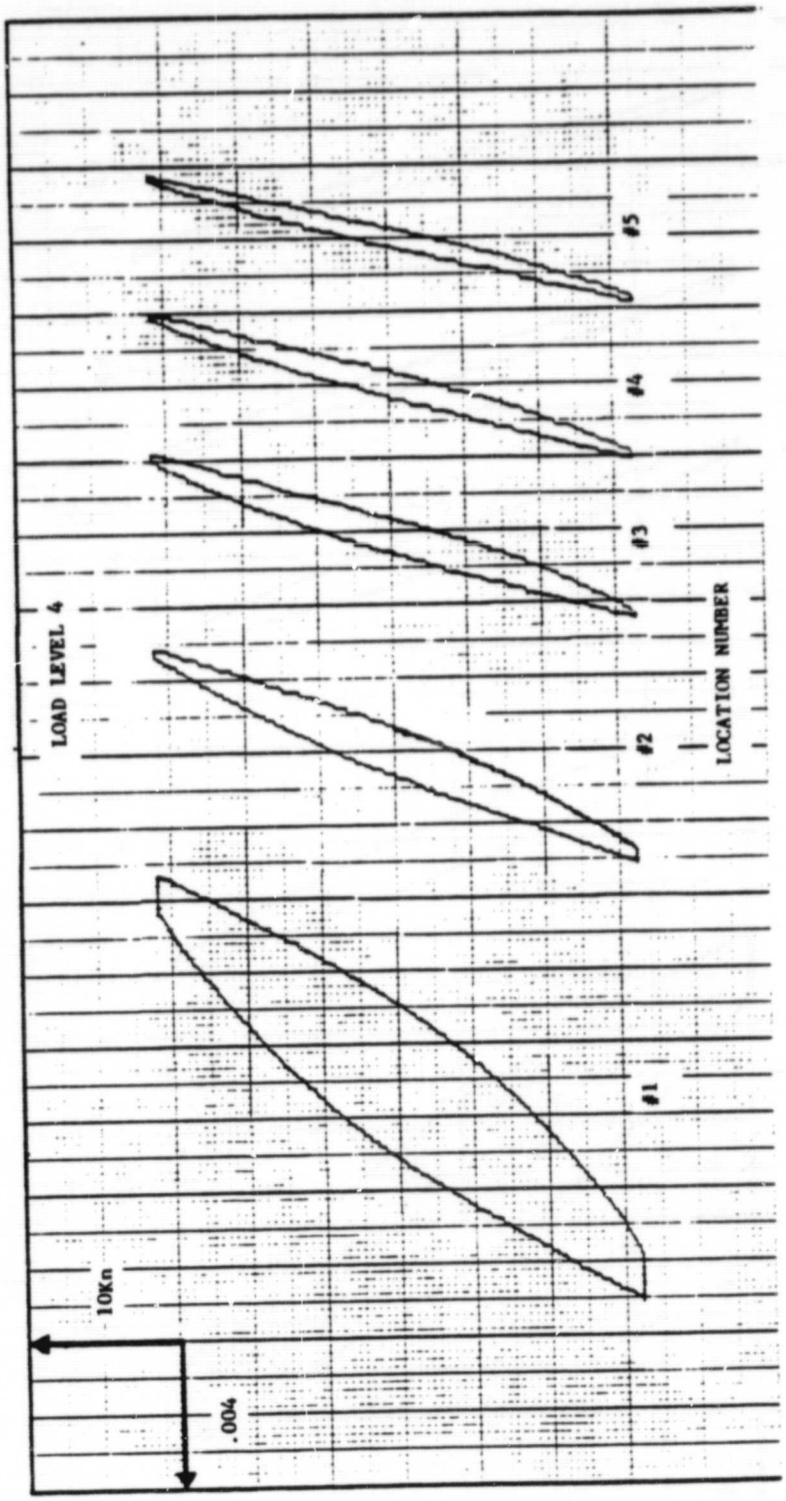

FIGURE 33 LOAD LEVEL 4 VERSUS STRAIN ACROSS NOTCHED SPECIMEN

as the distance from the notch increased. Also, when the load was raised from Level 1 to Level 4, the strain at the remote location (#5) increased by 21% while the local strain (#1) experienced a 50% increase. This gives an indication of the strain concentration near the notch.

5.2 Room Temperature Stress Simulation

These results were obtained by replaying the strain histories shown in Section 5.1 onto smooth specimens. Time plots of strain which had been measured with the I.S.G. were placed on a dual-pen recorder. As the pen moved across the recorder, the strain signal from a smooth specimen was controlled so that the original I.S.G.-measured strain plot would be retraced. The resulting stresses were plotted on the same recorder. This procedure was used to determine the stresses at the local and remote locations for both initial and stable behavior. The hysteresis loops for the first three cycles are shown in Figure 34.

Since these tests were run under strain control, stress was the independent variable and would increase if strain hardening occured. This effect is shown clearly for initial notch root data. There is an interesting relationship between the decrease in strain range and the increase in stress, both caused by cyclic hardening. The decrease in strain was experienced while cycling between constant load limits when I.S.G. measurements were recorded. The increase in stress peaks during the simulation was due to material

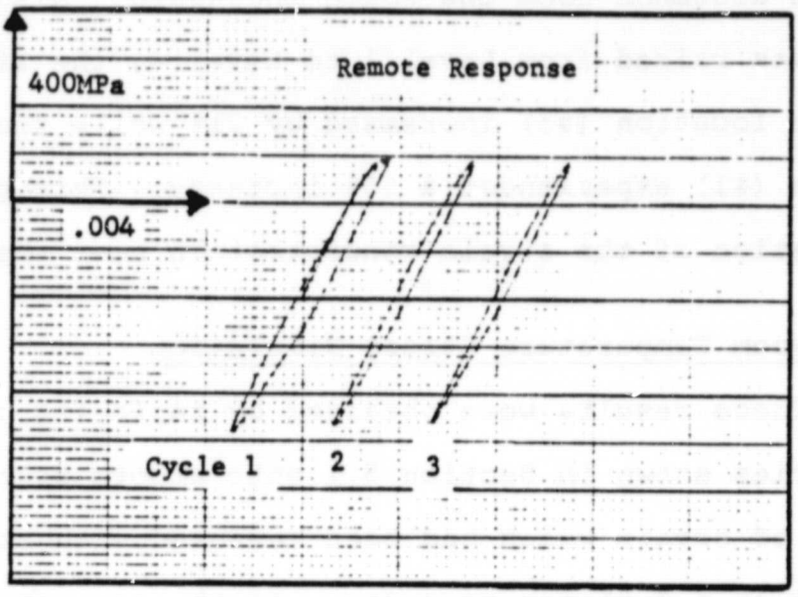

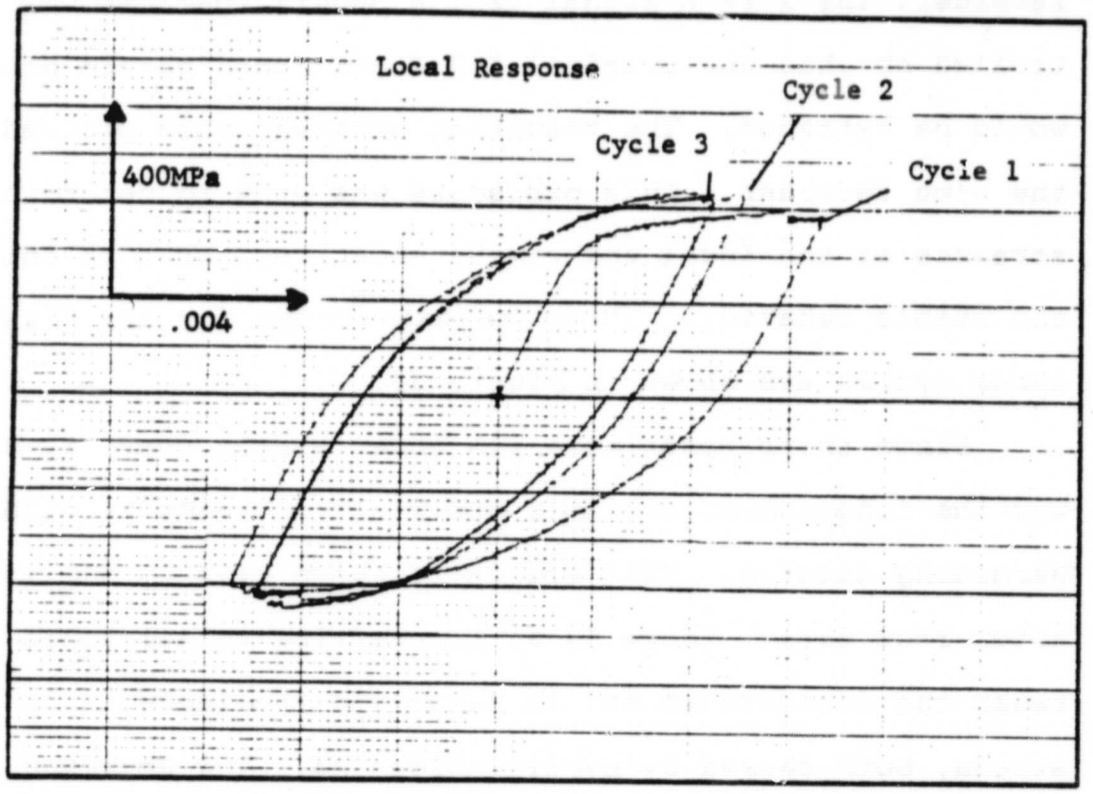

FIGURE 34 SMOOTH SPECIMEN SIMULATION OF INITIAL STRESSES

properties. The fact that the stress and strain have this upward and downward trend is not surprising. It is difficult, however, to separate the various factors which determine whether the stress or the strain is the more dominant characteristic. This study was more concerned with trying to duplicate this behavior than in trying to explain these interactions.

The remote location exhibited a small amount of strain hardening during the first three cycles. Figure 35 shows the remote strain and simulated stress on a time scale. The strain values in this Figure were replayed onto a smooth specimen to determine the stresses. The remote stress and strain information was used to conduct the Neuber prediction of notch root behavior as explained in Section 4.4.

The stable data are plotted in Figure 36 at each of four load levels. (Load levels refer to those used during I.S.G. measurements from Section 5.1.) The data for Level 1 show that the amount of plastic strain had decreased from the initial values in Figure 34. The hysteresis loops for the other three levels simply show increased stress and plastic strain at each location. Time plots of stress and strain for stable local response are shown in Figure 37 for Levels 3 and 4. Note the difference in the rate of increase between the stress and strain values.

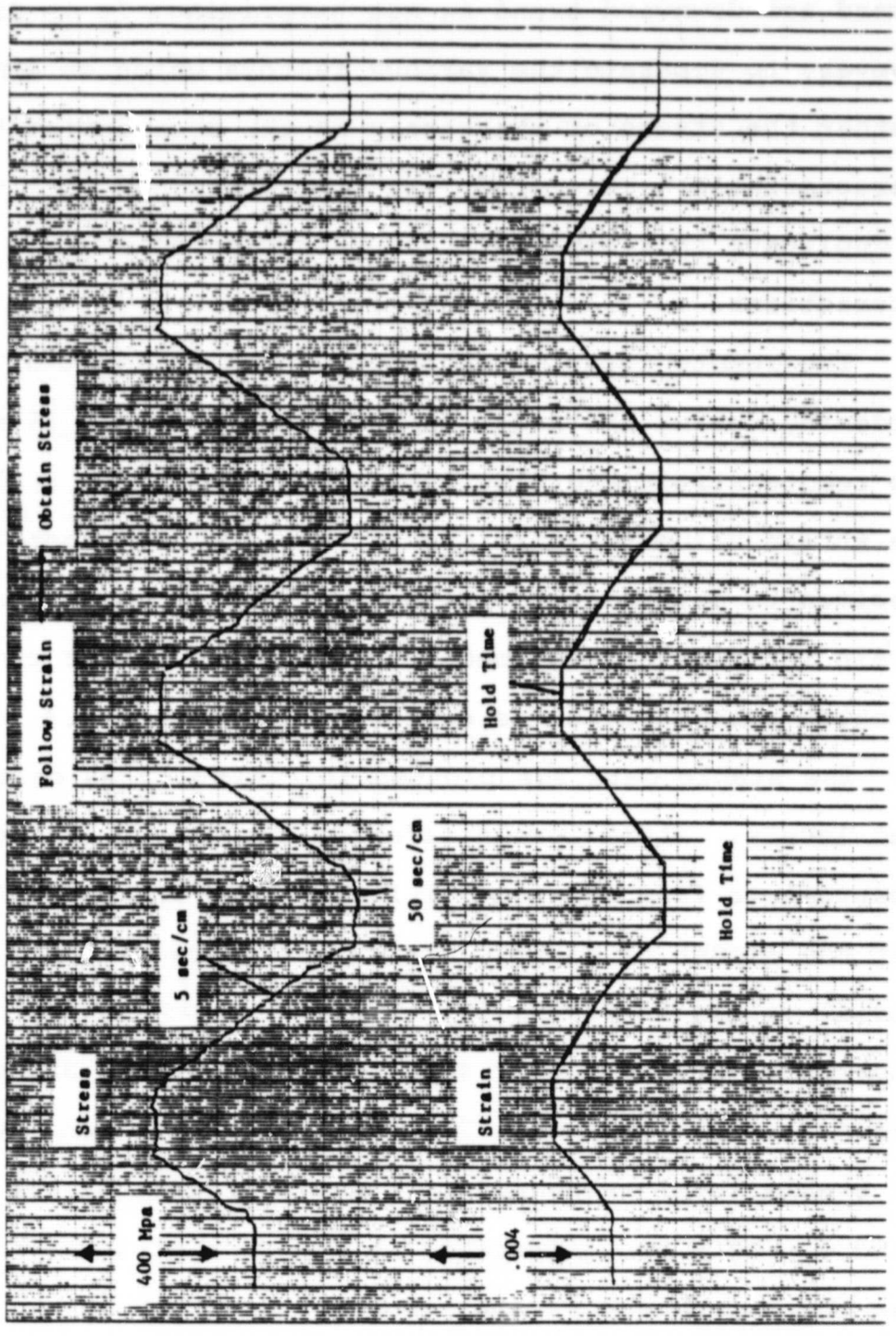

FIGURE 35 STRAIN AND SIMULATED STRESS FOR REMOTE REGION

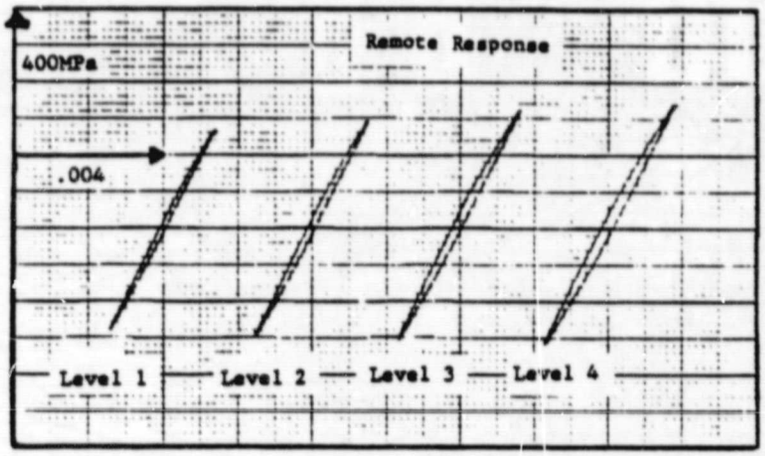

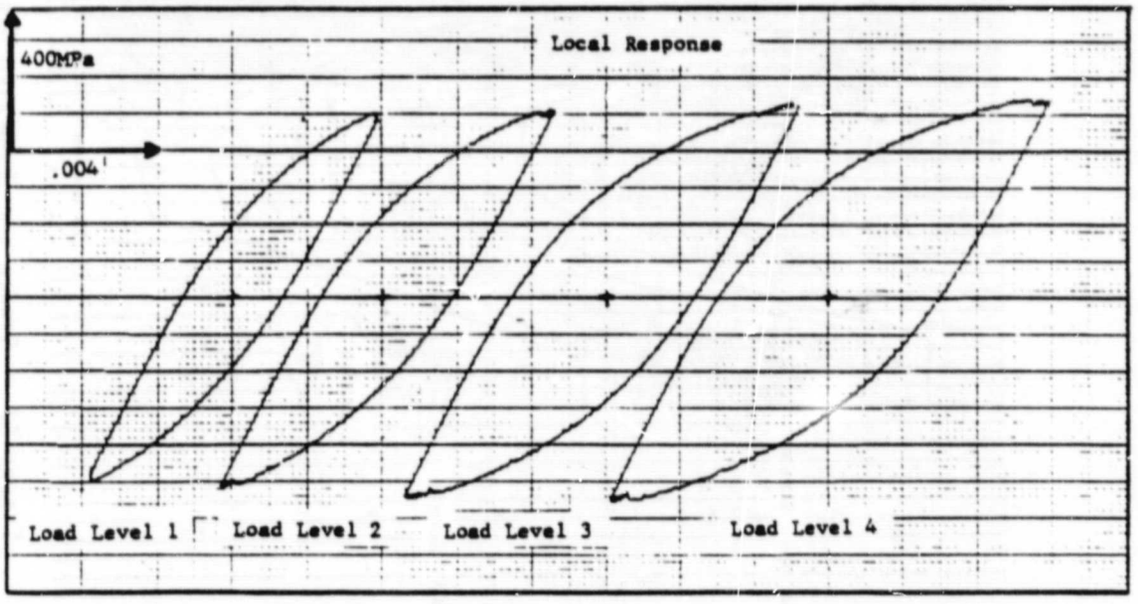

FIGURE 36 SMOOTH SPECIMEN SIMULATION OF STABILIZED STRESSES

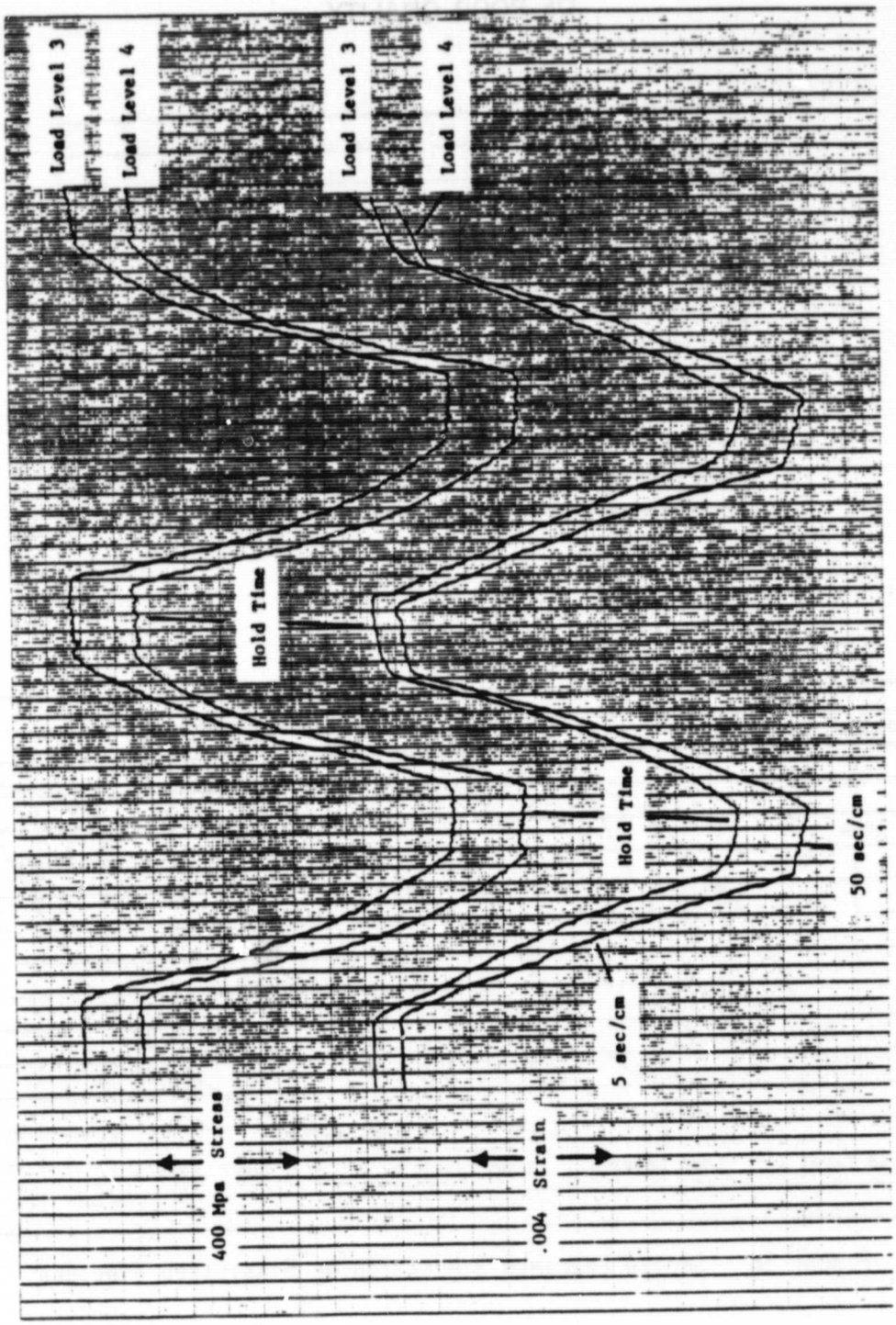

FIGURE 37 STRAIN AND SIMULATED STRESS FOR LOCAL REGION

5.3 Room Temperature Neuber Prediction

The remote stress and strain versus time plots were multiplied by $(K_t')^2$ so that $(K_t')^2 \Delta S \Delta e$ could be plotted (Section 4.4). Such a plot is shown in Figure 38 for initial behavior at Load Level 1. The stress-strain information from Figure 35 was used to construct this Neuber prediction curve. The same type of plots were drawn to predict stabilized local behavior in a notched specimen at four load levels.

A smooth specimen was manually controlled in the MTS testing system so that the product of stress and strain would follow the Neuber prediction curves. The resulting stress and strain values constituted the predicted notch root behavior. The Neuber prediction was then compared with data from the stress simulation of local response (Section 5.2).

The first three cycles were plotted in Figure 39. During the first cycle, the Neuber simulation was slightly high on stress which caused lower strain peaks to occur due to the multiplication. Actually, the tensile and compressive strains were only 9% low for the first cycle. The predicted tensile strain on the second cycle was low by 8% while the compressive strain was 13% lower than the stress simulation.

The stable stress-strain curves in Figure 40 were superimposed to show the excellent results obtained with the Neuber predictions. For Load Levels 1 and 2, the

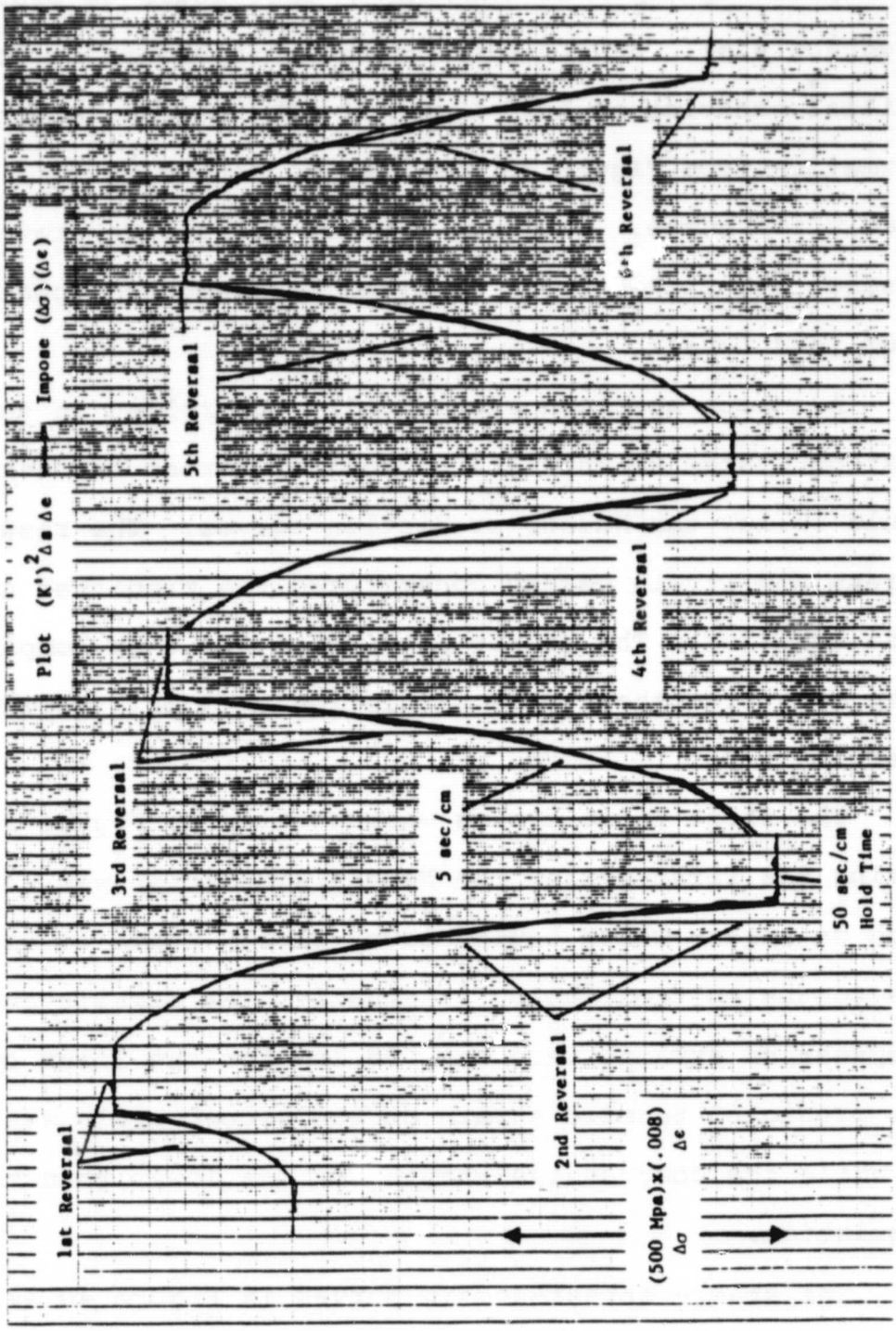

FIGURE 38 NEUBER PREDICTION CURVES FOR INITIAL LOCAL BEHAVIOR

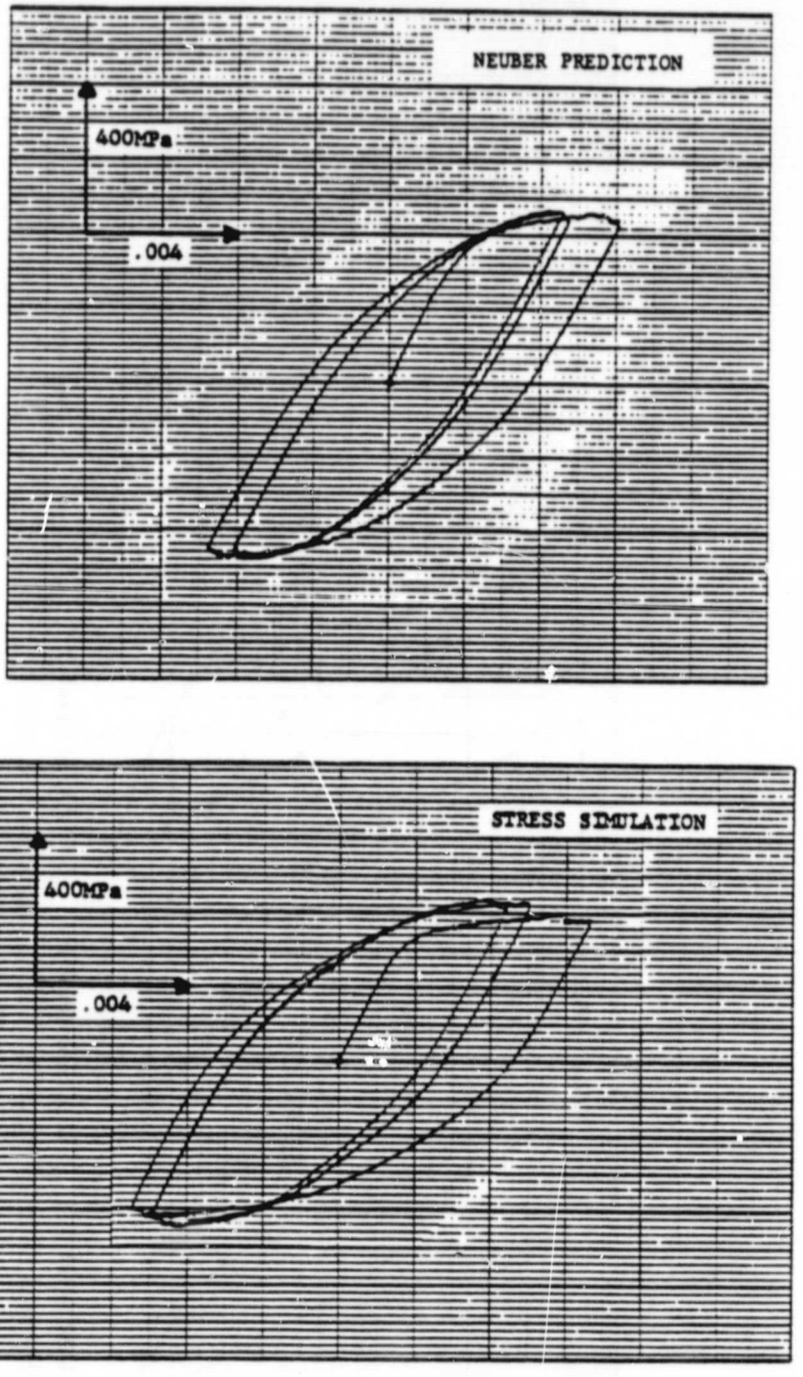

FIGURE 39 NEUBER PREDICTION AND STRESS SIMULATION OF INITIAL LOCAL BEHAVIOR

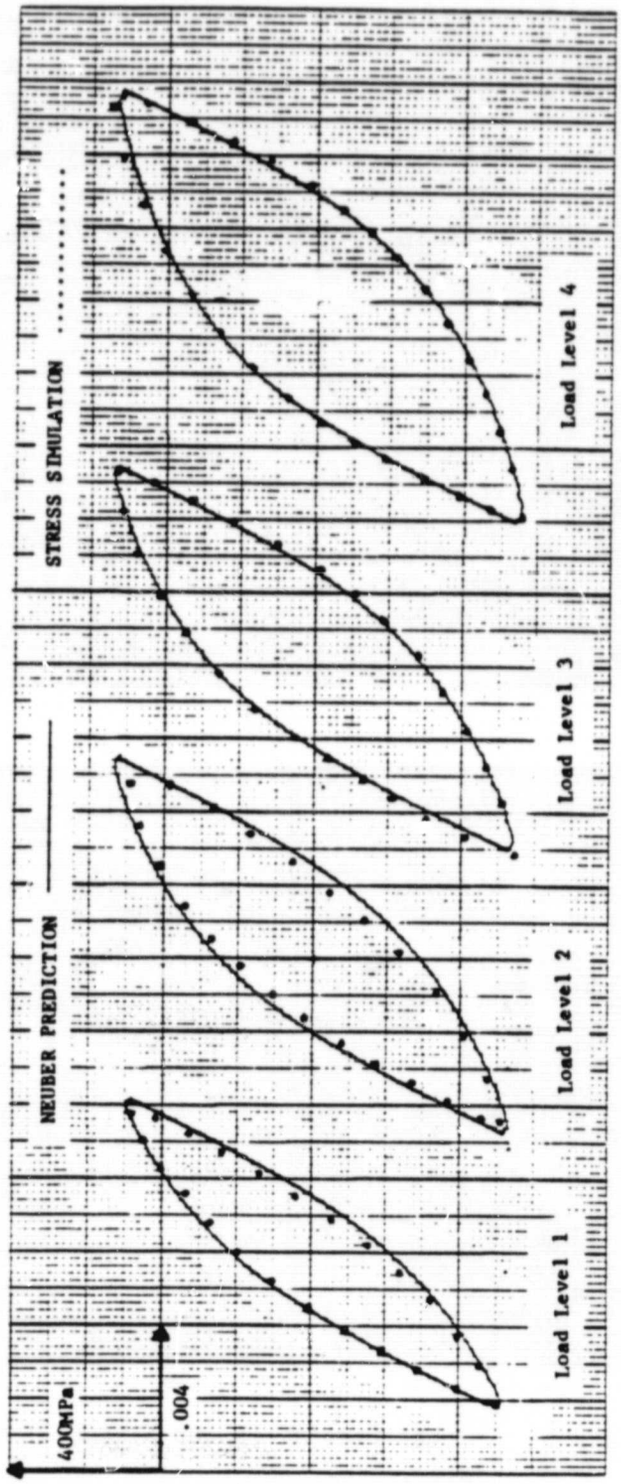

FIGURE 40 NEUBER PREDICTION AND STRESS SIMULATION OF STABILIZED LOCAL BEHAVIOR

Neuber method was approximately 6% high in predicting tensile and compressive strains. Load Levels 3 and 4 show nearly a perfect correlation between the two sets of curves.

5.4 High Temperature I.S.G. Strain Measurement

Notch root and remote strains were also measured at 1,200°F in a Hastelloy X specimen which had been cyclically stabilized. Four load levels were again used as follows:

Level #	Load (KN)
1	± 10.5
2	± 11.3
3	± 12.3
4	± 13.3

Hysteresis loops showing applied load vs. local strain at four different load levels are shown in Figures 41 and 42. Strain versus time plots for each of the corresponding load levels are shown in Figures 43 through 46.

Small increases in load produced large strains at this temperature; especially strain due to creep. During the 100 second hold time the amount of creep strain at each load level was as follows:

Level #	Creep Strain
1	0.05%
2	0.10%
3	0.13%
4	0.18%

These values were approximately equal for tension and compression. Note that the total measured strains were nearly

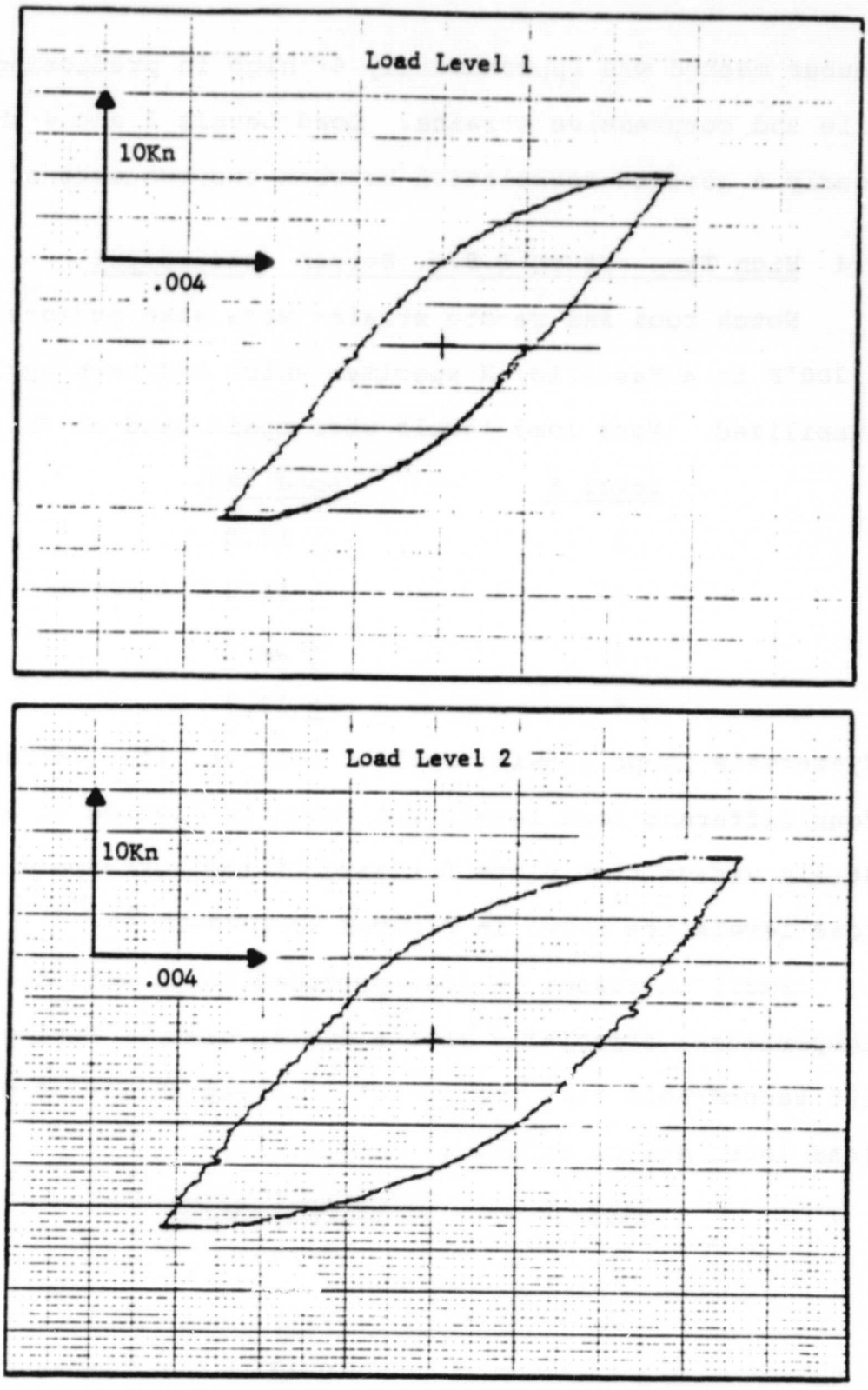

FIGURE 41 LOAD VERSUS LOCAL STRAIN AT 1,200°F

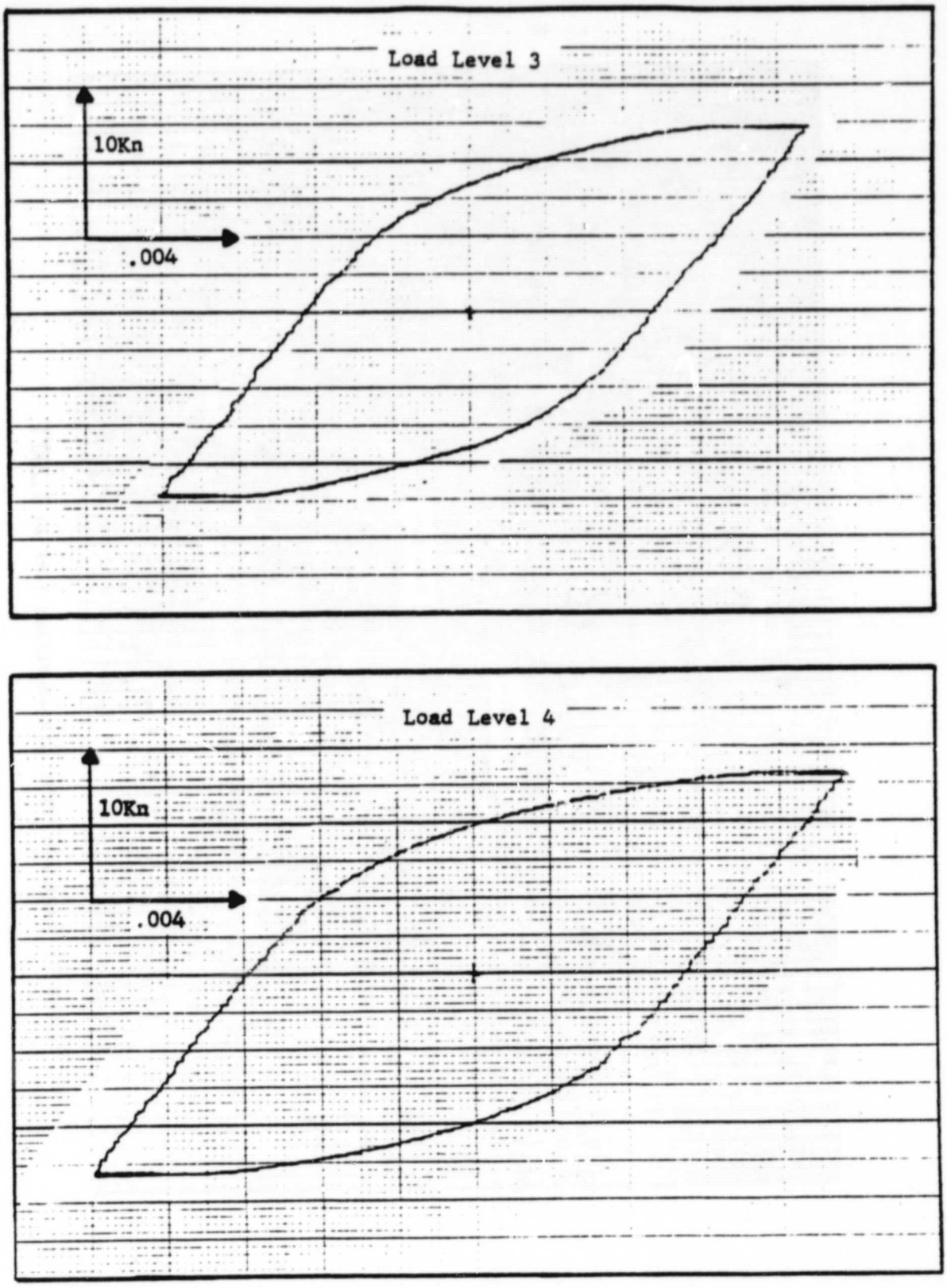

FIGURE 42 LOAD VERSUS LOCAL STRAIN AT 1,200°F

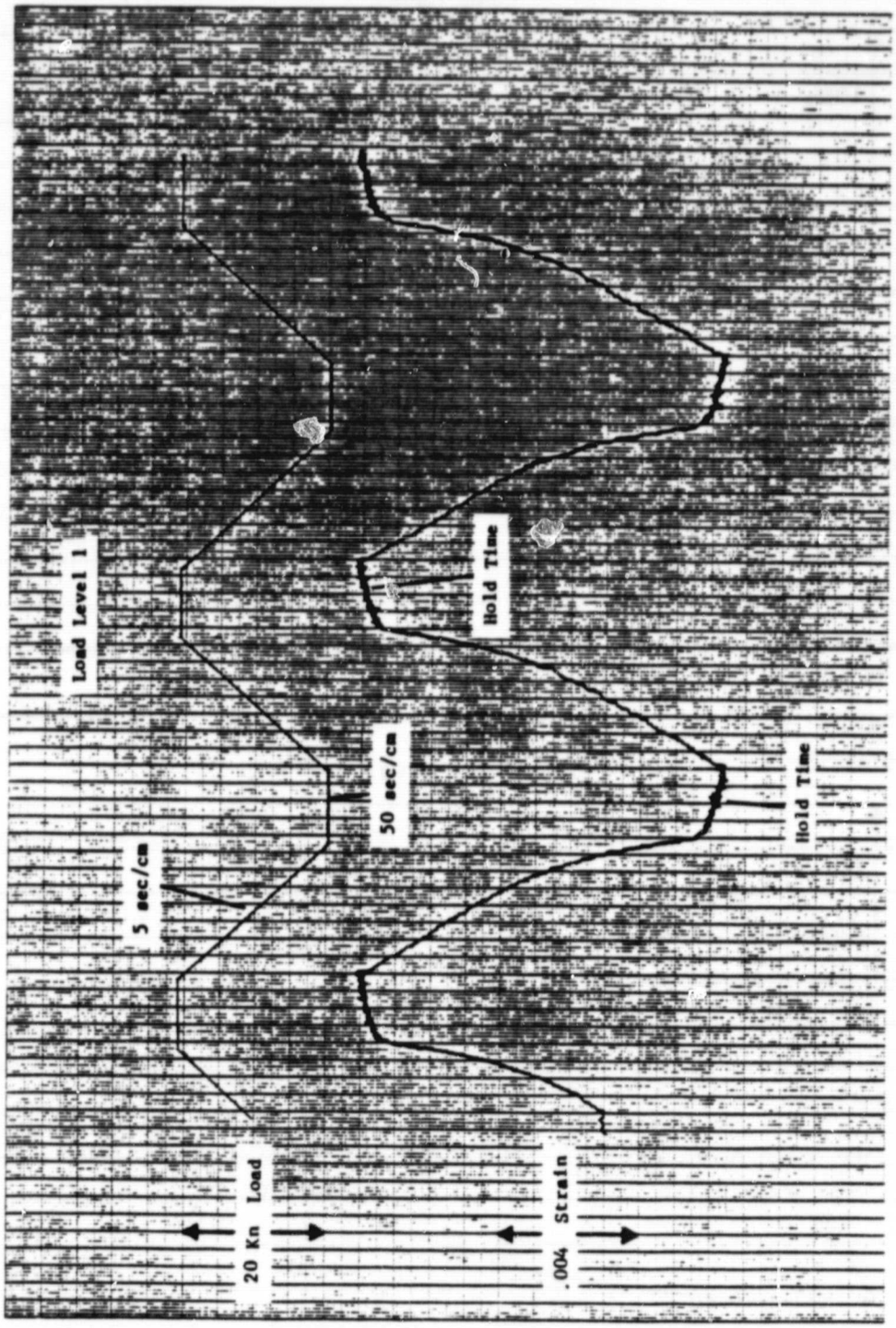

FIGURE 43 LOAD AND LOCAL STRAIN VERSUS TIME AT 1,200°F

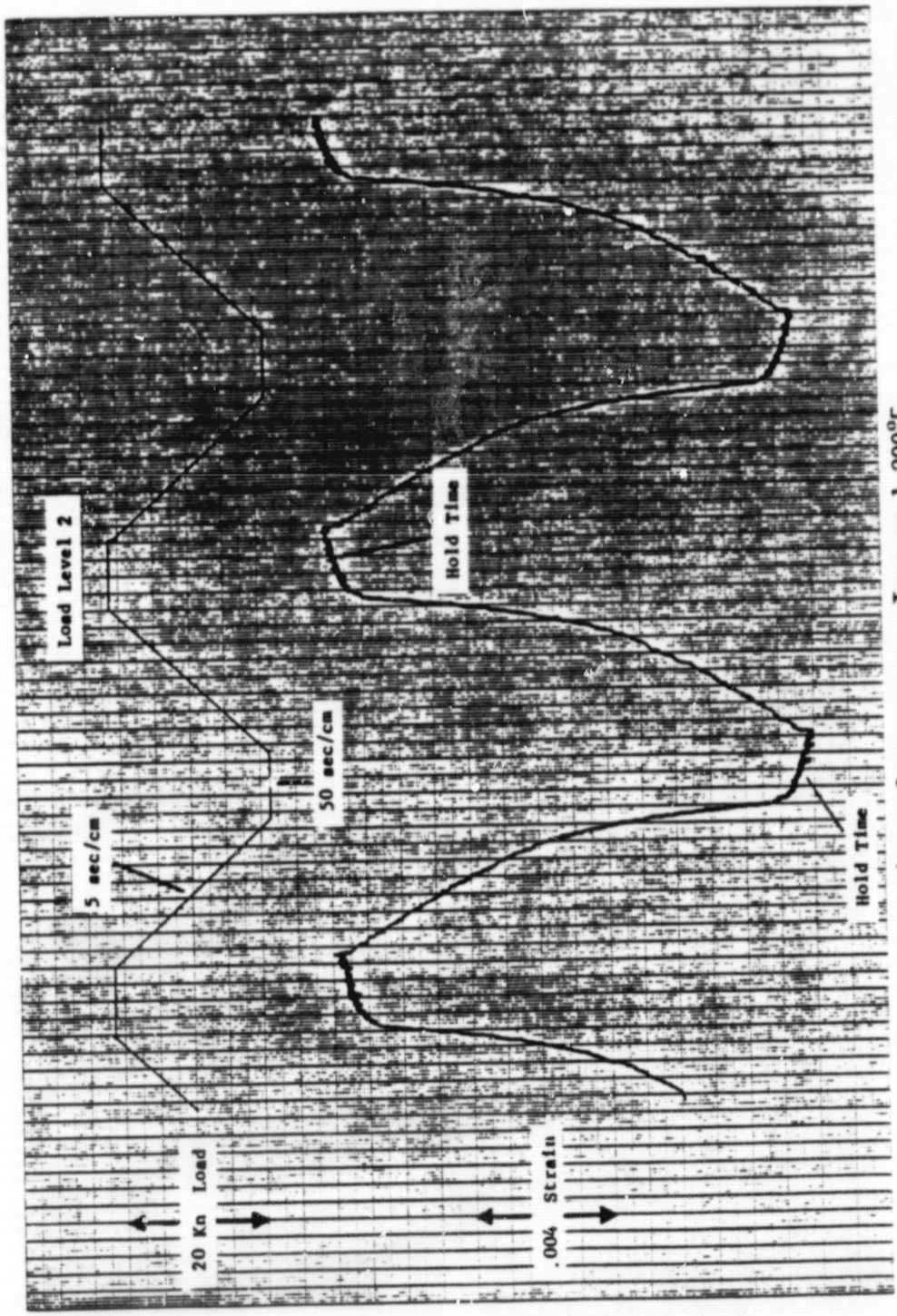

FIGURE 44 LOAD AND LOCAL STRAIN VERSUS TIME AT 1,200°F

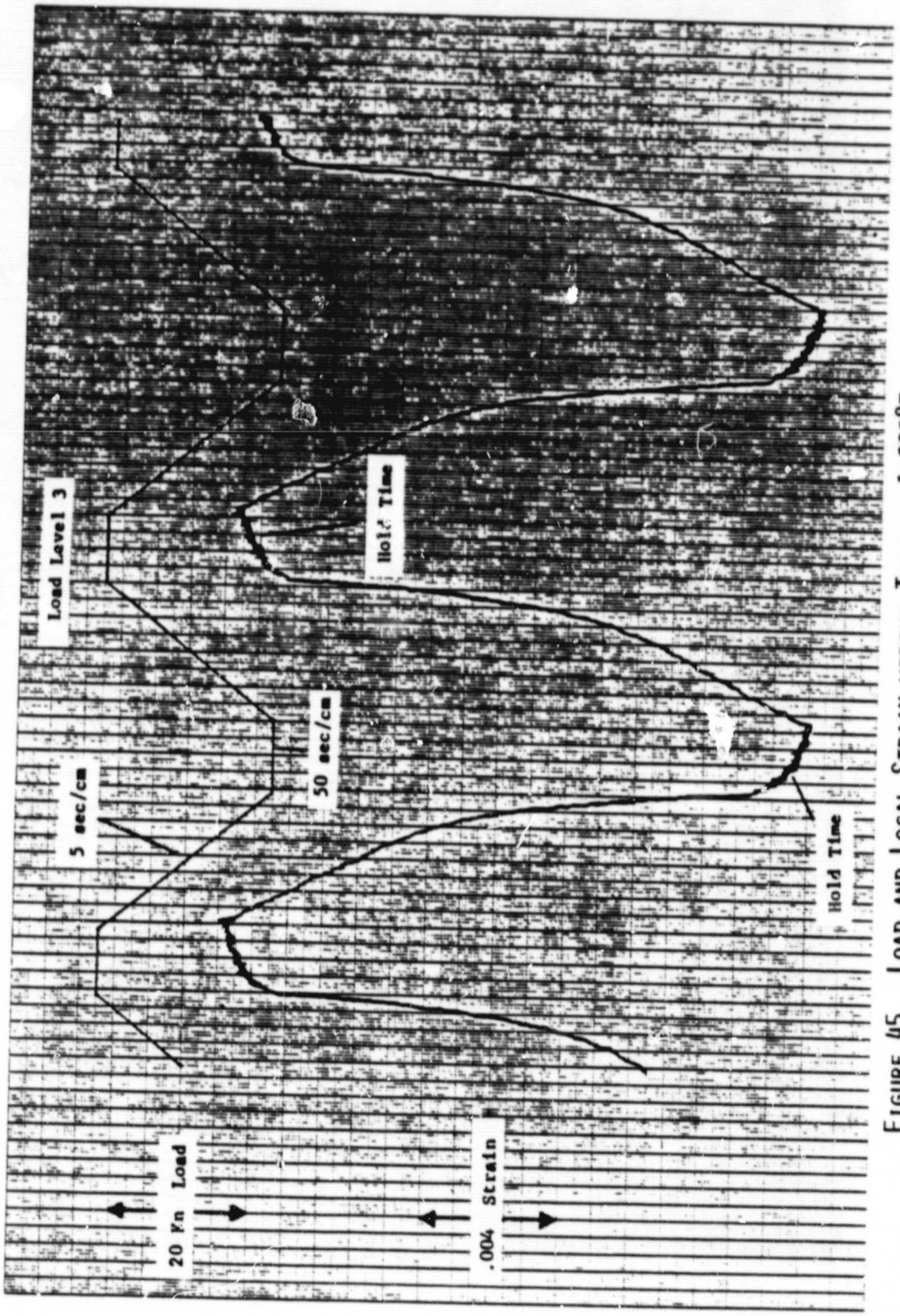

FIGURE 45 LOAD AND LOCAL STRAIN VERSUS TIME AT 1,200°F

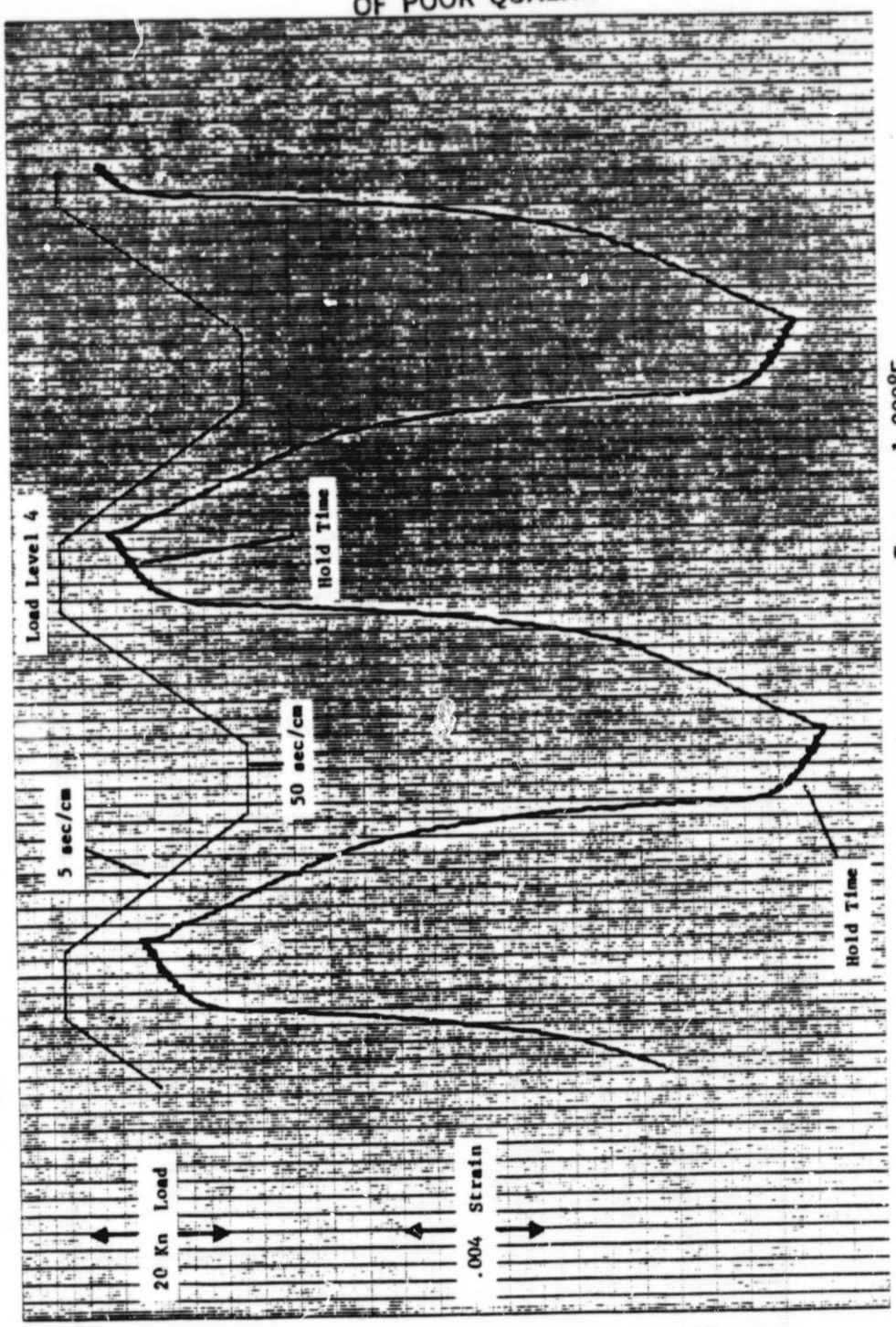

FIGURE 46 LOAD AND LOCAL STRAIN VERSUS TIME AT 1,200°F

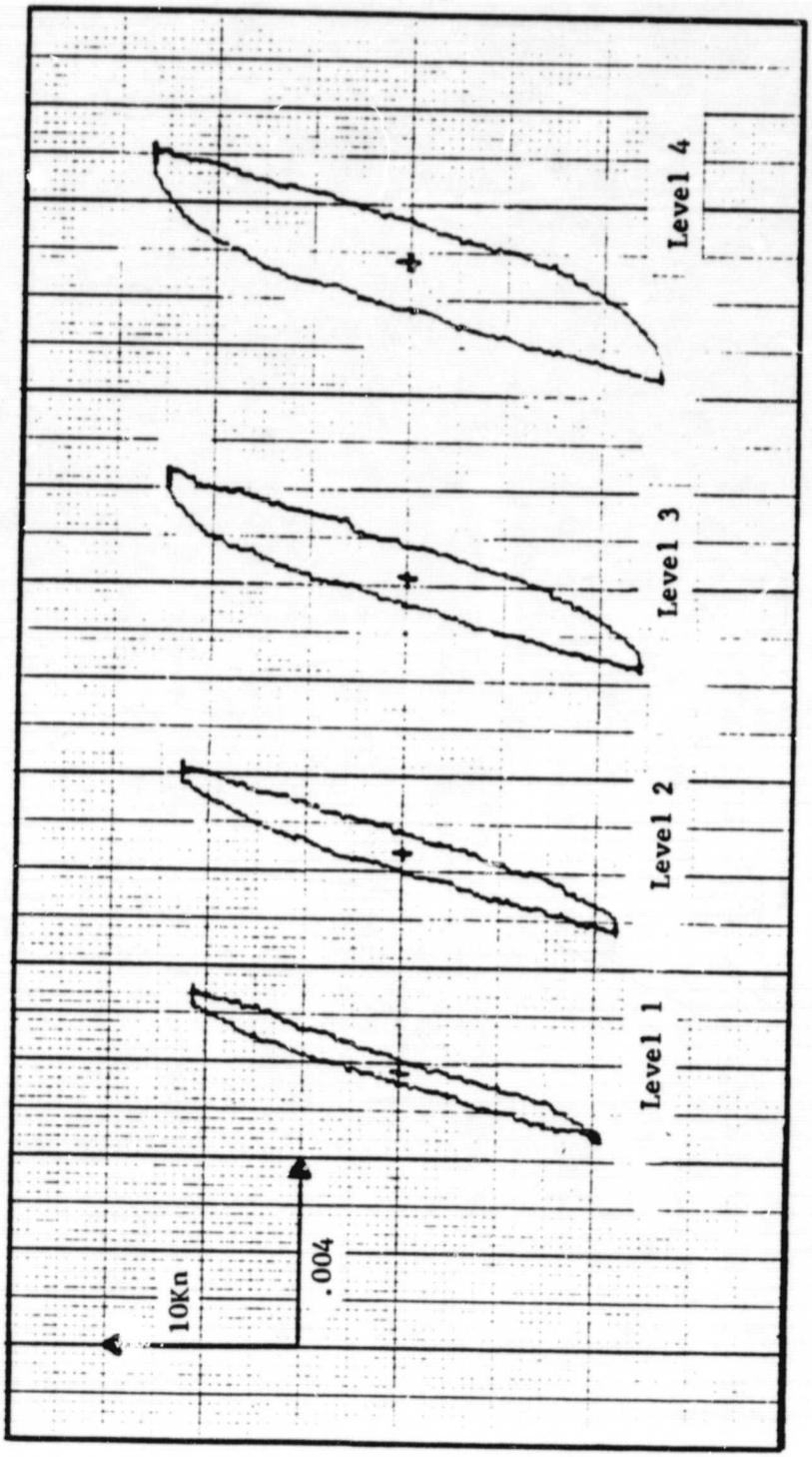

FIGURE 47 LOAD VERSUS REMOTE STRAIN AT 1,200°F

1.0% in both tension and compression during Load Level 4. The interferometric strain measurements were consistant even for these high strain ranges.

The remote data for the stabilized material exhibited much less creep and plastic strain. The load versus strain plots from each of the four load levels are shown in Figure 47. (Note: the four load levels used during the elevated temperature tests were different than the levels used at room temperature.) The amount of creep during the hold times was very small.

5.5 High Temperature Stress Simulation

The measured remote and local strains shown in Section 5.4 were imposed on an hourglass specimen at 1,200°F. The hourglass specimen was cyclically stabilized before performing the stress simulation. The resulting stress versus strain curves for stable notch root response at four different load levels are plotted in Figures 48 and 49. The relationship between stress and strain in time is illustrated in Figure 50 for Load Level 3. The increase in strain which was imposed during the hold period helped to balance the stress relaxation of the material. At Levels 1 and 2 there is almost no stress relaxation while Levels 3 and 4 show just a slight amount.

The remote data from the stress simulation is plotted in Figure 51. The time plot for Level 3 stresses and strains is shown in Figure 52. Very little creep had been measured

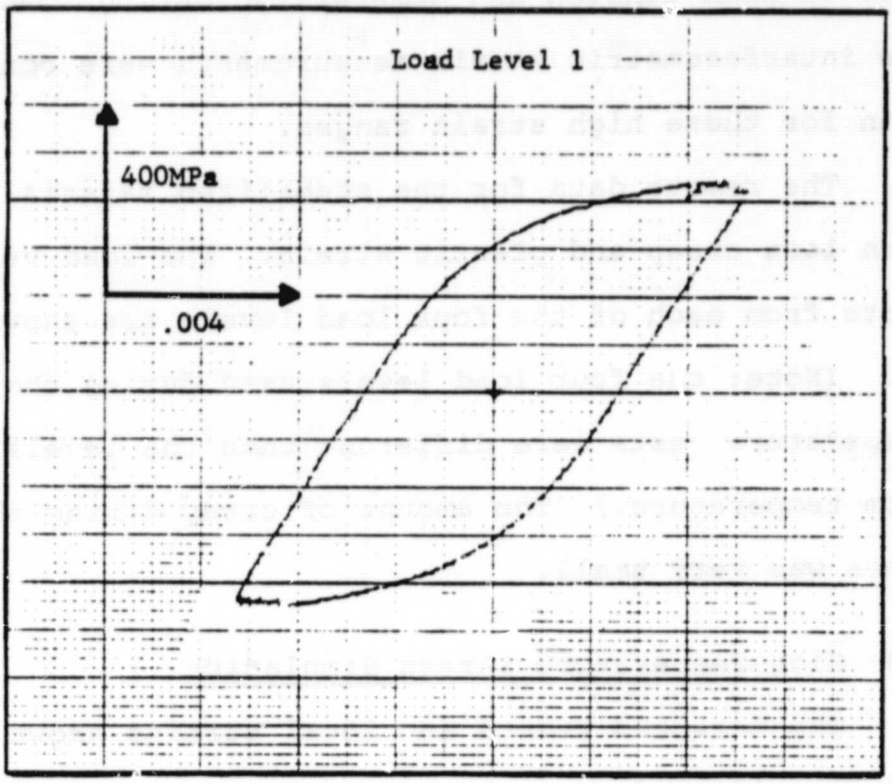

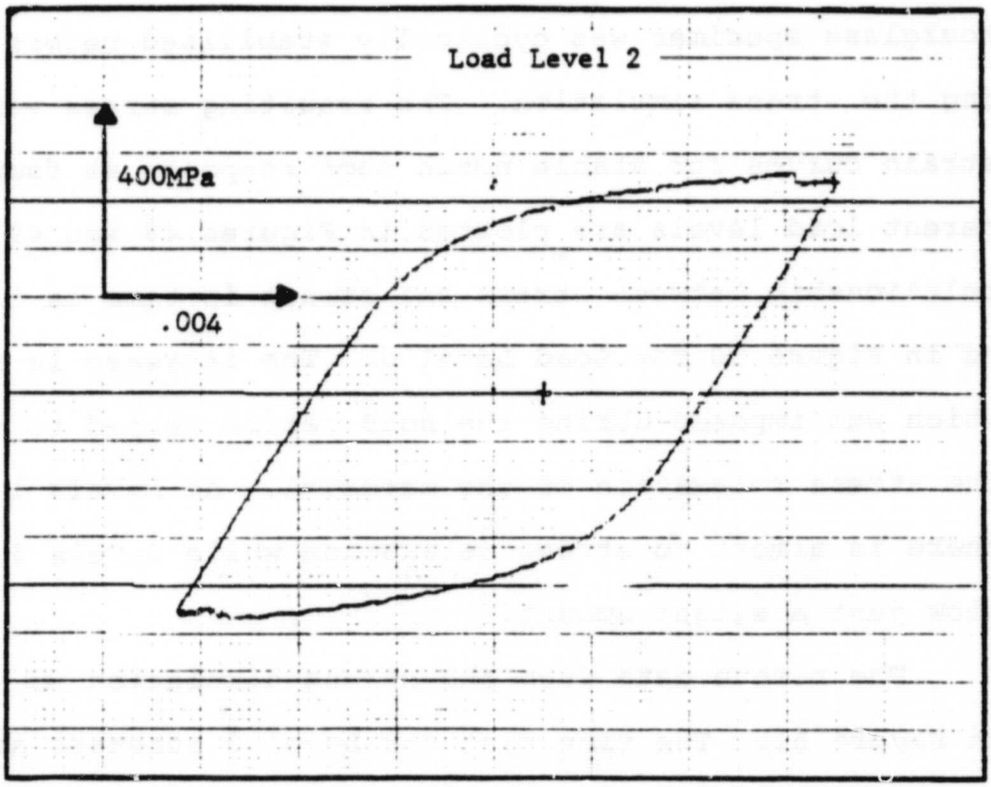

FIGURE 48 LOCAL SIMULATED STRESS VERSUS STRAIN AT 1,200°F

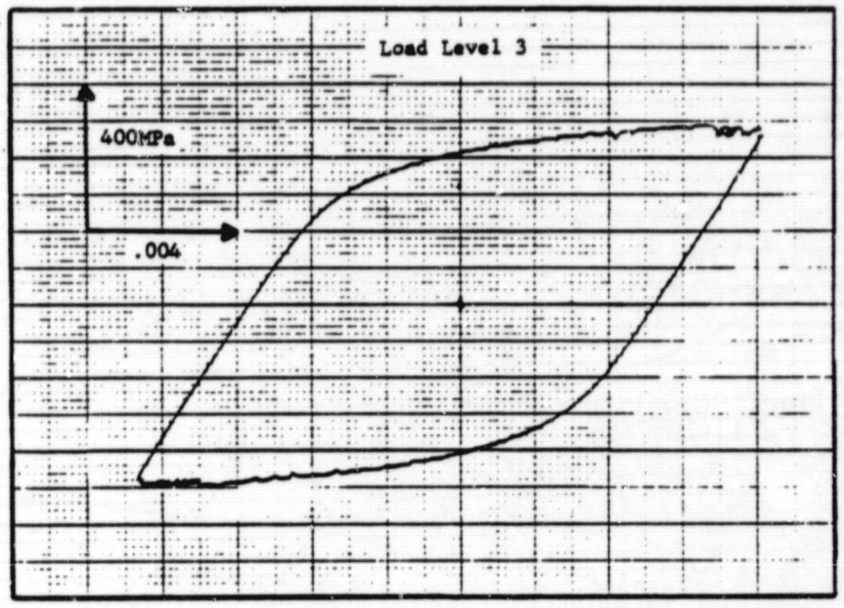

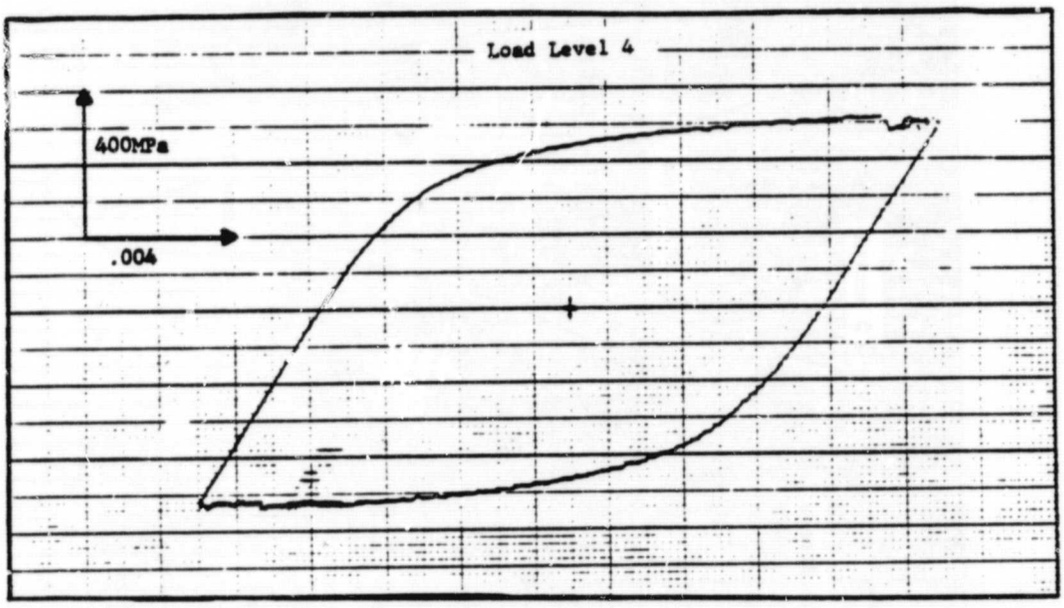

FIGURE 49 LOCAL SIMULATED STRESS VERSUS STRAIN AT 1,200°F

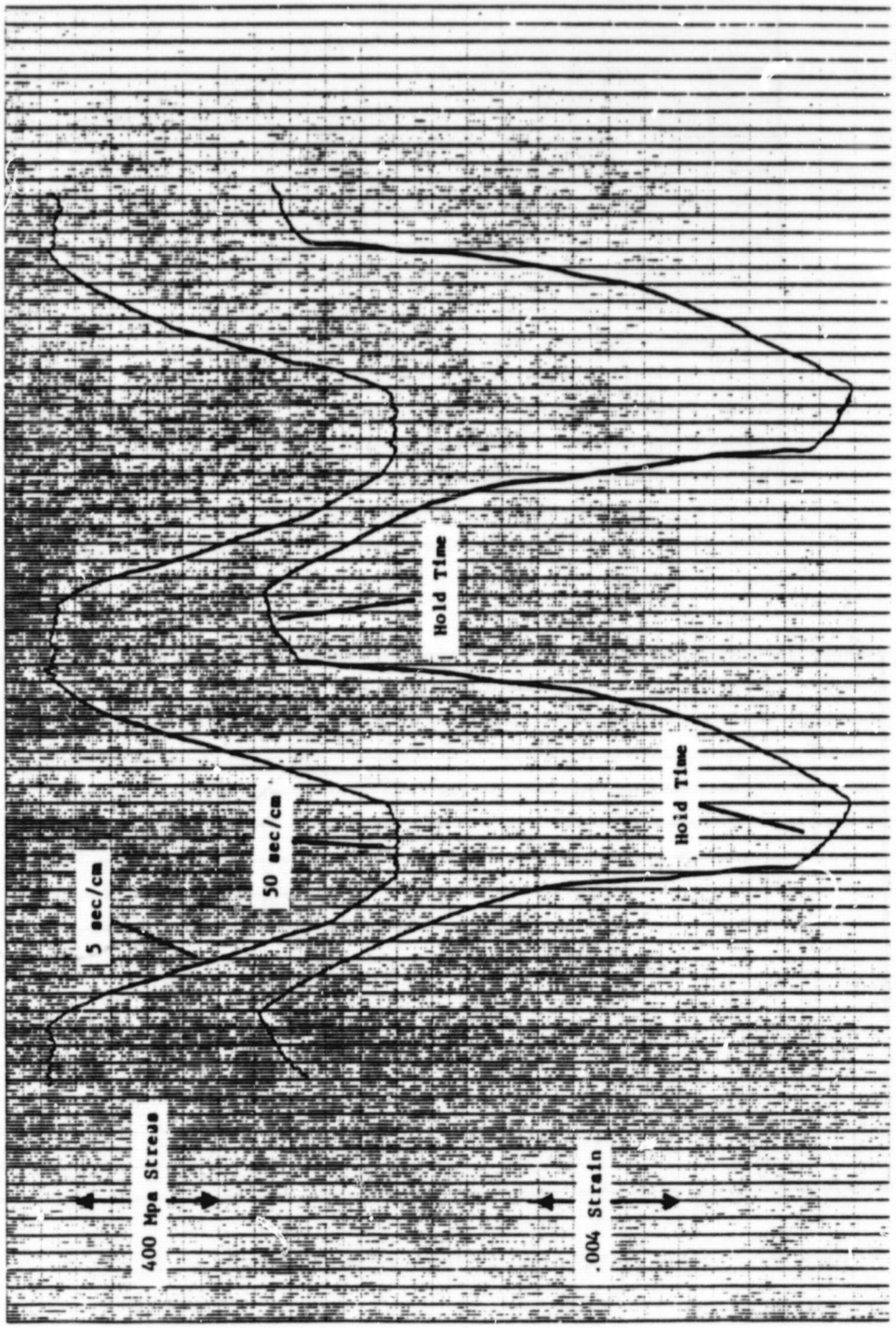

FIGURE 50 LOCAL STRAIN AND SIMULATED STRESS AT 1,200°F, LEVEL 3

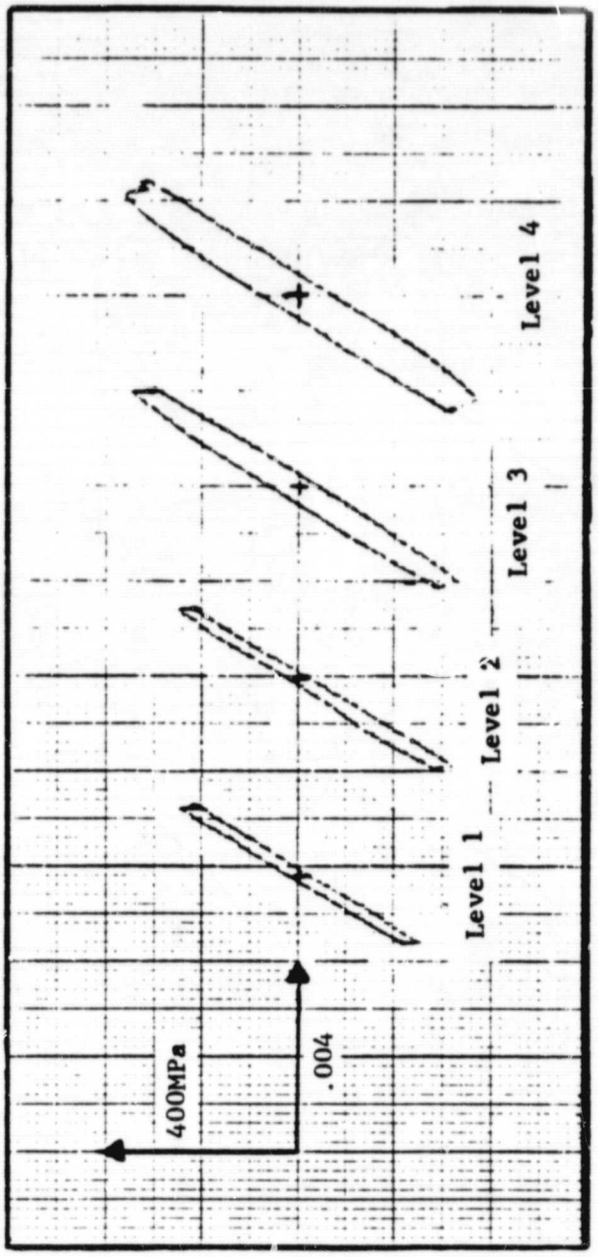

FIGURE 51 REMOTE SIMULATED STRESS VERSUS STRAIN AT 1,200°F

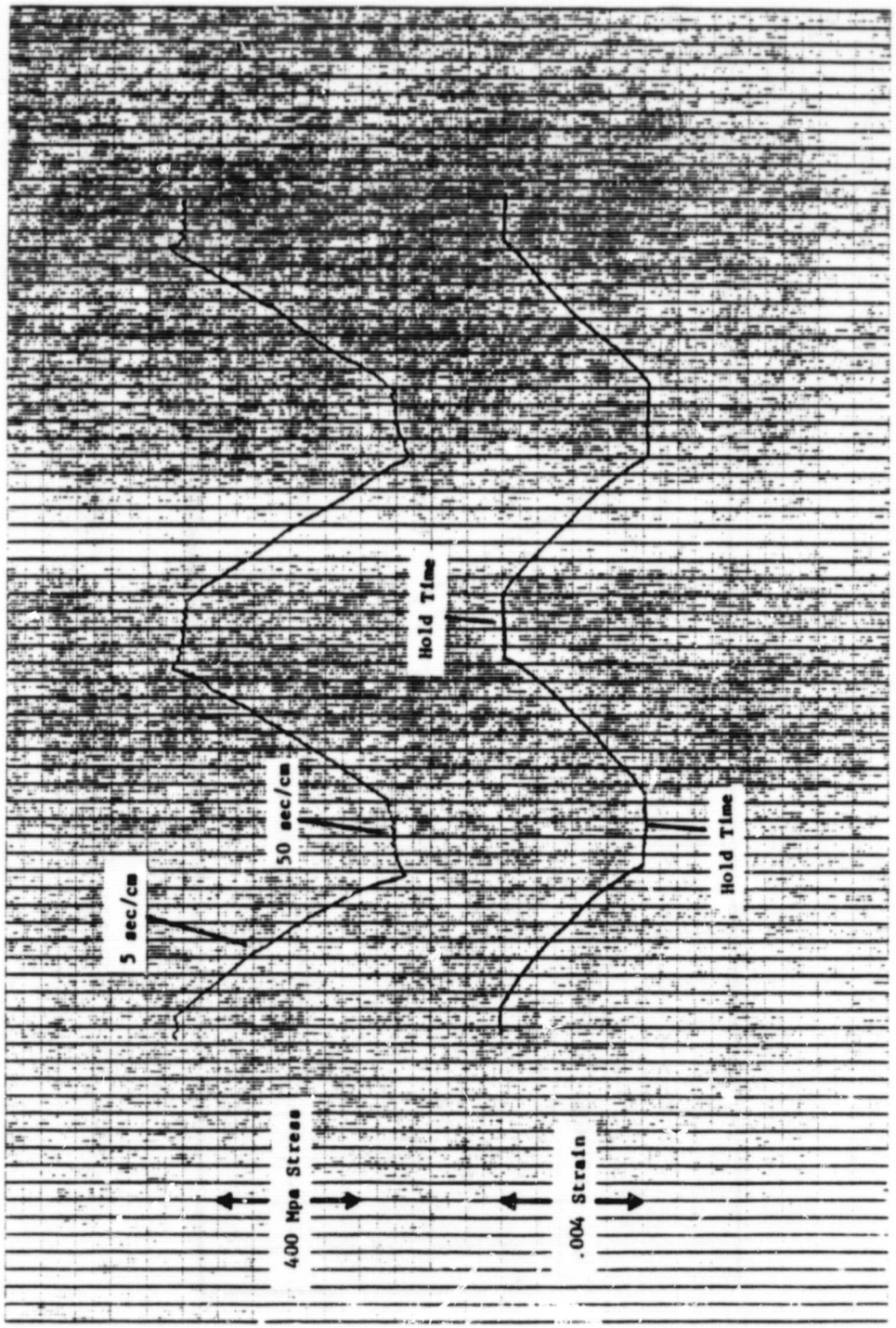

FIGURE 52 REMOTE STRAIN AND SIMULATED STRESS VERSUS STRAIN AT 1,200°F

with the I.S.G. at the remote location. Therefore, when these measured strains were replayed onto the smooth specimen, a large amount of stress relaxation occured during the hold times. This caused the stress vs. strain plots to take on an almost rectangular appearance.

The stress simulation data shows that as the distance from the notch increases, the amount of stress relaxation also increases. This is related to the fact that there is less creep strain to balance the relaxation of stress at the remote location. This information is valuable when trying to construct an overall picture of high temperature behavior in a notched plate.

5.6 High Temperature Neuber Prediction

The Neuber prediction of local behavior was entirely dependent upon remote stress and strain data. These remote data had been determined by the stress simulation described in Section 5.5. Therefore, it is not surprising that when the remote stress and strain values are multiplied by $(K_t')^2$ to construct the Neuber prediction curves, that these curves have decreasing slopes during the hold times. An example of this is shown in Figure 53 for Level 3. This figure shows the actual curves which were retraced during the smooth specimen Neuber prediction.

A cyclically stabilized hourglass specimen heated to 1,200°F was used to establish notch root behavior at four load levels. A comparison was made between the measured

strain/stress simulation and the Neuber prediction in Figures 54 and 55. The most noticeable trend at all four levels was the amount of stress relaxation predicted by the Neuber relation. For Load Levels 1 and 2, the stresses at the end of the 100 second hold times were low by 23% and 27% respectively. The stresses were predicted more accurately at the higher Load Levels. At load level 3 the stresses were 22% low and at Level 4 the stresses were 15% lower than the stress simulation. In terms of strain range, the error in predicting Level 1 strains was 20% low while the Level 4 strains were predicted within 10%.

The behavior during the hold times was quite interesting. The stress relaxation caused the product of stress and strain to decrease. This meant that the Neuber prediction curve's downward slope was automatically satisfied. However, continued stress relaxation forced the operator to increase the level of strain in the specimen so that the Neuber relation would still be satisfied. This accounted for the slanted corners of the Neuber hysterisis loops.

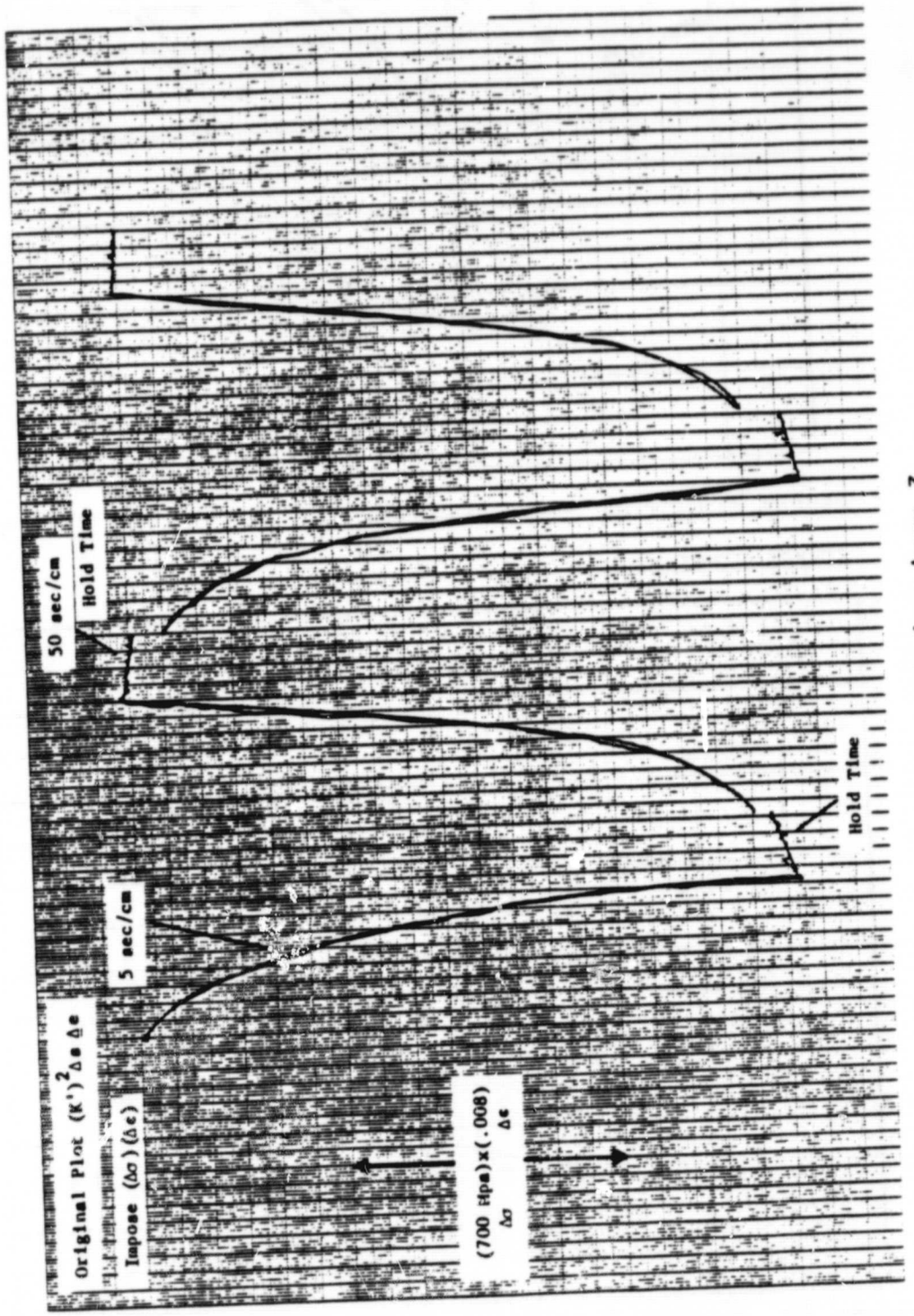

FIGURE 53 NEUBER PREDICTION CURVES FOR LOAD LEVEL 3

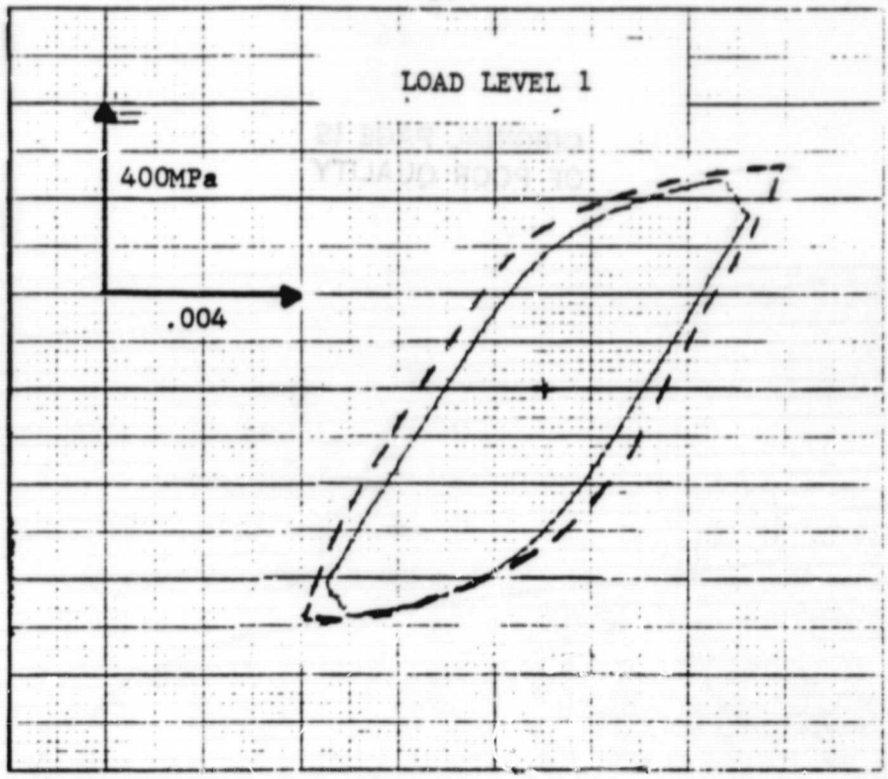

NEUBER PREDICTION ——————

STRESS SIMULATION ----------

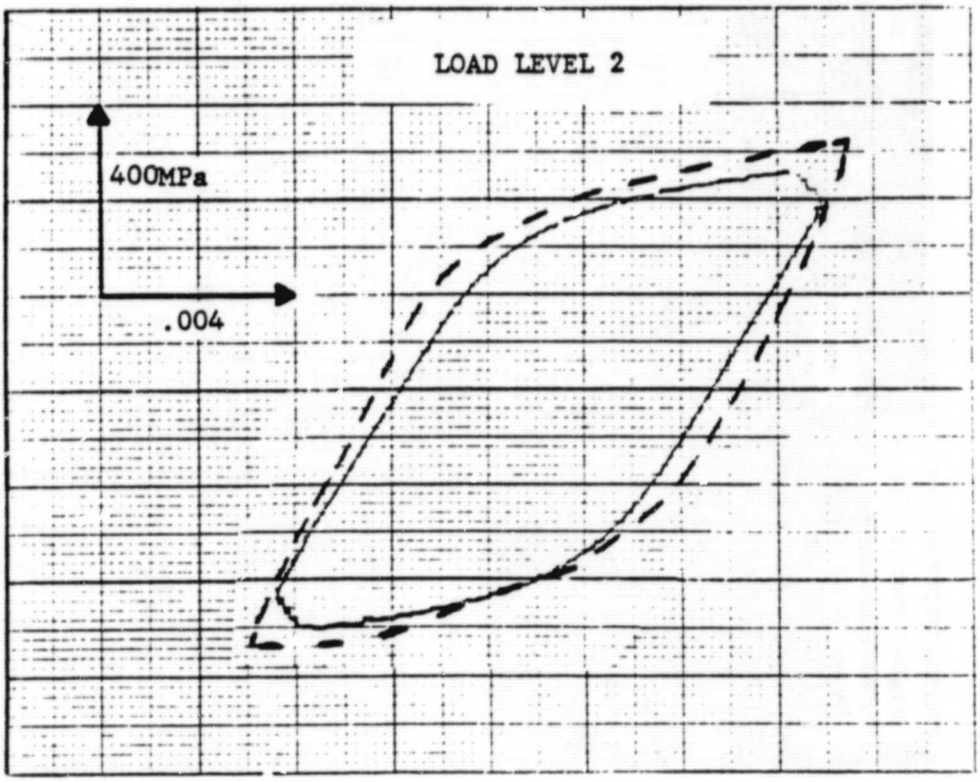

FIGURE 54 NEUBER PREDICTION AND STRESS SIMULATION AT 1,200°F

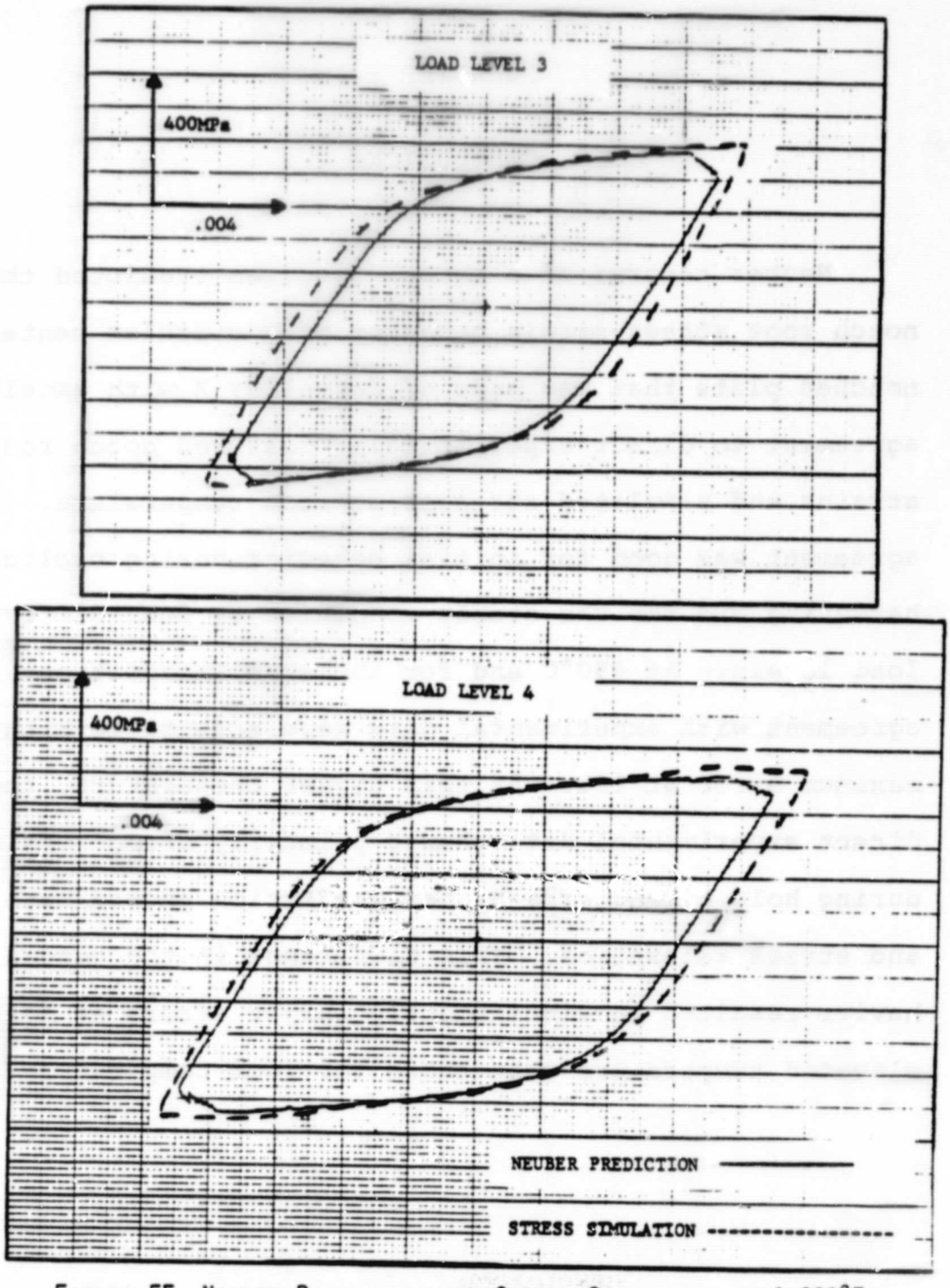

FIGURE 55 NEUBER PREDICTION AND STRESS SIMULATION AT 1,200°F

CHAPTER 6

CONCLUSIONS

Neuber control of a smooth specimen predicted the notch root stress-strain behavior of a circular center notched plate that was made of Hastelloy X with excellent agreement to direct experimentally measured notch root strains and simulated stresses at room temperature. The agreement was good for initial behavior during cyclic hardening and for the stable condition at four different load levels. At 650°C and for the stable conditions, agreement with experimental data were acceptable with the maximum error at 20%. At this higher temperature, the direct experimental data showed primarily creep strain during hold times. The Neuber prediction showed both creep and stress relaxation. This difference in the general behavior resulted in significantly larger errors at this elevated temperature than those for room temperature.

REFERENCES

REFERENCES

1. Signorelli, R. A., Glasgow, T. K., Halford, G. R. and Levine, S. R., "Materials and Structures Technology," NASA Conference Publication #2092, May 1979, pp. 150-162.

2. Avery, L. R., Carayanis, G. S. and Michky, G. L., "Thermal Fatigue Tests of Restrained Combustor Cooling Tubes," Experimental Mechanics, Vol. 7, No. 6, June 1967, pp. 256-264.

3. Walker, K. P., "Research and Development Program for Nonlinear Structural Modeling with Advanced Time-Temperature Dependent Constitutive Relationships," NASA Report No. CR-165533, November 1981.

4. Blatherwick, A. A. and Olson, B. K., "Stress Redistribution in Notched Specimens Under Cyclic Stress," ASD Technical Report 61-451, Aeronautical Systems Division, Wright-Patterson Air Force Base, Dayton, Ohio, 1961.

5. Bofferding, C. H., "A Study of Cyclic Stress and Strain Concentration Factors at Notch Roots Throughout Fatigue Life," Masters' Thesis, Michigan State Univeristy, 1980.

6. Guillot, M. W., "An Experimental Evaluation of Neuber's Cyclic Relation at Room and Elevated Temperatures," Ph.D. Thesis, Louisiana State University, May 1981.

7. Leis, B. N., Gowda, C. V. B., and Topper, T. H., "Some Studies of the Influence of Localized and Gross Plasticity on the Monotonic and Cyclic Concentration Factors," Journal of Testing and Evaluation, Vol. 1, No. 4, July 1973, pp. 341-348.

8. Sharpe, W. N., Jr., "The Interferometric Strain Gage," Experimental Mechanics, Vol. 8, No. 4, April 1968, pp. 164-170.

9. Sharpe, W. N., Jr., "Interferometric Surface Strain Measurement," International Journal of Non-Destructive Testing, 3, 1971, pp. 51-76.

10. Sharpe, W. N., Jr., "A Short Gage Length Optical Gage for Small Strain," Experimental Mechanics, Vol. 14, No. 9, 1974, pp. 373-377.

11. Sharpe, W. N., Jr., "Development and Application of an Interferometric System for Measuring Crack Displacements," Final report on Grant NSG 1148, June 1976.

12. Crews, J. H., Jr., and Hardrath, H. F., "A Study of Cyclic Plastic Stresses at a Notch Root," Experimental Mechanics, Vol. 6, No. 6, June 1966, pp. 313-320.

13. Stadnick, S. J., "Simulation of Overload Effects in Fatigue Based on Neuber's Analysis," T&AM Report No. 325, University of Illinois, Urbana, 1969.

14. Leis, B. N., Gowda, C. V. B., and Topper, T. H., "Cyclic Inelastic Deformation and the Fatigue Notch Factor," ASTM STP 519, American Society for Testing and Materials, 1973, pp. 133-150.

15. Wetzel, R. M., "Smooth Specimen Simulation of Fatigue Behavior of Notches," T&AM Report No. 295, University of Illinois, Urbana, May 1967.

16. Stadnick, S. J., and Morrow, Jo Dean, "Techniques for Smooth Specimen Simulation of the Fatigue Behavior of Notched Members," ASTM STP 515, American Society for Testing and Materials, 1972, pp. 229-252.

17. Sharpe, W. N., Jr., "Preliminary Development of an Interferometric Strain Gage for Use on Nosetip Materials Subjected to Thermal Shock," Final Report for Air Force Materials Laboratory TR 76-63, June 1976, pp. 14.

18. Jaske, C. E., Rice, R. C., Buchheit, R. D., Roach, D. B., Porfilio, T. L., "Low Cycle Fatigue of Type 347 Stainless Steel and Hastelloy X in Hydrogen Gas and in Air at Elevated Temperatures," NASA Report No. CR-135022, May 1976.

19. Cabot Corporation, "Hastelloy Alloy X," High Technology Materials Division, June 1976.

20. Peterson, R. E., "Stress Concentration Factors, John Wiley and Sons, Inc., 1974, pp. 150-196.

21. Boresi, A. P., Sidebottom, O. M., Seely, F. B., Smith, J. O., "Advanced Mechanics of Materials," John Wiley and Sons, Inc., 1978, pp. 576-579.

22. Slot, L., Stentz, R. H., Berling, J. T., "Controlled Strain Testing Procedures," Manual on Low Cycle Fatigue Testing, ASTM STP 465, American Society for Testing and Materials, 1969, pp. 100-128.